

AFG3L2 deficiency impairs axonal transport of mitochondria dependent on ROS and tau levels

Inaugural-Dissertation

zur

Erlangung des Doktorgrades

der Mathematisch-Naturwissenschaftlichen Fakultät

der Universität zu Köln



vorgelegt von

ARUN KUMAR KONDADI

aus Hyderabad, India

Köln 2014

Berichterstatter: **Prof. Dr. Elena Rugarli**
 Prof. Dr. Thomas Langer

Tag der mündlichen Prüfung: 23.06.2014

To my Guru Sri Sathya Sai Baba

ZUSAMMENFASSUNG

Die *m*-AAA Protease ist ein Protein der inneren mitochondrialen Membran, dessen katalytisches Zentrum zur Matrix hin ausgerichtet ist. Die Protease hat Funktionen im Abbau von fehlgefalteten Proteinen und der Prozessierung von Substraten. Patienten mit heterozygoten, nicht-synonymen Mutationen im *AFG3L2* Gen leiden unter Spinozerebellärer Ataxie Typ 28 (SCA28), wohingegen homozygote Mutationen in der *m*-AAA Protease Untereinheit zu akuten, rezessiven Formen von spastischer Ataxie (SPAX5) führen, deren Symptome bereits sehr früh in der Entwicklung erkennbar sind. Bekannt ist, dass der Verlust des *AFG3L2* Genes in nicht-polarisierten Zellen zur Fragmentierung des mitochondrialen Netzwerkes führt. Die neurodegenerative Erkrankung assoziiert mit dem Verlust von *AFG3L2* in Nervenzellen und der Effekt auf den mitochondrialen Transport ist bisher wenig erforscht.

Wir konnten zeigen, dass der Verlust von *AFG3L2* in einem spezifischen Defekt des anterograden Transportes in primären kortikalen Nervenzellen von Mäusen resultiert. Diese Beeinträchtigung des anterograden Transportes besteht auch bei gleichzeitigem Verlust von *AFG3L2* und *OPA1*, wodurch deutlich wird, dass der Abbau der GTPase OPA1 und somit die Hemmung der Fusion des mitochondrialen Netzwerkes nicht der Grund für diesen Transport Defekt ist. Die Störung des anterograden Transportes in *AFG3L2* defizienten Nervenzellen kann durch die Antioxidantien N-Acetylcystein (NAC) und Vitamin E beseitigt werden. Von Bedeutung ist auch, dass wir den mitochondrialen Transport teilweise durch runter Regulierung von Tau, einem Mikrotubuli bindendem Protein, retten können. Zusammenfassend kann man sagen, dass Nervenzellen mittels reaktiver Sauerstoff-Spezies (ROS), Modifikationen des Zytoskelettes und mitochondrialen Transport verbinden.

TABLE OF CONTENTS:

SUMMARY (p.1)

ABBREVIATIONS (p.2)

INTRODUCTION:

1.1) The *m*-AAA protease (p.5)

1.2) Neurodegeneration associated with *m*-AAA protease (p.14)

1.3) Link between mitochondrial dynamics and neurodegeneration (p.20)

1.4) Mitochondrial transport and neurodegeneration (p.25)

1.5) The role of tau in neurodegeneration and development (p.30)

METHODS:

2.1) Primary murine cortical neuronal culture and transfection (p.36)

2.2) Imaging and transfection of parkin-mCherry (p.37)

2.3) Live-cell imaging (p.38)

2.4) Immunofluorescence analysis (p.38)

2.5) TMRM staining and quantification of mitochondrial membrane potential
(p.39)

2.6) Measurement of cellular ROS levels (p.39)

2.7) Assessment of mitochondrial length, occupancy and transport (p.40)

2.8) Calculation of Mitochondrial velocities (p.41)

2.9) Statistical Analysis (p.41)

2.10) Quantification of proteins, SDS PAGE & Western blot analysis (p.42)

2.11) Cell treatments (p.43)

MATERIALS:

2.12) siRNA oligonucleotides used in the study (p.44)

2.13) Plasmids used (p.45)

2.14) Antibodies for western blot analysis (p.45)

3.0) FORMULATION OF THE RESEARCH PROJECT (p.47)

RESULTS:

3.1) Impaired mitochondrial fusion in *Afg3l2*^{Emv66/Emv66} MEFs (p.49)

3.2) Characterization of primary murine cortical neuronal culture (p.53)

3.3) Aberrant mitochondrial dynamics in neurons downregulated for *Afg3l2* (pp.56-69)

3.3.1) Neurons depleted for AFG3L2 have fragmented mitochondrial morphology

3.3.2) Neurons depleted for AFG3L2 have reduced mitochondrial occupancy

3.3.3) The reduced mitochondrial occupancy in *Afg3l2* downregulated neurons is independent of parkin-mediated mitophagic clearance

3.3.4) Kymographic analysis of neurons downregulated for *Afg3l2*

3.3.5) AFG3L2 depleted neurons have impaired anterograde transport of mitochondria but unchanged mitochondrial velocities

3.3.6) The mitochondrial membrane potential in *Afg3l2* downregulated neurons is unchanged

3.4) Depletion of OPA1 does not impair mitochondrial transport (pp. 70-74)

3.4.1) Neurons depleted for OPA1 have fragmented mitochondrial morphology and reduced mitochondrial occupancy

3.4.2) Mitochondrial transport analysis of neurons downregulated for *Opa1*

3.5) Aberrant mitochondrial dynamics in neurons depleted for AFG3L2 are independent of OMA-1 activation (pp. 75-79)

3.5.1) Mitochondrial morphology and occupancy in *Oma1*^{-/-} neurons downregulated for *Afg3l2*

3.5.2) Mitochondrial transport in *Oma1*^{-/-} neurons downregulated for *Afg3l2*

3.6) Tau affects mitochondrial dynamics in neurons deficient for AFG3L2 (pp.80-86)

3.6.1) Characterization of siRNA oligonucleotides directed against tau

3.6.2) Mitochondrial morphology and occupancy in neurons depleted for AFG3L2 and tau

3.6.3) Mitochondrial transport in neurons depleted for AFG3L2 and tau

3.7) NAC rescues mitochondrial defects observed in neurons depleted for AFG3L2 (pp.87-94)

3.7.1) Mitochondrial morphology and occupancy in AFG3L2 depleted neurons grown in the presence of NAC

3.7.2) Kymographic analysis of neurons downregulated for *Afg3l2* grown in the presence of NAC

3.7.3) Mitochondrial transport and velocity in AFG3L2 depleted neurons grown in the presence of NAC

3.8) Vitamin E rescues mitochondrial transport defects observed in AFG3L2 deficient neurons (pp.95-100)

3.8.1) Mitochondrial morphology and occupancy in AFG3L2 depleted neurons grown in the presence of vitamin E

3.8.2) Mitochondrial transport in AFG3L2 depleted neurons grown in the presence of vitamin E

3.9) Evaluation of cellular ROS levels in AFG3L2 deficient neurons by CellRox green (pp.101-104)

DISCUSSION (p.107)

REFERENCES (p.117)

ACKNOWLEDGEMENTS (p.130)

PUBLICATION OF THE THESIS (p.132)

ERKLÄRUNG (p.148)

CURRICULUM VITAE (p.149)

LIST OF FIGURES AND TABLES:

Figure 3.1: *Afg3l2*^{Emv66/Emv66} MEFs display reduced mitochondrial fusion

Figure 3.2: Characterization of primary murine cortical neuronal culture

Figure 3.3: Neurons depleted for AFG3L2 have fragmented mitochondrial morphology

Figure 3.4: Neurons depleted for AFG3L2 have reduced mitochondrial occupancy

Figure 3.5: Reduced mitochondrial occupancy in AFG3L2 depleted neurons is independent of parkin-mediated mitophagic clearance

Figure 3.6: Kymographic analysis of neurons downregulated for *Afg3l2*

Figure 3.7: Neurons depleted for AFG3L2 have impaired anterograde transport of mitochondria but unchanged mitochondrial velocities

Figure 3.8: The mitochondrial membrane potential in *Afg3l2* downregulated neurons is unchanged

Figure 3.9: Neurons depleted for OPA1 have fragmented mitochondrial morphology and reduced mitochondrial occupancy

Figure 3.10: Mitochondrial transport analysis of neurons downregulated for *Opa1*

Figure 3.11: *Oma1*^{-/-} neurons downregulated for *Afg3l2* do not show a significant difference in mitochondrial morphology and occupancy

Figure 3.12: *Oma1*^{-/-} neurons downregulated for *Afg3l2* do not rescue impaired anterograde transport of mitochondria

Figure 3.13: Characterization of siRNA oligonucleotides directed against tau

Figure 3.14: Neurons depleted for AFG3L2 and tau, when compared to AFG3L2 alone, show a rescue in fragmented mitochondrial morphology but not occupancy

Figure 3.15: Neurons depleted for AFG3L2 and tau partially rescue impaired anterograde transport of mitochondria but not mitochondrial velocities when compared to AFG3L2 depletion alone

Figure 3.16: NAC rescues fragmented mitochondrial morphology and occupancy in AFG3L2 depleted neurons

Figure 3.17: Kymographic analysis of neurons downregulated for *Afg3l2* grown in the presence of NAC

Figure 3.18: NAC rescues impaired anterograde transport in AFG3L2 depleted neurons and increases the velocity of anterogradely moving mitochondria in control neurons

Figure 3.19: AFG3L2 deficient neurons do not show a significant difference in mitochondrial morphology and occupancy when grown in the presence of vitamin E

Figure 3.20: Neurons depleted for AFG3L2 rescue impaired anterograde transport of mitochondria when grown in the presence of vitamin E

Figure 3.21: *Afg3l2* downregulated neurons do not display consistent increase in cellular ROS levels

Figure 3.22: NAC and vitamin E display antioxidant activity

Table 1: Percentage stationary mitochondria in the whole study (p. 105)

SUMMARY

The *m*-AAA protease, present in the inner mitochondrial membrane facing the mitochondrial matrix, degrades misfolded polypeptides and processes substrates. AFG3L2 is a subunit of *m*-AAA protease. In humans, heterozygous missense mutations in AFG3L2 lead to Spinocerebellar Ataxia type 28 (SCA28) whereas homozygous mutations in AFG3L2 cause a severe recessive form of spastic-ataxia with early-onset and rapid progression (SPAX5). While depletion of AFG3L2 causes mitochondrial fragmentation in non-polarised cells, the mechanisms of neurodegeneration associated with mitochondrial dynamics and trafficking were not studied in AFG3L2 deficient neurons.

We showed that depletion of AFG3L2 in murine primary cortical neurons leads to a selective defect of anterograde transport of mitochondria. The impaired anterograde transport defect was also observed upon concomitant depletion of AFG3L2 and OMA1 demonstrating that OMA1-mediated degradation of OPA1 (to inhibit mitochondrial fusion) was not the reason for mitochondrial transport defects. Anterograde transport defect of mitochondria in AFG3L2 depleted neurons could be rescued by antioxidants, N-acetyl cysteine (NAC) and vitamin E. Interestingly, we also observed a partial rescue in mitochondrial transport by depleting tau, a microtubule-associated protein. Hence, we conclude that neurons employ ROS to couple cytoskeletal modifications and mitochondrial transport.

ABBREVIATIONS

AAA: ATPase associated with diverse cellular activities

AFG3L1: ATPase family gene-3 like-1 or Afg3 like-1

AFG3L2: ATPase family gene-3 like-2 or Afg3 like-2

AD: Alzheimer's disease

APP: Amyloid Precursor Protein

CCCP: Carbonyl cyanide m-chlorophenyl hydrazine

CHO: Chinese Hamster Ovary

DIV: Days *in vitro*

DOA: Dominant Optic Atrophy

DRG: Dorsal Root Ganglion

DRP-1: Dynamin Related Protein-1

ETC: Electron transport chain

GFAP: Glial Fibrillary Acidic Protein

HSP: Hereditary Spastic Paraplegia

IMM: Inner mitochondrial membrane

KIFs: Kinesin Superfamily Proteins

MAP: Microtubule-associated protein 2

MEFs: Mouse Embryonic Fibroblasts

Mfn: Mitofusin 1

Mfn2: Mitofusin 2

Min: Minutes

MTOC: Microtubule organizing Centre

MTS: Mitochondrial targeting sequence

NAC: N-acetyl Cysteine

NFTs: Neurofibrillary tangles

OMA1: Overlapping activities with *m*-AAA protease

OPA1: Optic Atrophy 1

OMM: Outer mitochondrial membrane

pAcGFP: Photoactivable GFP

PARL: Presenilin-associated rhomboid-like protein

PBS: Phosphate buffer saline

PD: Parkinson's disease

PHFs: Paired helical Filaments

PINK1: PTEN Induced Putative Kinase 1

RGCs: Retinal Ganglion Cells

ROS: Reactive Oxygen Species

SCA 28: Spinocerebellar Ataxia type 28

Sec: Seconds

siRNA: Small interfering RNA

TCA: Trichloroacetic Acid

TMRM: Tetramethylrhodamine methyl ester perchlorate

WT: Wild type

Introduction

INTRODUCTION:

1.1) The *m*-AAA protease:

The *m*-AAA protease ('*m*' denotes 'matrix' and 'AAA' denotes 'ATPase associated with diverse cellular activities') located in the inner mitochondrial membrane has its catalytic subunits towards the mitochondrial matrix. The *m*-AAA protease is an important component of mitochondrial quality control mechanism as it degrades misfolded polypeptides (Pajic et al., 1994) and processes proteins important for mitochondrial ribosomal assembly (Nolden et al., 2005). In humans, *m*-AAA protease has two subunits namely AFG3L2 (ATPase family gene-3 like-2 or Afg3 like-2) and paraplegin. Heterozygous missense mutations in *AFG3L2* lead to Spinocerebellar Ataxia type 28 (SCA 28) (Di Bella et al., 2010) whereas mutations in *SPG7* encoding paraplegin leads to Hereditary Spastic Paraplegia (HSP) (Casari et al., 1998). Homozygous mutations in *AFG3L2* lead to an early onset Spastic Ataxia-Neuropathy syndrome (Pierson et al., 2011) Hence, deficiencies in *m*-AAA protease cause neurodegenerative diseases (Figure 1.1).

AFG3L2 and paraplegin are highly homologous to yeast Yta10 (Yta denotes Yeast Tat binding Analogs) and Yta12 respectively. The power of yeast genetics was used to establish the functions of *m*-AAA protease. In addition, in mammals, depletion of *m*-AAA protease causes mitochondrial fragmentation implicating an additional role in mitochondrial dynamics (Ehres et al., 2009). The functions of *m*-AAA protease are described in detail below:

1) Degradation of misfolded polypeptides: Yta10p was found to degrade the incompletely synthesized mitochondrial translation products, when

mitochondrial translation was carried out using ^{35}S -labelled methionine *in organello*, in the presence of limited concentrations of puromycin. The incompletely synthesized mitochondrial translation products did not assemble into functional active complexes, as assessed by the amount of radioactivity released into the TCA soluble supernatant fraction. The degradation was also dependent on the presence of divalent metal ions and ATP (Pajic et al., 1994).

2) Chaperone-like activity: *Δyta10* or *Δyta12* cells containing proteolytically inactive mutant forms, Yta10^{E559Q}p or Yta12^{E614Q}p (mutations in proteolytic domain in yeast), mediated the assembly of the F₀ ATPase subunit 9 into the ATP synthase complex deciphering an additional chaperone-like activity of the complex. The Yta10-12 complex also degraded the nonassembled ATPase 9 (Arlt et al., 1996).

3) Mitochondrial translation: Point mutations in the proteolytic centre of *m*-AAA protease subunits - Yta10^{E559Q} and Yta12^{E614Q} were used as a trap for finding out possible substrates (Nolden et al., 2005). The mutations did not affect the substrate binding capacity of *m*-AAA protease. Using affinity chromatography, *m*-AAA protease subunits used as trap were co-purified along with prohibitins. During these studies, MrpL32 (mitochondrial ribosomal protein of large subunit (39S)), a nuclear encoded protein of mitochondrial ribosomes, was found as a substrate of *m*-AAA protease. MrpL32 was processed from a precursor into a mature form and the first 71 N-terminal amino acid residues were essential for mitochondrial targeting. However, amino acid residues 72-77 were crucial in importing any protein attached with the presequence of MrpL32. It was demonstrated that MrpL32 processing was very important for conferring

respiratory competence to *m*-AAA protease deficient yeast cells. Analysis of ribosomal profiles by using a sucrose gradient showed no difference in the assembly of large ribosomal subunits (54S and 70S) and small ribosomal subunits (37 S) in wild type, *Δyta10*, *Δyta12* or *Δmrpl32* cells suggesting that the ribosome assembly occurs normally and is protected from proteolytic degradation (Nolden et al., 2005). How does the protease distinguish if it has to cleave a misfolded substrate or it has to process MrpL32 (the only known substrate till date)? The *m*-AAA protease cleaves MrpL32 from N-terminus until it reaches a conserved cysteine-rich domain resulting in the formation of a mature form from the precursor. Mutations in this domain destabilize the tightly folded domain resulting in the complete degradation of MrpL32 by the *m*-AAA protease (Bonn et al., 2011). Hence, *m*-AAA protease processes MrpL32 into mature forms. A direct link to neurodegeneration was obtained when impaired mitochondrial protein synthesis was observed *in organello* in murine brain tissues from the constitutive knock out of *Afg3l2* due to impaired mitochondrial ribosomal assembly (Almajan et al., 2012).

4) Mitochondrial dynamics: In MEFs knocked down for *Afg3l1* and *Afg3l2*, mitochondria are fragmented. Therefore, the mitochondrial dynamics are aberrant. This occurs due to accumulation of short OPA1 (Optic Atrophy 1) forms mediated by proteolytic cleavage by OMA1 (Overlapping activities with *m*-AAA protease) (Ehse et al., 2009; Head et al., 2009), a protease also present in the inner mitochondrial membrane. OMA1 was identified as a peptidase cleaving misfolded polypeptides when *m*-AAA protease was inactivated (Kaser et al., 2003). OPA1, a dynamin-related GTPase responsible for inner mitochondrial

membrane (IMM) fusion, has 8 splice variants (Delettre et al., 2001). Two isoforms 'a' and 'b' are abundant in MEFs corresponding to long forms of OPA1. Proteolytic processing at S1 and S2 sites by OMA1 and YME1L respectively yield a combination of short forms 'c', 'd' and 'e' (Song et al., 2007). Under steady state conditions, all forms from 'a-e' are observed. When AFG3L1 and AFG3L2 are depleted, the balance is shifted towards accumulation of short forms. The proteolytic site to cleave OPA1 is present in the intermembrane space. OMA1 enhances conversion to short forms 'c' and 'e' upon treatment by different stress conditions like antimycin, CCCP etc. and is also autocatalytically degraded (Baker et al., 2014). Consistently, downregulation of *Oma1* in *m*-AAA protease depleted MEFs rescues mitochondrial fragmentation.

Oma1^{-/-} mice developed normally and did not show any differences in survival rates when compared to littermates (Quiros et al., 2012). *Oma1*^{-/-} mice showed an increase in body weight compared to controls when kept on a high-fat diet due to adipocyte hypertrophy in white adipose tissue. Livers from *Oma1*^{-/-} mice have higher triglycerides showing steatosis. *Oma1*^{-/-} mice also showed a significant decrease in body temperature compared to controls upon exposure to cold stress (4°C) pointing to an impaired adaptive thermogenic response mediated by BAT (brown adipose tissue). Under these conditions, histological analysis showed reduced lipid droplets in control mice whereas *Oma*^{-/-} mice retained most of the lipid droplets. Quantitative PCR showed that *Oma1* deficiency reduces expression of nuclear genes encoding mitochondrial proteins and β -oxidation genes accompanied by increase in lipogenic genes and PGC1 α . Treatment of wild type (WT) cells with CCCP, oligomycin (ATP synthase

inhibitor) or staurosporine (apoptosis inducer) results in the formation of OPA1 short forms ('c' –'e'). Accordingly, mitochondria are resistant to fragmentation and less sensitive to apoptosis in *Oma*^{-/-} cells (Baker et al., 2014; Quiros et al., 2012). β -oxidation of fatty acids was impaired in liver and BAT in *Oma1*^{-/-} mice when fed on normal or high fat diet. The decreased palmitate oxidation rates in differentiated adipocytes obtained from *Oma1*^{-/-} mice was dependent on OPA1 levels (Quiros et al., 2012).

Conditional deletion of AFG3L2 in Purkinje cells results in mitochondrial fragmentation and altered distribution of mitochondria in the dendritic tree (Almajan et al., 2012). EM studies show mitochondria with abnormal cristae. Hence, the contribution of mitochondrial dynamics to disease progression upon depletion of AFG3L2 remains to be understood. In polarized neurons, the situation becomes even more complex as mitochondrial dynamics include efficient transport of mitochondria over long distances. This led to the formulation of my research project, which will be discussed later.

How do the different subunits of *m*-AAA protease interact to make up the whole complex?

Assembly of *m*-AAA protease subunits: In yeast, Yta10 and Yta12 form hetero-oligomers (instead of homo-oligomers) to form the functional *m*-AAA protease complex. What prompts the hetero-oligomerisation of this complex? $\Delta yta10$ $\Delta yta12$ yeast cells carrying Yta12 do not support growth. However, only 2 mutations in *yta12* are sufficient to rescue the growth defect, suggesting that these mutations allow homo-oligomerization. Hence, minor differences in the proteolytic domain are required to promote hetero-oligomerization of Yta12 and

Yta10 (Lee et al., 2011). As mentioned before, the murine *m*-AAA protease has three subunits namely AFG3L1, AFG3L2 and paraplegin with AFG3L1 being a pseudogene in humans (Kremmidiotis et al., 2001). AFG3L2 forms hetero-oligomers with paraplegin as shown by co-immunoprecipitation and gel filtration elution profiles (Atorino et al., 2003). Blue native PAGE of mitochondria solubilized with detergent in fibroblasts derived from patients suffering from HSP also showed a complex of 900 KDa similar to hetero-oligomeric complex of *m*-AAA protease. Hence, it can be concluded that AFG3L2 also forms homo-oligomers. Mitochondria isolated from murine liver and brain showed pulldown of AFG3L1, AFG3L2 and paraplegin with each other (Koppen et al., 2007). Interestingly, AFG3L1 and AFG3L2 also interact with each other forming hetero-oligomers in *Spg7*^{-/-} (paraplegin deficient) mice. Hence, different subunits of *m*-AAA protease interact in different combinations to form either homo-oligomers or hetero-oligomers (Koppen et al., 2007).

Domain structure of AFG3L2 and the *m*-AAA protease structure: Human AFG3L2 consists of 17 exons on chromosome 18p11.21 spanning 48 kilobases (Figure 1.2). Amino acids 1-65 encode a mitochondrial targeting sequence (MTS), whereas amino acids 146-163 and 252-271 encode two transmembrane domains to insert the protein into the mitochondrial inner membrane (Di Bella et al., 2010). The AAA domain spanning amino acid residues 343-534 has a highly conserved three-dimensional structure made of Walker A motif (residues 348-355) and Walker-B motif (residues 403-410). Walker A motifs help in the nucleotide binding whereas Walker-B motif aids to hydrolyze ATP (Hanson and Whiteheart, 2005). A third conserved region called second region of homology

(SRH, 453-470) helps in efficient ATPase activity (Karata et al., 1999). The proteolytic domain spans amino acids 541-744 (Di Bella et al., 2010). Cryo-Electron microscopic (EM) studies show that yeast *m*-AAA protease showed a bipartite structure with a height of 137 Å and width of 130 Å. The upper body sitting on the lower and larger main body consists of a central mass from which six smaller arms project out. The lower main body also has 6 approx. 25 Å wide holes through which cleaved peptides can exit the protease complex (Lee et al., 2011). Elegant experiments showed that ATP hydrolysis within the subunits of *m*-AAA protease is coordinated but not stochastic where ATP binding to a subunit prevents its hydrolysis by the neighboring subunit eg. Yta10 by Yta 12 or vice versa (Augustin et al., 2009).

Diseases	Hereditary spastic paraplegia	Spinocerebellar ataxia (SCA28)	Spastic ataxia neuropathy syndrome
Genes	Homozygous mutations in <i>SPG7</i>	Heterozygous mutations in <i>AFG3L2</i>	Homozygous mutations in <i>AFG3L2</i>



Fig 1.1: Diseases occurring due to deficiency in m-AAA protease
Source: (Rugarli and Langer, 2012)

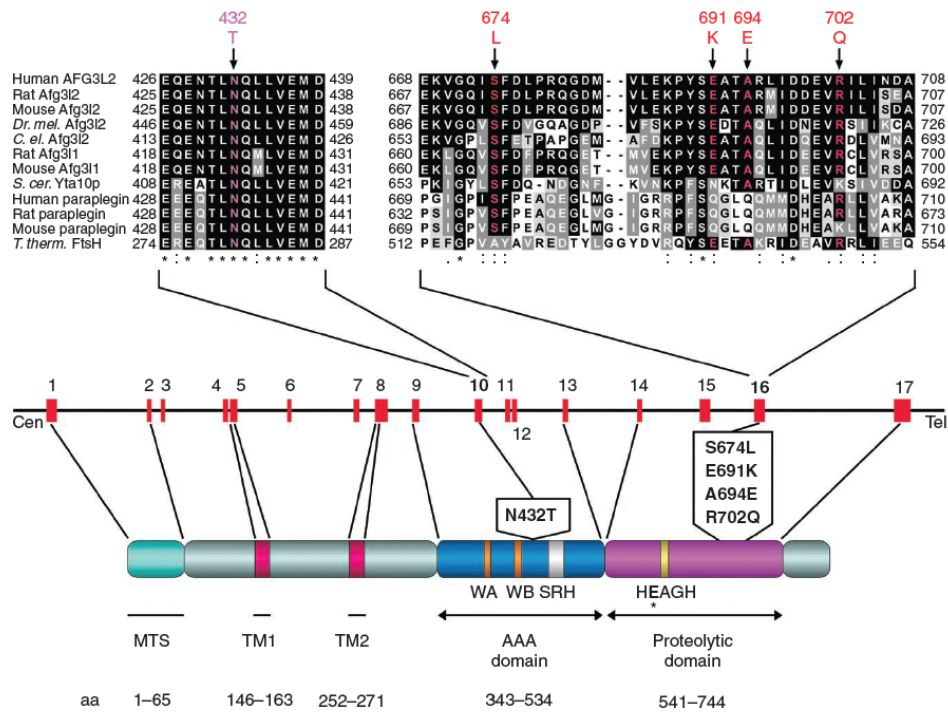


Figure 1.2: Domain Structure of Human AFG3L2 showing different domains and associated mutations. The mutation sites in patients are highly conserved across different species.
Source: (Di Bella et al., 2010)

1.2) Neurodegeneration associated with *m*-AAA protease:

Mutations in various subunits of *m*-AAA protease cause various neurodegenerative diseases in humans. As mentioned previously, heterozygous missense mutations in *AFG3L2* lead to Spinocerebellar Ataxia type 28 (SCA 28) (Di Bella et al., 2010) whereas mutations in *SPG7* encoding paraplegin lead to Hereditary Spastic paraplegia (HSP) (Casari et al., 1998). Homozygous mutations in *AFG3L2* lead to an early onset Spastic Ataxia-Neuropathy syndrome harboring combined symptoms of ataxia and paraplegia (Figure 1.1)(Pierson et al., 2011).

1) Spinocerebellar Ataxia type 28: Spinocerebellar ataxias are a class of neurodegenerative diseases characterized by imbalance, progressive gait, limb ataxia, dysarthria and ophthalmoparesis. Loss of AFG3L2 leads to Spinocerebellar Ataxia type 28. SCA 28 is an autosomally inherited trait, which may occasionally lead to complicated disease phenotype characterized by parkinsonism or spasticity in the limbs (Cagnoli et al., 2010). Owing to high amounts of AFG3L2 expression in Purkinje cells, the patients display degeneration of the cerebellum (Di Bella et al., 2010). The disease was first mapped in a four-generation Italian family on chromosome 18 at 18p11.22-q11.2 spanning a 7.9 Mb of genomic DNA (Cagnoli et al., 2006). Sequencing of candidate genes led to the identification of heterozygous point mutation in this region (Mariotti et al., 2008). The gene was later identified as *AFG3L2* where most of the missense mutations in the gene were present in the proteolytic domain of the protein (Di Bella et al., 2010).

Yeast cells expressing the targeted deletions of Yta10 and Yta12 (homologous to AFG3L2 and paraplegin respectively) show impaired respiratory growth on glycerol, a nonfermentable carbon source required for respiration (Di Bella et al.,

2010). This phenotype can be suppressed by the introduction of mammalian AFG3L2 indicating evolutionary conservation. However, variants of the human protein, harboring 4 different pathological mutations in proteolytic domain and one mutation in the ATPase domain, when expressed individually, could not rescue the growth phenotype. All the mutations could also not rescue the COX activity and the levels of different subunits of COX protein (Di Bella et al., 2010). It is noteworthy to observe that *Δyta10Δyta12* yeast cells expressing paraplegin and carrying the mutant AFG3L2^{S674L}, AFG3L2^{A694E} or AFG3L2^{R702Q} had normal respiration whereas the mutants AFG3L2^{E691K} or AFG3L2^{E575Q} failed to rescue the respiration. This would point that the first set of mutations namely: AFG3L2^{S674L}, AFG3L2^{A694E} and AFG3L2^{R702Q} gave rise to haploinsufficiency, whereas the mutations in AFG3L2^{E691K} and AFG3L2^{E575Q} acted as dominant negative mutations. Consequently, a higher number of patients were observed when they harbored dominant negative mutations. Thus, the heterozygous missense mutations exert differential effects. Screening of 366 Caucasian families having autosomal dominant cerebellar ataxias, excluded for those suffering from trinucleotide expansions (which cause most part of ADCA), concluded that an appreciable 1.5 % of Europeans suffer from SCA 28 (Cagnoli et al., 2010) pointing out the widespread nature of SCA 28. With time, more mutations are being identified in patients (Lobbe et al., 2014; Musova et al., 2013).

Two mouse models of *Afg3l2* were *described* where one of them was a homozygous spontaneous missense mutation denoted as *Afg3l2*^{par/par} and the other was denoted as *Afg3l2*^{Emv66/Emv66} (Maltecca et al., 2008). The first mutation namely *paralysée* was a spontaneous mutation, which occurred at the Pasteur

institute. The second mutation was a homozygous null mutant where an ecotropic murine leukemia virus integrated within intron 14 of the *Afg3l2* gene on chromosome 18 leading to the deletion of the last 210 amino acids in the 802 amino acid protein. Further 24 amino acids were added before prematurely terminating in a stop codon leading to no detection of the full-length or truncated protein on a western blot (Maltecca et al., 2008). Both the mouse models display significant paraparesis by the second week and do not survive beyond their third week. Mice have reduced thickness of the spinal cord, aberrant myelination and also display massive vacuolization in Purkinje cells and dorsal root ganglia. The sciatic nerve has reduced axonal diameter. At the cellular level, the brains of these mice synthesized lesser ATP due to aberrant complex I and III (Maltecca et al., 2008). It has been proposed that haploinsufficiency in *Afg3l2*^{Emv66/+} mice is sufficient to induce motor defects in mice and cause Purkinje cell death by dark degeneration. Increased mitochondrial ROS has also been proposed to play a role in the pathological advancement (Maltecca et al., 2009). Therefore, the mice models comprehensively show the mechanism of disease progression.

2) Hereditary Spastic Paraplegia: Depletion of paraplegin encoded by *SPG7* results in Hereditary Spastic Paraplegia (HSP) (Casari et al., 1998). HSPs are a diverse group of diseases characterized by spasticity in the lower limbs due to degeneration of long motor neuron axons in the corticospinal tracts. HSPs are categorized as pure when accompanied by lower limb spasticity and complicated if accompanied by other clinical symptoms such as dementia, ataxia and seizures. Unlike SCA 28, HSP caused by deficiency of *SPG7* is an autosomal recessive trait.

A study that examined 135 HSP patients found approximately 5 % of the patients (seven patients) harboured deficiencies in paraplegin confirming the magnitude of its pathological contribution (Arnoldi et al., 2008).

Spg7^{-/-} mice displayed motor defects at 4 months by a rotarod test (Ferreirinha et al., 2004). Spinal cords of these mice display swollen mitochondria characterized by degenerating fibers in the anterolateral funiculi at 15 months of age. In keeping with the late onset neurodegeneration, mitochondria isolated from spinal cord of *Spg7*^{-/-} mice at 23 months of age displayed reduced ability to synthesize ATP. An abnormal accumulation of neurofilaments was also observed in *Spg7*^{-/-} mice. When Cholera toxin subunit B (conjugated with a fluorescent dye) was injected into the gastrocnemius muscle of *Spg7*^{-/-} mice at 17 weeks, lesser motor neurons were labeled when compared to control. The reduction was limited to long motor neuron axons (Ferreirinha et al., 2004). Remarkably, adenoassociated virus-mediated intramuscular delivery of paraplegin rescued mitochondrial abnormalities and sciatic nerve abnormalities (Pirozzi et al., 2006). Indeed, *Spg7*^{-/-} mice paved the way for deciphering the disease progression occurring in HSP patients.

3) Spastic Ataxia-Neuropathy syndrome (SPAX5): Homozygous missense mutation in *AFG3L2* (*AFG3L2*^{Y616C}) lead to an early onset ataxia-neuropathy syndrome in two brothers born from a consanguineous marriage. The symptoms included cerebellar atrophy, lower limb spasticity, peripheral neuropathy, ptosis and epilepsy. The mutation was found in the exon 15 at the beginning of the proteolytic domain. *Δyta10Δyta12* yeast cells harboring human *AFG3L2* restored the growth and processing of MrpL32 whereas *Δyta10Δyta12* cells expressing

AFG3L2 having mutations in the Walker A motif of AAA domain (AFG3L2^{K354A}) or in its proteolytic centre (AFG3L2^{E575Q}) were unable to do so. However, AFG3L2^{Y616C} mutation found in the siblings was able to rescue the growth and MrpL32 processing phenotype suggesting that the mutation acted as a hypomorph. This could also explain the reason for the survival of brothers, at least to their teens. Blue native PAGE electrophoresis conducted on primary fibroblasts from a patient also demonstrated that AFG3L2 assembled less efficiently with itself, where the parents' samples showed more efficient assembly albeit less when compared to the control sample. The same was true for paraplegin assembly with AFG3L2 (Pierson et al., 2011).

Notably, *Spg7*^{-/-}*Afg3l2*^{Emv66/+} mice showed an acceleration of axonopathy and degeneration of the cerebellum demonstrating a genetic interaction between the subunits of *m*-AAA protease (Martinelli et al., 2009). *Spg7*^{-/-}*Afg3l2*^{Emv66/+} mice had a median survival time of 13 weeks with all the mice dying by the 20th week. They showed diminished motor abilities beginning at 7 weeks of age, which worsened very rapidly with time. Mice displayed uncoordinated gait, loss of balance suggesting ataxia and also developed a prominent kyphosis. Axonal swellings were observed in the spinal cord of *Spg7*^{-/-}*Afg3l2*^{Emv66/+} mice. A number of axons of the sciatic nerve show abnormal and enlarged mitochondria with disrupted cristae structure. Abnormal Purkinje cell ramification was observed along with abnormal vacuolization in the soma. Axonal loss in the granular layer of cerebellum was detected in these mice. The mice also showed loss of mitochondrial DNA content (Martinelli et al., 2009).

The *m*-AAA protease corroborates the relationship between mitochondrial dynamics, due to its connection with OPA1 and OMA1, and associated neurodegeneration with SCA28, HSP and spastic ataxia-neuropathy syndrome (SPAX5). What is the connection between mitochondrial dynamics and neurodegeneration?

1.3) Link between mitochondrial dynamics and neurodegeneration:

Mitochondria are highly dynamic organelles constantly undergoing fission and fusion at steady state (Bereiter-Hahn and Voth, 1994). They play key roles in ATP production, calcium buffering and apoptosis. During interphase, fission helps to remove dysfunctional mitochondria by mitophagy (Twig et al., 2008). During cell division, it helps to distribute mitochondria to daughter cells (Kashatus et al., 2011). Fusion helps in the intermixing of mitochondrial DNA and proteins and also to maintain mitochondrial DNA stability (Chen et al., 2010; Ono et al., 2001). OPA-1 is responsible for the inner mitochondrial membrane (IMM) fusion whereas Mitofusin-1 (Mfn1) and Mitofusin-2 (Mfn2) are responsible for outer mitochondrial membrane (OMM) fusion. All of them belong to dynamin family and typically contain a GTPase domain and a hydrophobic heptad repeat domain. The hydrophobic heptad repeat domains help to tether opposing mitochondria facilitating fusion (Chan, 2006). Mitochondrial fission machinery mainly includes DRP1, which has a GTPase domain, a central domain and a GTPase Effector domain (GED).

Molecules primarily responsible for mitochondrial fission and fusion are also associated with neurodegenerative diseases. Mutations in *MFN-2* cause Charcot-Marie-Tooth Type 2A (Zuchner et al., 2004). The gene was mapped to chromosome 1p36.2 where five different missense mutations were identified in the GTPase domain and one mutation was mapped to the mitofusin coiled-coil domain. Mice knocked out for *Mfn1* or *Mfn2* were embryonic lethal and died in midgestation (Chen et al., 2003). *Mfn2*^{-/-} mice embryos had a disrupted placental trophoblast giant cell layer. This layer is especially prone to high metabolic

demands of energy because of endoreplication. Depending on the tissue specificity, it was found that Mfn1 and Mfn2 form homo-oligomers and/or hetero-oligomers. Mfn2 did not form any hetero-oligomers with Mfn1 in the placental giant cells and thus could not compensate for the loss of mitofusin pool (Chen et al., 2003).

Conditional deletion of *Mfn2* using an EN1-Cre (actively expressed in the cerebellar primordia from midgestation) resulted in smaller animals unable to coordinate body movements which crawled on their abdomen and died by three weeks of age (Chen et al., 2007). Immunohistological analysis confirmed that area of the mutant cerebella decreased to about 60 % of WT by P7 and 25 % by P15-17 accompanied loss of Purkinje cells. By P10, there is an extensive loss of arborisation of the dendrites of Purkinje cells projecting into the molecular layer. At P6, an increased staining of Complex V is observed possibly to compensate for insufficient respiration. Primary cerebellar cultures depleted of Mfn2 using a lentivirus showed loss of dendritic branches and spines when the control had nicely developed them. Mitochondrial clustering in the soma of cerebellar neurons depleted of Mfn2 could be rescued by the introduction of Mfn1 pointing out that the overcoming abnormalities of mitochondrial fusion can rescue the phenotype. This process was found to be cell autonomous as L7-Cre solely expressed in the Purkinje cells also recapitulated the phenotype observed, albeit at a slower pace, where all the Purkinje cells were lost by 6 month of age. As the L7-cre is expressed from P7, it can also exclude any effects observed because of developmental abnormalities. Immunohistochemical sections also reveal

abnormal COX-SDH staining. Mitochondria also lacked mtDNA nucleoids (Chen et al., 2007).

Dominant Optic Atrophy (DOA) is a hereditary optic neuropathy characterized by progressive loss of vision resulting from atrophy of the optic nerve. Two back-to-back studies mapped the disease to aberrancies in the mitochondrial gene *OPA1* on the chromosome 3q28-q29 (Alexander et al., 2000b; Delettre et al., 2000). In one study, the mutations from 7 independent families included missense mutations and nonsense deletions and insertions while in the other study frameshift and missense mutations were found. Although ubiquitously expressed, the susceptibility of the patients is due to a high expression of *OPA1* in the retina. A mouse model of *OPA1* was obtained when a splice site mutation in *Opa1* led to the deletion of exon 10 encoding part of the GTPase domain (Alavi et al., 2007). Homozygous mutations in *Opa1* were embryonic lethal whereas heterozygous mutations were viable but display progressive loss of retinal ganglion cells (RGCs), reduction in the number of axons in optic nerves and axonal swelling. Mitochondria also had disorganized cristae in these axons (Alavi et al., 2007). Another mouse model also recapitulated the symptoms where *Opa1*^{-/-} animals were embryonic lethal at 13.5 and heterozygous animals displayed impaired vision around 6 months of age showing a slow onset of the disease (Davies et al., 2007).

Drp1 is responsible for mitochondrial fission (Smirnova et al., 2001). An isolated case of neonatal death was observed at 37 days where the infant developed microcephaly, optic atrophy and hypoplasia. The mutation A395D was found in the middle domain of DRP1 and was characterized as a *de novo* mutation as none

of the parents possessed it (Waterham et al., 2007). Defective mitochondrial and peroxisomal fission were observed in human skin fibroblasts. Because of the ability of the mutant DRP1 to induce mitochondrial and peroxisomal elongation in control cells, it was characterized as dominant negative. This mutation was shown to impair intermolecular interactions, as tested by yeast two-hybrid assays. The stimulation of DRP1 GTPase activity dependent on higher order assembly was also reduced (Chang et al., 2010). Knocking out *Drp1* in mice leads to embryonic lethality (Ishihara et al., 2009; Kageyama et al., 2012; Wakabayashi et al., 2009). In primary cultured neurons, there are decreased number of neurites and defective synapse formation.

The intricate relationship between mitochondrial dynamics and neurodegenerative diseases is further highlighted in Parkinson's disease (PD) as the parkinsonian mimetic, MPP⁺ specifically impairs mitochondrial transport in dopamine axons (Kim-Han et al., 2011). Further, mutations in *PINK1* (*PTEN-induced kinase 1*) and *parkin* cause familial form of PD in an autosomal recessive inheritance. PINK1 is a mitochondrially-targeted molecule, which is proteolytically degraded from a 63 KDa fragment into 52 KDa by the proteasome under physiological conditions in healthy cells (Beilina et al., 2005; Zhou et al., 2008). Presenilin-associated rhomboid-like protein (PARL) was found to proteolytically cleave PINK1 into a 52 KDa band after its import into the inner mitochondrial membrane (Jin et al., 2010), which is rapidly degraded by an unknown peptidase. Loss of mitochondrial membrane potential compromises the health of cells that stabilizes the PINK1 on the surface of mitochondria and recruits parkin (Narendra et al., 2010). Parkin is known to mediate the turnover

of damaged mitochondria by mitophagy (Narendra et al., 2008). Deletion of *Mfn2* in mouse cardiac myocytes abolished depolarization-induced Parkin recruitment on to the mitochondrial membrane suggesting that PINK1 phosphorylated Mfn2 acts as an anchor to recruit Parkin on to the surface of mitochondria (Chen and Dorn, 2013). However, it is also proposed that PINK1 phosphorylation of parkin promotes its mitochondrial translocation via a linker region (Kim et al., 2008). Mitochondria are distributed away from the axons in pyramidal neurons in Alzheimer's disease (AD) (Wang et al., 2008). Mice overexpressing human huntington (Htt) in hippocampal neurons also displayed mitochondrial anterograde transport defects (Shirendeb et al., 2012). Indeed, there is ample evidence indicating the importance of mitochondrial dynamics in neurodegeneration. As there is additional burden to transport mitochondria over long distances in neurons, mitochondrial transport is nevertheless linked to neurodegeneration. What are the mechanisms of mitochondrial transport in neurons?

1.4) Mitochondrial transport and neurodegeneration:

Neurons are highly polarized cells with three distinct compartments: a soma, dendritic compartment and an axon that can be as long as 1 m in a human adult. It is generally thought that most of the biosynthetic as well as degradative machineries like DNA replication, translation and autophagy occurs in the soma of neurons. Therefore, neurons have an additional level of complexity to transport all organelles including mitochondria over long distances from time to time. All the long-range transport of organelles occurs using microtubules as tracks whereas short-range transport uses actin. Short-range transport mediated by actin is active in the pre-synaptic, post-synaptic compartments and in the growth cones of neurons. Motors belonging to kinesin superfamily (KIFs) and cytoplasmic dynein are the main microtubule-based motor proteins. Myosin motors drive the actin-based transport. However, the directionality of motors is based on the polarity of the compartments. Axons have a defined polarity of microtubules whereas dendrites have a mixed polarity. In the axons, microtubules are uniformly arranged with the growing ends (+ ends of microtubules) towards the distal regions, whereas minus ends lie in proximal position near the soma (Duncan and Goldstein, 2006; Hirokawa et al., 2010; Sheng and Cai, 2012). In congruence, kinesins being plus-end driven motors transport cargoes like mitochondria and vesicles in an anterograde manner, whereas the minus-end driven dynein motors transport cargoes in a retrograde manner (Sheng and Cai, 2012). As dendrites exhibit mixed polarity, both kinesin and dynein motors can drive cargo like mitochondria in either retrograde or anterograde direction. Axonal transport is classified as slow or fast depending on

the kinetics of cargo transport. Cargo speeds of 0.5-10 $\mu\text{m}/\text{sec}$ occurring both anterogradely and retrogradely include membrane-bound organelles, neurotransmitters, endosomes etc. Slow axonal transport possesses cargo speeds of 0.01-0.001 $\mu\text{m}/\text{sec}$ where the cargo includes neurofilaments, tubulin, actin, clathrin, enzymes etc (Goldstein and Yang, 2000).

Kinesin proteins encoded by 45 genes are divided into 14 superfamilies based on phylogenetic classification in mammals (Hirokawa et al., 2010; Lawrence et al., 2004). Kinesin superfamily proteins are made up of a motor domain and a coiled-coil domain. Additionally, the tail region possesses a pleckstrin homology (PH) domain, CAP domain, PX domain and a region consisting of WD40 repeats. However, they are mainly classified based on the location of motor domain in the protein (present C-terminally, N-terminally or in the middle region). The motor domains hydrolyze ATP and move on the microtubules whereas the tail regions recognize different cargoes. Most of the KIFs have motor domain in the N-terminal region while only 3 proteins belong to groups where motor domain is present either in the middle region or C-terminally. There is a significant homology (30-60%) in the motor domain while other domains exhibit considerable variance (Hirokawa and Noda, 2008). Different kinesins carry different kind of cargo like mitochondria, vesicles, mRNA and plasma membrane precursors. What confers the selectivity of different cargoes to kinesins? The selectivity of different cargo is conferred at two levels: 1) Differential organization of different domains namely motor domain, coiled-coil and tail domain, based on which they are divided into different families; 2) Variable assembly pattern to form a functional unit of specificity. For example, a

functional kinesin motor eg. Kinesin 1 consists of two KIF5s and two KLCs (kinesin light chain). Members of the kinesin-1 superfamily including KIF5A, KIF5B and KIF5C are responsible for mitochondrial transport. While KIF5B is expressed in most cell types, KIF5A and KIF5C are found only in neurons. Mutations in kinesin motor (KIF5A) encoded by *SPG10* cause hereditary spastic paraplegia (HSP), a neurodegenerative disease accompanied by degeneration of long corticospinal axons leading to lower limb weakness (Reid et al., 2002). In mice, constitutive knockout of KIF5A was leading to lethality soon after birth. Conditional knockout of KIF5A in neurons resulted in 75% lethality accompanied by seizures along with accumulation of neurofilaments in the dorsal root ganglion (DRG) sensory axons. The transport profiles of other cargoes such as Amyloid Precursor protein (APP), Rab3 and synaptophysin were not altered. This indicates that KIF5A apart from carrying mitochondria also transports slow cargoes like neurofilaments eliciting an additional role of KIF5A in pathological advancement of the disease (Xia et al., 2003). *KIF5B*^{-/-} mice were embryonic lethal (Tanaka et al., 1998). There are various other pathological symptoms associated with deletion of kinesin super family (KIFs) proteins (Hirokawa et al., 2010).

Dyneins are a smaller family of motor proteins (compared to kinesins) that comprise two dynein heavy chain motor subunits and few light chain subunits. Even so, what confers the selectivity of different cargoes to dyneins? Since, isoforms of each component of different subunit chains can recognize different cargoes, one cytoplasmic dynein can transport many types of cargoes (Hirokawa et al., 2010). Murine embryonic knockouts of dynein heavy chain were

embryonic lethal. When the blastocysts were cultured *in vitro*, they showed fragmented Golgi spread throughout the cytoplasm accompanied by abnormal endosomal and lysosomal distribution (Harada et al., 1998). Dyneins are linked to cargo by means of an adaptor called dynactin. Dynactin is made up of subunits namely, dynamitin and p150^{Glued} (Karki and Holzbaur, 1999). Single base-pair substitution in a conserved motif of the p150^{Glued}, responsible for binding to the microtubules, resulted in human lower motor neuron disease (Puls et al., 2003). In addition, disruption of murine dynactin, by overexpressing dynamitin, led to a motor neuron degeneration characterized by hind limb weakness, abnormal gait and decreased forelimb strength (LaMonte et al., 2002). Fluoro-gold neurotracer was injected into the muscles and its accumulation was traced in the motor neuron pools that innervate the injected muscle. Transgenic mice only displayed few neurons with accumulation of the dye at a time point when all the control neurons had the dye suggesting delayed retrograde transport. Degeneration of motor neurons was observed in the ventral horns of the transgenic mice around 17 weeks of age (LaMonte et al., 2002). Indeed, affecting the transport motors, kinesins or dynein, detrimentally influences widespread functions leading to lethality or pathological conditions.

Between the motors and cargoes, there are specific adaptors. Kinesins are connected to mitochondria by TRAK1 and TRAK2 in mammals. TRAK1 is localized mainly in the axons and is capable of binding to kinesin-1 and dynein/dynactin whereas TRAK2 capable of binding to dynein/dynactin is predominantly present in the dendrites aiding in dendritic development (van Spronsen et al., 2013). Knockdown of *TRAK1* by shRNA in rat hippocampal

neurons causes impaired mitochondrial transport (Brickley and Stephenson, 2011). A genetic screen to decipher mutants defective in photoreceptor function identified *milton* as a novel candidate in *Drosophila*. *Milton* mutant flies had impaired mitochondrial transport to the synapses resulting in defective synaptic transmission (Stowers et al., 2002). The adaptors (TRAKs in mammals and *Milton* in *Drosophila*) are connected to the mitochondria by a mitochondrially targeted protein namely Miro. In mammals, there are two GTPases, Miro 1 and Miro 2, the role of which has not been elucidated hitherto. Mitochondria enriched fractions from HEK293 cells expressing human PINK1 (FLAG tag) were immunoisolated and analyzed by mass spectrometry. Miro2 was found to be a strong candidate interacting with PINK1. PINK1 also interacted with Miro1 and *Milton* (Weihs et al., 2009). PINK1 is known to phosphorylate Miro and target its degradation via parkin, an ubiquitin ligase (Wang et al., 2011). So, dysfunction at all three levels – motors (kinesins and dynein), adaptors (TRAKs or *Milton* and dynactin) and Miro lead to pathological conditions conferring a high level of complexity and control for mitochondrial transport.

Microtubules serve as tracks to transport mitochondria. Therefore, it is absolutely essential that microtubules are in a perfect condition to transport mitochondria. Tau (a microtubule-associated protein (MAP)) is essential for microtubule assembly and stabilization (Morris et al., 2011). What does tau do and how is it involved in neurodegeneration?

1.5) The role of tau in neurodegeneration and development:

Tau was discovered around forty years ago when microtubules isolated from porcine brains had bound tau. It was found that tau was essential for microtubule assembly and the capacity of microtubule growth was restored by the addition of tau (Weingarten et al., 1975; Witman et al., 1976). Later, it was demonstrated that neurofibrillary tangles in Alzheimer's disease patients consisted of hyperphosphorylated, insoluble tau (Grundke-Iqbal et al., 1986; Kosik et al., 1986). Hence, neurodegenerative disorders consisting of tau inclusions are collectively called tauopathies. Some of the tauopathies include Frontotemporal dementia and parkinsonism linked to chromosome 17 (FTDP-17), Pick's disease, down's syndrome and corticobasal degeneration.

The domain structure of tau consists of a N-terminal projection domain, a proline-rich domain, a microtubule-binding domain and a C-terminal region. Alternative splicing at the N-terminal region and microtubule-binding domain generates different isoforms. The microtubule-binding domain consists of repeat domains (Morris et al., 2011). Human adult harbors 6 isoforms of tau, which form proteins of sizes ranging from 352-441 amino acids. Only three tau isoforms are present in adult rodents. The isoforms of tau change from shorter ones to longer ones from fetal through adult stages (Bullmann et al., 2009; Takuma et al., 2003). Number of N-terminal projection domains (which could be 0,1 or 2) and the presence of three or four repeat domains characterize different tau isoforms. Tau is modified by a variety of post-translational modifications like phosphorylation (Martin et al., 2013), acetylation (Min et al., 2010) and O-GlcNAcylation (Arnold et al., 1996). Pathologically, tau phosphorylation attains

the prominence as it is found in Alzheimer's patients. The positive charges of amino acids in the repeat domain of microtubule binding region help tau to bind to negatively charged residues on tubulin. Phosphorylation of tau affects the positive charges of repeat domain and interferes with binding to microtubules (Jho et al., 2010). This causes tau to dissociate from the microtubules leading to accumulation of phosphorylated tau in the form of neurofibrillary tangles (NFTs) and microtubule instability (Lee et al., 2001; Mandelkow et al., 1996).

Overexpression of *tau40* (longest isoform of tau) in Chinese hamster ovary (CHO) cells resulted in the accumulation of mitochondria near the microtubule organizing centre (MTOC) (Ebner et al., 1998). The specificity was confirmed by injecting a recombinant tau protein. Mitochondrial clustering near the MTOC was dependent on microtubules as destabilization of microtubules (by using nocodazole) inhibited the mitochondrial clustering. Tau overexpression also leads to lesser branching and shrinkage of endoplasmic reticulum. Inhibition of dynein (by overexpressing dynamitin), a '-' end driven motor, rescued the mitochondrial clustering near MTOC pointing out that kinesin was inhibited upon tau overexpression. Moreover, transport of mitochondria to the neurites of differentiated neuroblastoma N2 cells was impaired leading to shorter neurites (Ebner et al., 1998). Acute reduction of tau in the developing embryonic brains at E14.5 *in utero* resulted in slower migration of layer II/III pyramidal neurons to the superficial layers of the cortex. Organotypic slices from *tau* shRNA electroporated brain sections revealed that mitochondria were present to a lesser extent in the axons (Sapir et al., 2012). Thus, overexpression as well as depletion of tau is not healthy for neurons. A study also proposes that tau can

act as cargo and thus compete with other cargo like neurofilaments transported into axon. This would lead to retarded growth of the axons (Dubey et al., 2008).

Tau^{-/-} mice display normality in the brains upon histological examination. However, small calibre cerebellar parallel fibers show decreased microtubule stability and organization (Harada et al., 1994). Primary hippocampal neuronal culture from *tau*^{-/-} mice show delayed axogenesis rescued by introduction of tau. This study also reported that *tau*^{+/-} and *tau*^{-/-} mice were phenotypically indistinguishable from their littermates (Dawson et al., 2001). To eliminate a possible compensation of *tau* deletion by other possible MAPs, *tau*^{+/-}*map1b*^{+/-} mice were crossed to obtain double knockout of *tau* and *MAP1B*. *Tau*^{+/-}*map1b*^{-/-} mice displayed only a mild reduction in corpus callosum, forebrain commissural fiber bundles, anterior and hippocampal commissure. This condition was exacerbated severely in *tau*^{-/-}*map1b*^{-/-} mice. Defects were also observed in the pyramidal layer formation in the hippocampus accompanied by a marked reduction in the axonal area and microtubule number in the anterior commissure. Primary cultured hippocampal neurons depleted of tau and MAP1B exhibited growth defects (Takei et al., 2000).

Mice deficient for superoxide dismutase 2 (SOD2) die within first week of life by developing mitochondrial dysfunction and oxidative stress. Antioxidant treatment increases the lifespan of these mice to 3 months. Mitochondrial oxidative stress can also give rise to tau hyperphosphorylation (Melov et al., 2007; Melov et al., 2001). Deletion of kinesin light chain motor subunit, a component of kinesin-1 complex causes abnormal tau hyperphosphorylation mediated by JNK. Deletion of murine *KLC* (kinesin light chain) did not affect the

polarization of neurons nor mitochondrial transport. However, the anterograde movement of APP into axons was impaired accompanied by an increased retrograde APP transport. *KLC*^{-/-} mice were normal at young age but developed axonal pathologies like increased APP accumulation, phosphorylation of neurofilaments in hippocampus and spinal cord (Falzone et al., 2009). Thus, either oxidative stress or transport defects are also sufficient to cause tau hyperphosphorylation.

Transfection of tau in CHO cells disrupted the organization of microtubules, which normally emanate from MTOC. These cells display microtubule bundling forming a spiral around the cell circumference. Cells co-transfected with both tau and GSK3- β (Glycogen synthase kinase-3 β) showed normal microtubule morphology as untransfected cells suggesting that GSK3- β mediated phosphorylation of tau dissociated tau from the microtubules (Wagner et al., 1996). GSK3- β overexpression increases the number of anterogradely and retrogradely moving mitochondria while dominant negative version of GSK3- β decreased the number of motile mitochondria. GSK3- β mediated increase in the number of motile mitochondria was abolished in *tau*^{-/-} neurons saying that the phenomenon is dependent on tau. To add to this, GSK3- β also increased the formation of paired helical filaments (PHFs) reflecting hyperphosphorylation of tau in the axons of primary neurons (Llorens-Martin et al., 2011). Hence, transport defects can cause tau hyperphosphorylation and reduction of tau phosphorylation can increase mitochondrial motility. Indeed, a number of sites are phosphorylated by tau (Querfurth and LaFerla, 2010).

Overexpression of tau can also effect mitochondrial fission by preventing the localization of DRP1 onto the mitochondrial surface. Increasing mitochondrial fission by depleting Marf (*Drosophila* Mitofusin) or overexpressing DRP1 rescued the mitochondrial length, neurotoxicity (TUNEL staining) and also ROS levels in neurons of *Drosophila* (DuBoff et al., 2012). Prevention of tau mediated stabilization of actin by expressing an actin severing protein gelsolin (UAS transgene in *Drosophila*) rescued mitochondrial length, neurodegeneration and ROS levels associated with increased localization of DRP1 to mitochondria. Concurrently, actin stabilization in flies overexpressing WASP increased mitochondrial length by decreasing DRP1 recruitment in mitochondrial fractions as assessed by western blots. This study places tau action upstream of altered mitochondrial dynamics. Therefore, the mechanisms connecting tau, mitochondrial dynamics and neurodegeneration are rather interconnected.

Materials and Methods

METHODS:

2.1) Primary murine cortical neuronal culture and transfection

The E18.5 CD1 pregnant mouse was sacrificed according to standard animal procedures and the abdominal region was sterilized. The skin was cut to access the embryonic sac containing the embryos and the embryos were placed in fresh ice-cold sterile phosphate buffer saline (PBS). The embryos were decapitated and the heads were transferred to fresh ice-cold dissection medium (a solution made up of 30 ml EBSS (Earle's Balanced salt solution) (Gibco), 15 ml horse serum (Gibco), 6 ml glucose (30 %), 1.5 ml hepes Buffer (1 M, Gibco)) and the brains of the embryos were dissected out. A stereomicroscope was used to separate out the cerebellum and hippocampus. After removing the meninges, the cortices were collected and cut into smaller pieces. All further steps were performed under sterile conditions. Very gently, the small pieces of cortices were transferred to a falcon and washed twice with 5 ml of pre-warmed (37° C) EBSS. The supernatant was removed (leaving little EBSS so that the cells were not dry) and 1 ml of complete neuronal medium (a solution containing 500 ml neurobasal medium (Gibco), B-27 (10 ml solution, Gibco) and glutamine (0.5 mM, Gibco) was added. The cortices were gently dissociated with a glass Pasteur pipette (Volac) for 10-12 times (where the speed of dissociation is very critical). A small fire-polished Pasteur pipette having almost half the diameter of the original tip was obtained (by pulling the tip in the middle after heating with fire). With the modified Pasteur pipette, neurons were gently dissociated 6-8 times again. Later, the neurons were spun for 5 min at 100g and the supernatant was discarded. The pellet was resuspended in 3 ml of neuronal medium and the neurons were

filtered through a 100 μ M mesh to avoid clumps. After making 1 in 10 dilution, the viable cells were counted by using Trypan Blue (1:20 dilution of standard 0.4 % standard solution in PBS was used).

500 ng of mito-mCherry was used to transfect 125,000 neurons using a micro-electroporation system (Microporator MP-100 apparatus, Digital Bio). The mito-mCherry was co-transfected together with 100 nM of control or appropriate siRNA to downregulate the respective genes. The transfected neurons were gently mixed in an eppendorf and plated on microwell area of the dish (P35G-1.5-14-C, MatTek corporation), coated with poly-D-lysine hydrobromide (0.1 mg/ml, (Sigma)), in 300 μ l of complete neuronal medium, for at least 1 hour to allow efficient attachment to the dish, a process known as seeding. After an hour, the volume of the neuronal medium was made up to 2 ml and the neurons were grown for 72 hours in the incubator at 37° C and 5 % CO₂. For harvesting neurons for western blots, at least 250,000 neurons were plated in 35 mm wells.

2.2) Imaging and transfection of parkin-mCherry

200 ng of mito-GFP and 400 ng of parkin-mCherry were co-transfected with 100 nM of the respective siRNA in primary cortical neuronal cultures by electroporation as mentioned previously. As a positive control, neurons were treated with 100 μ M of antimycin A, a mitochondrial complex III inhibitor (Wang et al., 2011). Axons were imaged at excitation wavelength of 488 nm for mito-GFP and 561 nm for parkin-mCherry.

2.3) Live-cell imaging

After 72 hours of plating the neurons, mitochondria were imaged in the axons as they were identified morphologically as processes arising from the soma twice or thrice longer than other processes. Axons selected for analyses had a minimum length of 200 μm and were imaged at least 50 μm distal to the soma. Video recordings were acquired at 1000 X 1000 pixel resolution every 10 sec for a period of 10 min (61 image stacks/movie) using a Perkin-Elmer Ultra View spinning disc confocal microscope, equipped with a CCD camera (Hamamatsu, C9100-50), at 60X magnification (oil-immersion objective, N.A = 1.49, illumination wavelength = 561 nm). The stage enclosing the dishes was set to 37°C and 5 % CO₂ to imitate the viable conditions in an incubator.

2.4) Immunofluorescence analysis

Two-thirds of the complete medium covering the neurons was drained out using a Pasteur pipette. The neurons were fixed in 4 % PBS for 30 min, permeabilized using 0.2 % Triton-X 100 for 10 min and blocked in PBS having 10 % goat serum for a further 10 min. Appropriate dilution of primary antibody (1:1000 for MAP2) was used to incubate in PBS containing 1 % goat serum for 3 hours. The neurons were washed thrice for 5 min and incubated with appropriate secondary antibody conjugated with Alexa-fluor 488 for 1 hour and again washed thrice for 5 min.

2.5) TMRM staining and quantification of mitochondrial membrane potential

TMRM (Tetramethylrhodamine methyl ester perchlorate) (sigma), is a cell-permeable, cationic dye, which is taken up by the mitochondria depending on the membrane potential (Ehrenberg et al., 1988) and is extensively used in mitochondrial biology research. It is used to qualitatively compare the mitochondrial membrane potential. 10 nM TMRM was applied to primary murine cortical neuron cultures for 3 hours. The neurons were imaged in a time window of 30 min for each condition in the same medium. No washing step is necessary. Images were obtained at excitation wavelength of 561 nm and average pixel intensities of all optical planes were quantified in the soma of neurons by using Volocity 6.1 (Perkin-Elmer). 20 μ M CCCP (sigma) was added after one hour of adding TMRM to the primary neurons and was used as a control to avoid TMRM accumulation inside primary neurons.

2.6) Measurement of cellular ROS levels

Cellular ROS levels were measured qualitatively using CellRox green dye (life technologies), a cell-permeable probe which fluoresces brighter upon oxidation by ROS. Upon oxidation, the dye binds to DNA in mitochondrial nucleoids and nucleus. Primary cortical neurons were stained with 2.5 μ M CellROX green for 30 min. The neurons were washed twice with pre-conditioned medium and imaged in the pre-conditioned medium after 15 min to allow some time to stabilize. Images of the soma were obtained at excitation wavelength of 488 nm and average pixel intensities of all the optical planes were quantified using Volocity 6.1 (Perkin-Elmer). For the menadione experiment, average intensity of the

nuclear staining of CellRox green was quantified. To compare ROS levels upon AFG3L2 depletion with the mock, average soma intensity was quantified.

2.7) Assessment of mitochondrial length, occupancy and transport

Mitochondrial length was quantified from the first image of the video recordings, by drawing a line along the major axis or along the diameter of circular mitochondria. The analysis was performed in Volocity 6.1 (Perkin-Elmer). All the mitochondrial lengths from different axons in an experiment were pooled into uniform length bins of 0.5 μm till 2.5 μm . All the mitochondria having a size greater than 2.5 μm were pooled into a single bin. The percentage of mitochondria belonging to a given mitochondrial length bin was then averaged from different experiments.

Mitochondrial occupancy was calculated as the total length of all mitochondria in an axon divided by total axonal length. For each axon, a value of mitochondrial occupancy was calculated and then averaged for the experiment. Average of averages from different experiments was then plotted.

Over a timespan of 10 min, mitochondrial transport was quantified into anterograde, retrograde and oscillatory modes of transport. Mitochondria were defined as oscillatory if they changed direction to move a distance greater than 5 μm , while they were considered stationary if they moved less than 5 μm during the video recordings. The number of stationary mitochondria was deduced as the number of motile mitochondria subtracted from the total number of mitochondria. Calculation of mitochondrial transport is complicated when mitochondria undergo fission and fusion. When mitochondria undergo a fission

event, the resulting daughter mitochondria were considered as separate from the parent mitochondrion. When two mitochondria undergo a fusion event, daughter mitochondrion after fusion was considered as separate from the parent mitochondria. Classification of mitochondrial movements was manually performed from the video recordings obtained in Volocity 6.1 (Perkin-Elmer) as the position of soma was noted while image acquisition.

2.8) Calculation of mitochondrial velocities

Mitochondrial velocity was calculated between two frames (10 sec timespan) in all the timeframes where a mitochondrion was moving. After putting all the split velocities of a particular mitochondrion together, a velocity cutoff of 0.1 μ /sec was used and velocity averaged. Each mitochondrion was represented by an averaged velocity value. All the velocities of mitochondria were averaged for a particular experiment and the average mitochondrial velocity calculated from the respective number of experiments.

2.9) Statistical analysis

Mitochondrial length was obtained from at least 3 independent experiments where each experiment had 8-10 axons. Data were classified into different bins after calculating the average across all the experiments and were represented as mean \pm standard error (SEM). The *p*-values were calculated using Graphpad Prism software (Version 6.02), and are indicated when lower than 0.05.

Mitochondrial length: Statistical evaluation of the difference of frequency distribution of different mitochondrial length bins was performed using the χ^2 test.

Mitochondrial occupancy, transport and velocity: Unpaired two-tailed Student's *t* test was used for statistical comparison of mitochondrial occupancy, transport and average velocity.

2.10) Quantification of proteins, SDS PAGE and Western blot analysis

The protein amounts were measured using the classical and widely established Bradford's method. Whole cell lysates containing the cellular proteins were mixed with Bradford's reagent and the absorbance was measured by using a spectrophotometer at 595 nm (Bradford, 1976). Using known concentrations of Bovine Serum Albumin (BSA), a standard curve was plotted. The standard curve was used to infer the amount of proteins from the absorbance obtained for different samples.

Proteins were suspended in SDS sample buffer containing 20 mM Tris-HCl (pH 6.8), 2 % SDS, 5 % mercaptoethanol, 2.5 % glycerol and 2.5 % bromophenol blue. The solution was denatured for 3 min at 100°C. 30 µg of proteins were loaded in all cases. The gels were run at 30 mA, using SDS PAGE running buffer having 25 mM Tris, 192 mM glycine and 0.1% SDS. Commercially available protein weight markers (Thermo Scientific PAGE ruler plus prestained protein ladder) were used to identify the size of proteins. Biorad gel apparatus were used to run the SDS PAGE.

The proteins resolved on a SDS PAGE were transferred onto a polyvinylidene fluoride (PVDF) membrane (Amersham) using a wet blotter (biorad) at 300 mA for 90 min in a blotting buffer comprising of 25 mM Tris, 192 mM glycine and 20% Methanol. To prevent non-specific binding of antibodies to the membrane,

they were blocked in Tris-buffered saline (TBS) solution (20 mM tris, 150 mM NaCl, pH 7.4) containing 5 % milk powder and 0.1 % tween-20 for 30 min. The membrane was then incubated with primary antibodies overnight at 4°C. Later, the membrane was washed 3 times, for a duration of 10 min each, with TBST (TBS solution with 0.1 % tween-20). The membranes (containing the bound primary antibodies) were then incubated for 1 hour with respective Horse-radish peroxidase conjugated secondary antibodies depending on the host species in which the primary antibody was raised. Again, the membrane was washed 3 times, for a duration of 10 min each, with TBST. The membrane was then exposed to ECL reagents (Amersham) according to the manufacturer's protocols and developed after optimum exposure time on X-ray film.

2.11) Cell treatments

NAC treatment: 1mM of NAC (Sigma-Aldrich) was used to supplement the complete neuronal medium for growing primary neurons.

Vitamin E treatment: 200 µM of vitamin E (Sigma-Aldrich) was used to supplement the complete neuronal medium for growing primary neurons. Vitamin E was replenished every 24 hours.

MATERIALS:

2.12) siRNA oligonucleotides used in the study

Stealth small interfering RNAs (siRNAs) were synthesized by Invitrogen, with the following sequences to knockdown *Afg3l2*:

siRNA A (used in most of the study):

5'-CCUGCCUCCGUACGCUCUAUCAAUA-3'

siRNA B: 5'-GCGUUCUCUGCUGAGGGAUGUAAUU-3'

siRNA C: 5'-GGUUGAUGGGCAAUACGUCUGGUUU-3'

To downregulate *Opa1*, we used Stealth siRNAs synthesized by Invitrogen with the following sequences:

siRNA A: 5'-CAAGAGCAGUGUGUUCACAACGAAA-3'

siRNA B: 5'-CAGUGUUCUGUAUUCAGGAACGCUU-3'

To downregulate *Mapt*, we used Stealth siRNAs synthesized by Invitrogen with the following sequence:

siRNA 36: 5'-CAGUCGAAGAUUGGCUCCUUGGAUA-3'

siRNA 37: 5'-CAGGAGGUGGCAAGGUGCAGAUAAU-3'

siRNA 38: 5'-CAGGAGGUGGCCAGGUGGAAGUAAA-3'

The medium GC stealth-negative control (Invitrogen) was used for all experiments.

2.13) Plasmids used in the study

1) Mito-GFP or Su9-GFP (Eura et al., 2003)

2) Mito-mCherry (The coding sequence of mitochondrial targeting sequence from Su9-GFP was amplified by PCR using the primers:

5'-CCGGAATTCATGGCCTCCACTCGTGTC-3'

5'-GCCGGATCCGGAAGAGTAGGCGCGC-3'). The PCR fragment was digested with *EcoRI* and *BamHI*, and inserted in-frame before the N3-mCherry. The construct was confirmed by sequencing.

3) Mito-pAcGFP (Zunino et al., 2007)

4) Murine parkin-mCherry (a kind gift of Prof. Nils-Göran Larsson)

5) Rat Tau Plasmid (A construct containing the full length sequence of rat *Mapt* cDNA (Accession No: BC126095) in the vector pExpress-1 (kind gift of Dr. Walter Becker).

2.14) Antibodies for Western blot analysis

S.No	Antibody name	Source	Dilution used
1	Anti-tau1	Mouse	1:1000
2	Anti-GAPDH	Mouse	1:2000

3	Anti-MAP2	Mouse	1:1000
4	Anti- β 3 tubulin	Mouse	1:2000
5	Anti-GFAP	Rabbit	1:2000

3.0) Formulation of the research project:

AFG3L2 depletion in Purkinje cells leads to mitochondrial fragmentation and altered distribution of mitochondria in the dendritic tree (Almajan et al., 2012) pointing out to aberrant mitochondrial dynamics. Given the general connection between mitochondrial dynamics and neurodegeneration and the specific connection between *m*-AAA protease and OPA1 and OMA1, it is interesting to study the role of mitochondrial dynamics and transport in the patients suffering from neurodegeneration of Spinocerebellar Ataxia type 28 (SCA28). Hence, our project aims to uncover the contribution of mitochondrial dynamics and transport in SCA28 disease by using murine primary cortical neurons as the model system.

Results

RESULTS:

3.1) Impaired mitochondrial fusion in *Afg3l2*^{Emv66/Emv66} MEFs

Mitochondria constantly undergo fusion and fission at steady state (Bereiter-Hahn and Voth, 1994). Mitochondrial fragmentation occurs in MEFs knocked down for *Afg3l1* and *Afg3l2* (Ehse et al., 2009). Mitochondria could be fragmented because of increase in fission or decrease in fusion. A decrease in mitochondrial fusion can be inferred by performing a mitochondrial photoactivation assay. In this method, a mitochondrial matrix-targeted photoactivable GFP when illuminated with a 405 nm laser fluoresces 100 times brighter. Therefore, when certain mitochondria in a cell are photoactivated, the GFP fluorescence would spread as non-photoactivated mitochondria would fuse with photoactivated mitochondria due to mixing of matrix contents. The extent of GFP spread between the mitochondria can be used as an index of mitochondrial fusion (Zunino et al., 2007). Photoactivation assay clearly indicated that *Afg3l2* knockout MEFs (*Afg3l2*^{Emv66/Emv66} MEFs) have defective mitochondrial fusion (Figure 3.1). Figure 3.1A shows an increased redistribution of mitochondrially targeted photoactivable GFP (pAcGFP) in wild type (WT) MEFs compared to the *Afg3l2*^{Emv66/Emv66} MEFs after 45 min. Consistently, the pseudocoloured images also show a greater decrease in high-intensity pixels in WT MEFs compared to *Afg3l2*^{Emv66/Emv66} MEFs confirming that *Afg3l2*^{Emv66/Emv66} MEFs have impaired fusion. After 45 min, the increase in number of mitochondrial pixels per cell having photoactivable GFP was quantified in all the optical planes, as shown in Figure 3.1B, where *Afg3l2*^{Emv66/Emv66} MEFs showed a

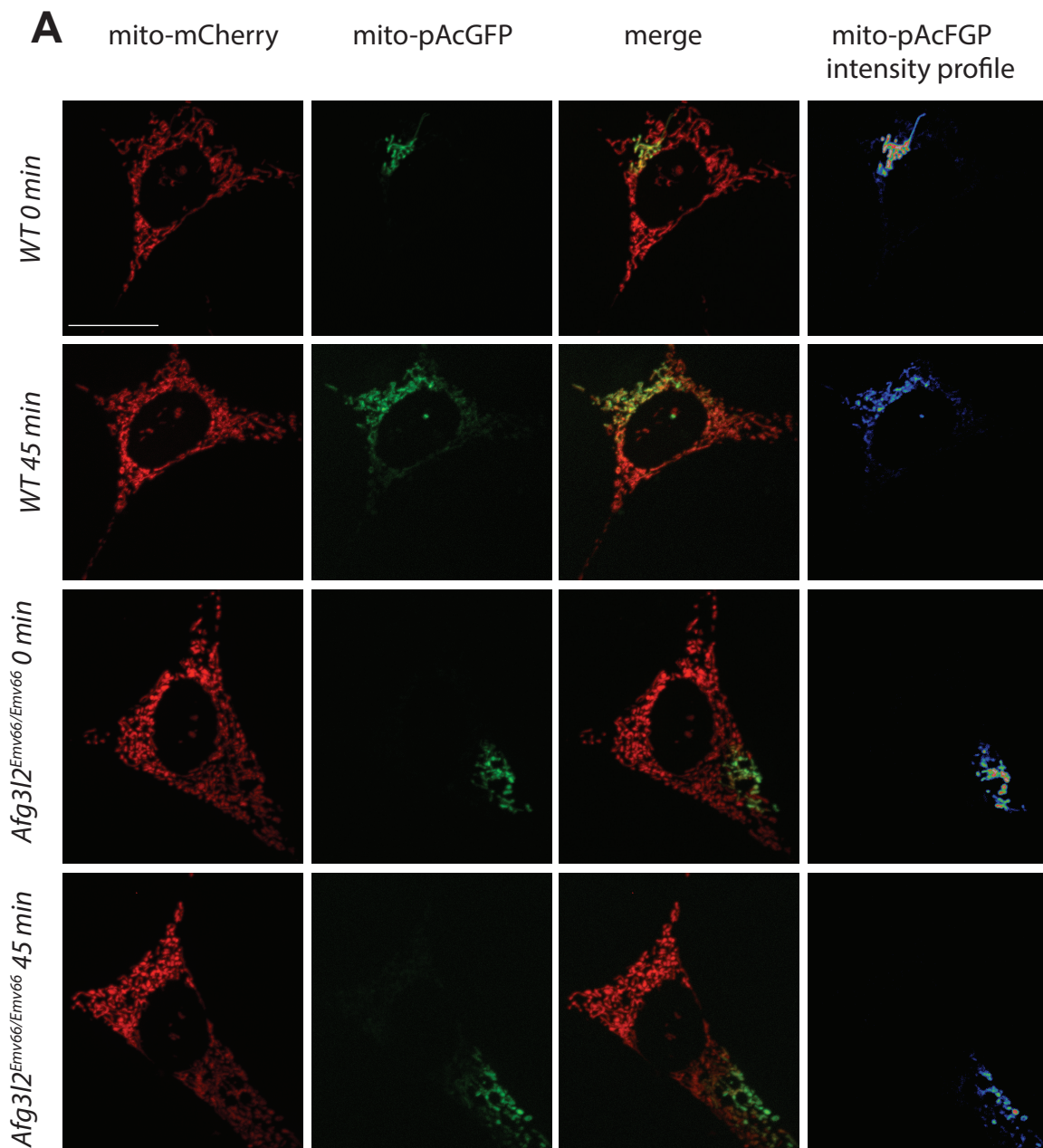
lesser spread of photoactivable GFP. We were interested in the mechanisms of neurodegeneration mediated by mitochondrial dynamics occurring in AFG3L2 deficient neurons. Due to strong connection between mitochondrial dynamics and neurodegeneration (as mentioned in the introduction), we investigate mitochondrial dynamics and transport in polarised cells like neurons upon AFG3L2 depletion. Therefore, we standardised the preparation of primary murine cortical neuronal culture.

FIGURE LEGENDS

Figure 3.1: *Afg3l2*^{Emv66/Emv66} MEFs display reduced mitochondrial fusion

A) After 45 min, WT MEFs show a greater spread of mito-pAcGFP compared to the *Afg3l2*^{Emv66/Emv66} MEFs. This is also inferred by a greater reduction in pseudo-colour pixel intensities. Scale bar: 10 μ m.

B) Quantification of pixel increase of mito-pAcGFP in WT MEFs (n = 8) and *Afg3l2*^{Emv66/Emv66} MEFs (n = 10) after 45 min as shown by a representative experiment.



B

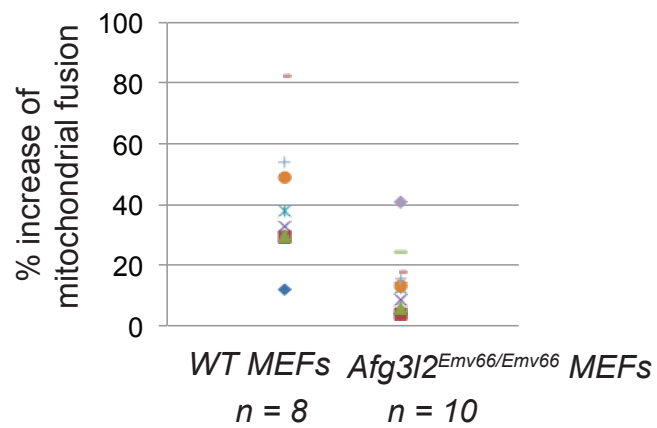


Figure 3.1

3.2) Characterization of primary murine cortical neuronal culture

To understand how mitochondrial dynamics contribute to neurodegeneration in patients suffering from spinocerebellar ataxia, we established primary murine cortical neuronal cultures from embryos at E18.5 stage (Figure 3.2A & B). In all the experimental conditions, the neurons were cultured for 3 days *in vitro* (DIV). The neurons were characterized by checking different markers on 2-week-old cultures. MAP2 antibody labeling dendrites was shown to stain the neuronal culture by immunofluorescence (Figure 3.2C). Western blots showed the neuronal lysate stained for antibodies against β -3 tubulin (marking whole neurons) and tau (present in axons) (Figure 3.2D). We also detected the presence of astrocytes by checking with antibody against GFAP, which confirmed the mixed nature of neuronal culture. However, when examined morphologically, they were present to a much lesser extent than the neurons.

FIGURE LEGENDS

Figure 3.2: Characterization of primary murine cortical neuronal culture

A) E18.5 embryos from wild type CD1 dam.

B) Dissected mice brains from the embryos used for collecting the primary cortical neurons.

C) Immunofluorescent image of MAP2 showing the dendrite of a neuron from two-week old cortical neuronal culture.

D) Western blots of two-week old primary neuronal cortical culture showing different neuronal markers: β -3 tubulin (whole neurons) and tau (axons). Presence of glia shown by Glial fibrillary acidic protein (GFAP) staining indicates mixed nature of culture.

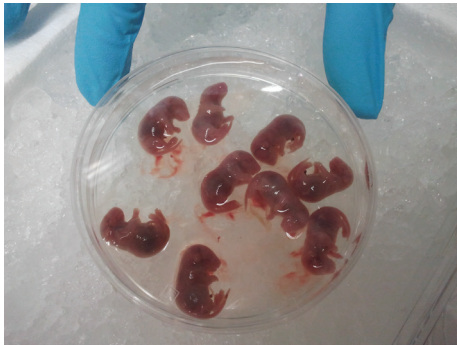
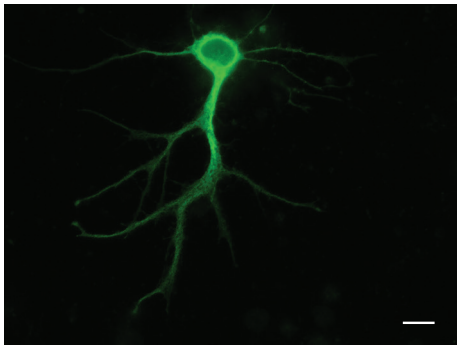
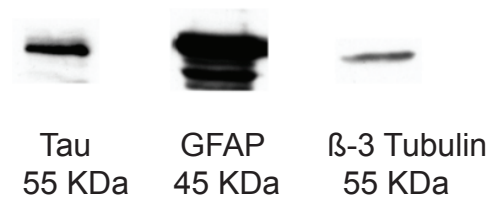
A**B****C****D**

Figure 3.2

3.3) Aberrant mitochondrial dynamics in neurons downregulated for *Afg3l2*

We co-transfected 100 nM of control siRNA oligonucleotides or three different siRNA oligonucleotides against *Afg3l2* together with 500 ng of mitochondrial targeted Cherry (called as mito-mCherry from now onwards) to study mitochondrial morphology, occupancy, transport and velocities in the axons. Axons were distinguished morphologically and always imaged at least 50 μm distal to the soma of the neurons where the axons had a minimum length of 200 μm .

3.3.1) Neurons depleted for AFG3L2 have fragmented mitochondrial morphology

While the mitochondrial morphology in the axons of control neurons was composed of long and short tubules, neurons downregulated for *Afg3l2* predominantly had only short tubules or spheres (Figure 3.3A). A detailed quantification of mitochondrial length was done. Mitochondria were classified into bins of different lengths from each individual experiment and data were averaged from different experiments. Figures 3.3B and 3.3C show a higher percentage of mitochondria belonging to shorter length bins and lesser percentage of mitochondria belonging to longer length bins in neurons downregulated for *Afg3l2* when compared to control neurons. Moreover, comparison of the frequency distribution of bins of mitochondrial length in control neurons and neurons downregulated for *Afg3l2* show a statistical difference by chi-square test.

3.3.2) Neurons depleted for AFG3L2 have reduced mitochondrial occupancy

Mitochondrial occupancy is described as the sum length of all mitochondria put together in an axon per unit length of axon. For instance, a mitochondrial occupancy of 20 % would mean that one-fifth of the axonal length is occupied by the mitochondria. Neurons depleted for AFG3L2 have lesser mitochondrial occupancy than control neurons. Quantification of average mitochondrial occupancy from 3 different experiments clearly show a reduction in AFG3L2 depleted neurons (Figure 3.4A) with statistical significance attained in most cases (Figure 3.4B).

3.3.3) The reduced mitochondrial occupancy in Afg3l2 downregulated neurons is independent of parkin-mediated mitophagic clearance

One of the plausible hypothesis for reduced mitochondrial occupancy in neurons downregulated for *Afg3l2* could be parkin-mediated mitophagy (Narendra et al., 2008). Therefore, we checked if parkin-mCherry was targeted to mitochondria in AFG3L2 depleted neurons. However, we could not find any recruitment of parkin onto the mitochondria in such conditions (Figure 3.5). In order to validate the assay, a positive control was used where control neurons were treated with antimycin, a complex III inhibitor of electron transport chain (ETC). Treatment of neurons with antimycin resulted in a shift of parkin-mCherry from cytosolic to punctate distribution colocalising with mitochondria as shown by arrows (Figure 3.5). Antimycin was previously shown to recruit parkin on the surface of mitochondria and mediate mitophagy (Wang et al., 2011). Hence, we conclude that the reduced mitochondrial occupancy in AFG3L2 depleted neurons is independent of parkin-mediated mitophagy.

3.3.4) Kymographic analysis of neurons downregulated for *Afg3l2*

Control neurons and neurons deficient for AFG3L2 were extensively analyzed by classifying different kinds of mitochondrial transport. Movies of mitochondrial transport were acquired for 10 min with a frame rate of 10 Sec per frame where the mitochondria were moving anterogradely or retrogradely. If a mitochondria moving in anterograde direction changed course and moved retrogradely or vice-versa, it was classified as oscillatory. The percentage of motile mitochondria was in accordance with previous literature (Brickley and Stephenson, 2011) where one-third of the mitochondria are motile.

A representative kymograph of control neurons and neurons downregulated for *Afg3l2* is shown (Figure 3.6). Here, the soma can be extrapolated to be present on the left side of the respective kymographs. If the kymograph is represented as a graph, the X-axis represents the distance in the axons whereas the Y-axis represents the time period of acquiring the movie (tracing the mitochondrial motility). Consequentially, the negative slope represents anterograde transport whereas positive slope represents retrograde transport. The perpendicular lines represent immotile mitochondria. Hence, the kymographs have been used as a two-dimensional pictorial depiction of objects moving through space and time. The kymographs of control neurons show a healthy mix of anterograde and retrograde transport whereas axons of neurons depleted for AFG3L2 show impaired anterograde transport and normal retrograde transport.

3.3.5) AFG3L2 depleted neurons have impaired anterograde transport of mitochondria but unchanged mitochondrial velocities

The percentage of mitochondria moving in different directions was extensively quantified. It was very interesting to observe that neurons downregulated for *Afg3l2* had impaired anterograde mitochondrial transport (Figure 3.7A & B). Approximately 10% of mitochondria moved anterogradely in AFG3L2 depleted neurons (using 3 different siRNA oligonucleotides) compared to around 20% in control neurons (Figure 3.7A & B). Owing to similar observation of mitochondrial anterograde transport defects with 3 different siRNA oligonucleotides for depleting AFG3L2, it can be concluded that observed transport defects are not a result of off-target effects of the siRNA oligonucleotides. The percentage of mitochondria moving in the retrograde or oscillatory direction did not show a statistical difference. However, it was noteworthy that in some cases where *Afg3l2* was downregulated, we found a statistical increase in the number of stationary mitochondria (table 1, p.105).

We also checked if the mitochondrial velocities changed upon *Afg3l2* downregulation. The average velocities of mitochondria moving in the retrograde or anterograde direction were calculated. Quantification of average mitochondrial velocities revealed no differences in either anterogradely or retrogradely moving mitochondria in AFG3L2 depleted neurons (Figure 3.7C).

3.3.6) The mitochondrial membrane potential in Afg3l2 downregulated neurons is unchanged

It was previously suggested that mitochondrial membrane potential and axonal transport are correlated (Miller and Sheetz, 2004). Mitochondria having higher membrane potential were preferentially transported anterogradely whereas those having lower membrane potential were transported retrogradely. As a corollary, it is possible that the impaired anterograde transport observed in AFG3L2 depleted neurons is due to reduced membrane potential. In other words, mitochondrial membrane potential might act as a sensor for regulating the anterograde transport of mitochondria. Therefore, we qualitatively measured the mitochondrial membrane potential by using TMRM. Pseudo-colour images of TMRM intensities do not show any appreciable difference between control neurons and AFG3L2 depleted neurons (Figure 3.8A). Negligible TMRM staining was observed by the addition of CCCP (used to abolish mitochondrial membrane potential) in control neurons validating the TMRM assay. Descriptive analysis by means of a boxplot clearly indicated that only few neurons had very low membrane potential in AFG3L2 depleted neurons while such neurons were not observed in the control neurons (Figure 3.8B). This would argue against the mechanism of coordinated control of mitochondrial membrane potential and transport. However, few neurons having very less mitochondrial membrane potential in AFG3L2 depleted neurons also suggests that all is not well with the mitochondrial membrane potential in all the neurons depleted for AFG3L2.

FIGURE LEGENDS

Figure 3.3: **Neurons depleted for AFG3L2 have fragmented mitochondrial morphology**

A) Mitochondrial morphology shown in axons of control neurons and neurons downregulated for *Afg3l2* with three different siRNA oligonucleotides (A, B and C).

B) Quantification of mitochondrial length, comparing siRNA oligonucleotides against control and *Afg3l2* (oligo A), shown as the percentage of mitochondria belonging to a given length bin, averaged from 3 independent experiments (120-150 mitochondria were measured in each experiment). Bars represent SEM. Chi-square test: $p = 0.002$.

C) Quantification of mitochondrial length, comparing siRNA oligonucleotides against control and *Afg3l2* (oligo B and oligo C), shown as the percentage of mitochondria belonging to a given length bin, averaged from 3 independent experiments (124-167 mitochondria were measured in each experiment). Bars represent SEM. p values were calculated with the Chi-square test. Control vs. *Afg3l2* (oligo B): $p = 0.008$; Control vs. *Afg3l2* (oligo C): $p = 0.009$.

Figure 3.4: **Neurons depleted for AFG3L2 have reduced mitochondrial occupancy**

A) Histogram showing quantification of mitochondrial occupancy of axons of control neurons and neurons downregulated for *Afg3l2* (Oligo A), ($n = 3$ experiments; 7-8 axons per experiment).

B) Histogram showing quantification of mitochondrial occupancy of axons of control neurons and neurons downregulated for *Afg3l2* (Oligo B & C), (n = 3 experiments; at least 8 axons per experiment). *p* values were determined with Student's *t*-test.

Figure 3.5: Reduced mitochondrial occupancy in AFG3L2 depleted neurons is independent of parkin-mediated mitophagic clearance

Cytosolic staining of parkin-mCherry observed in control and AFG3L2 depleted neurons (top two panels), whereas control neurons treated with antimycin A show punctate parkin-mCherry staining colocalising with mitochondria (arrows).

Figure 3.6: Kymographic analysis of neurons downregulated for *Afg3l2*

Axons showing representative kymographs from neurons co-transfected with mito-mCherry and control or *Afg3l2* siRNAs. Schematic of different color-coded transport types is shown below. Scale bars: 10 μ m.

Figure 3.7: Neurons depleted for AFG3L2 have impaired anterograde transport of mitochondria but unchanged mitochondrial velocities

(A) Quantification of mitochondrial transport types in the axon (Control siRNA Vs siRNA oligonucleotide A against *Afg3l2*). Data represent mean \pm SEM of 3 independent experiments. 7-8 axons from each experiment were analyzed.

(B) Quantification of mitochondrial transport types in the axon (Control siRNA Vs siRNA oligonucleotides B & C against *Afg3l2*). Data represent mean \pm SEM of 3 independent experiments. At least 8 axons from each experiment were analyzed.

(C) Average mitochondrial velocity (from at least 5 axons per experiment) in the anterograde and retrograde direction. Data represent mean \pm SEM of 3 independent experiments. *p* values in A, B and C were determined with Student's *t*-test.

Figure 3.8: The mitochondrial membrane potential in *Afg3l2* downregulated neurons is unchanged

(A) Representative TMRM images as shown by pseudo-colour coded intensities along with mitochondrial staining by mito-GFP.

(B) Quantification of TMRM staining from two different experiments.

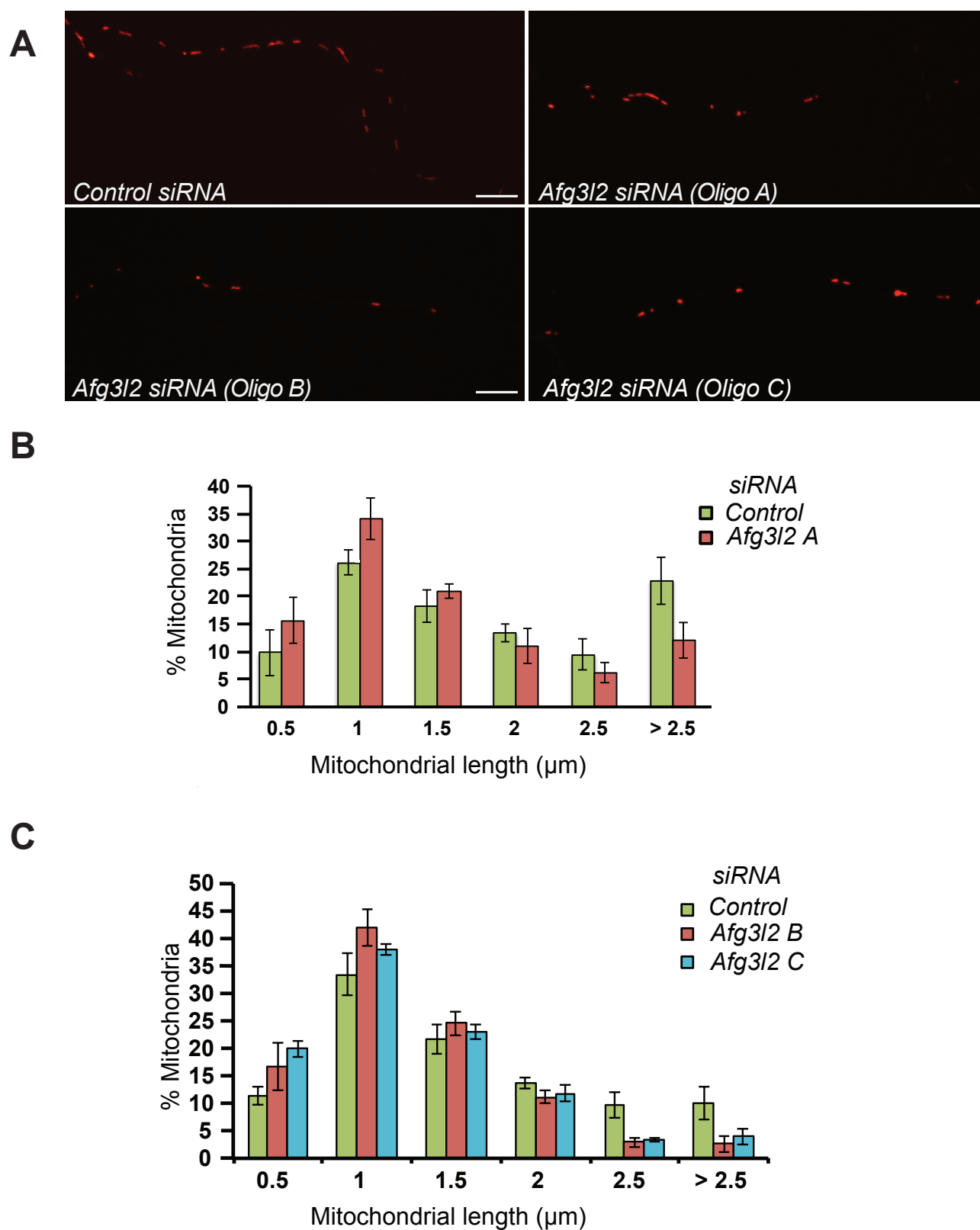


Figure 3.3

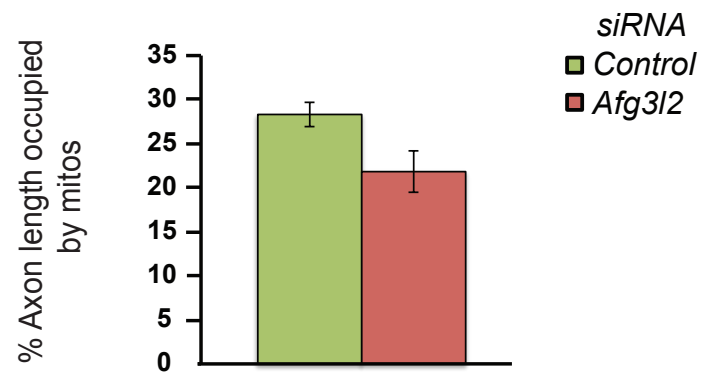
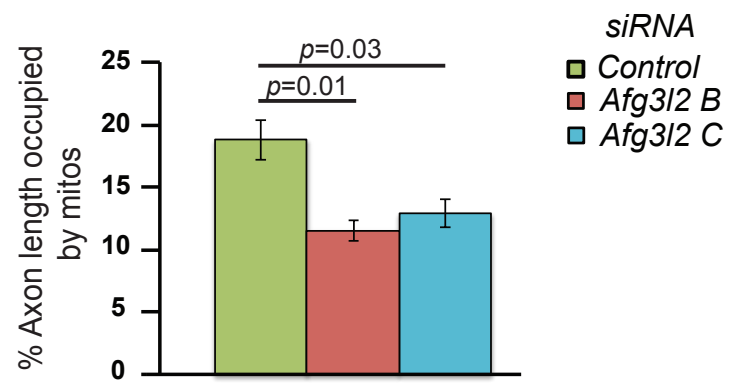
A**B**

Figure 3.4

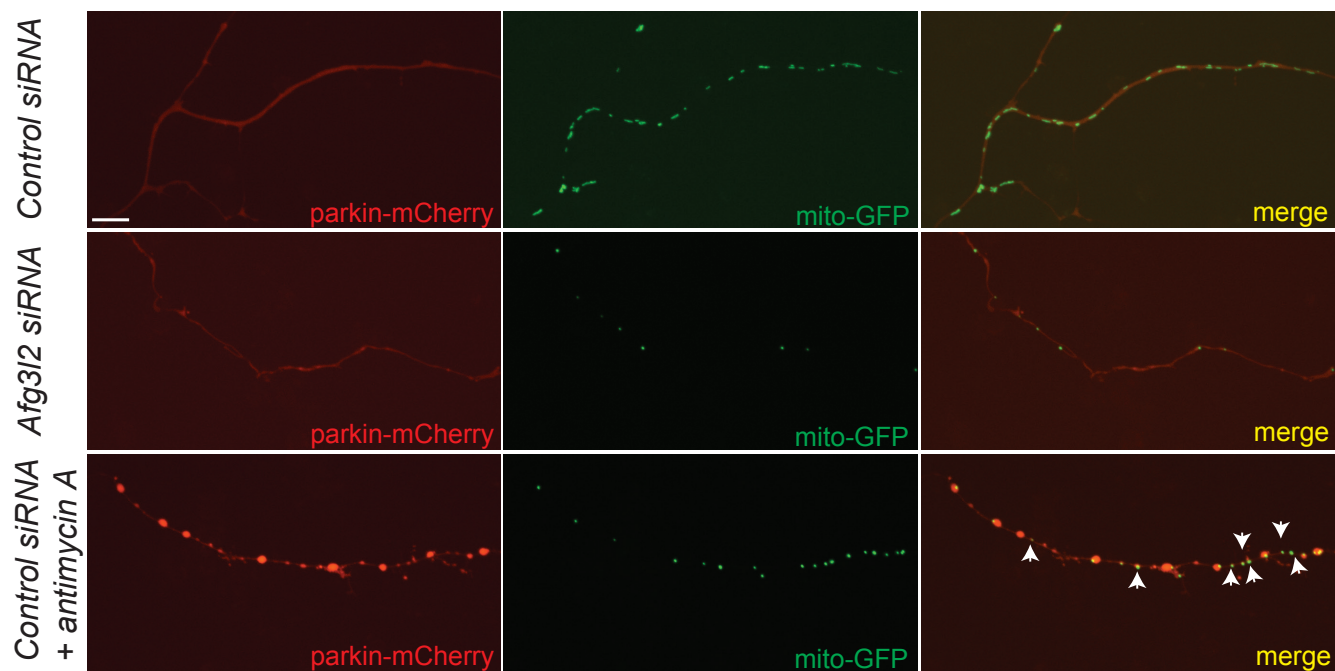


Figure 3.5

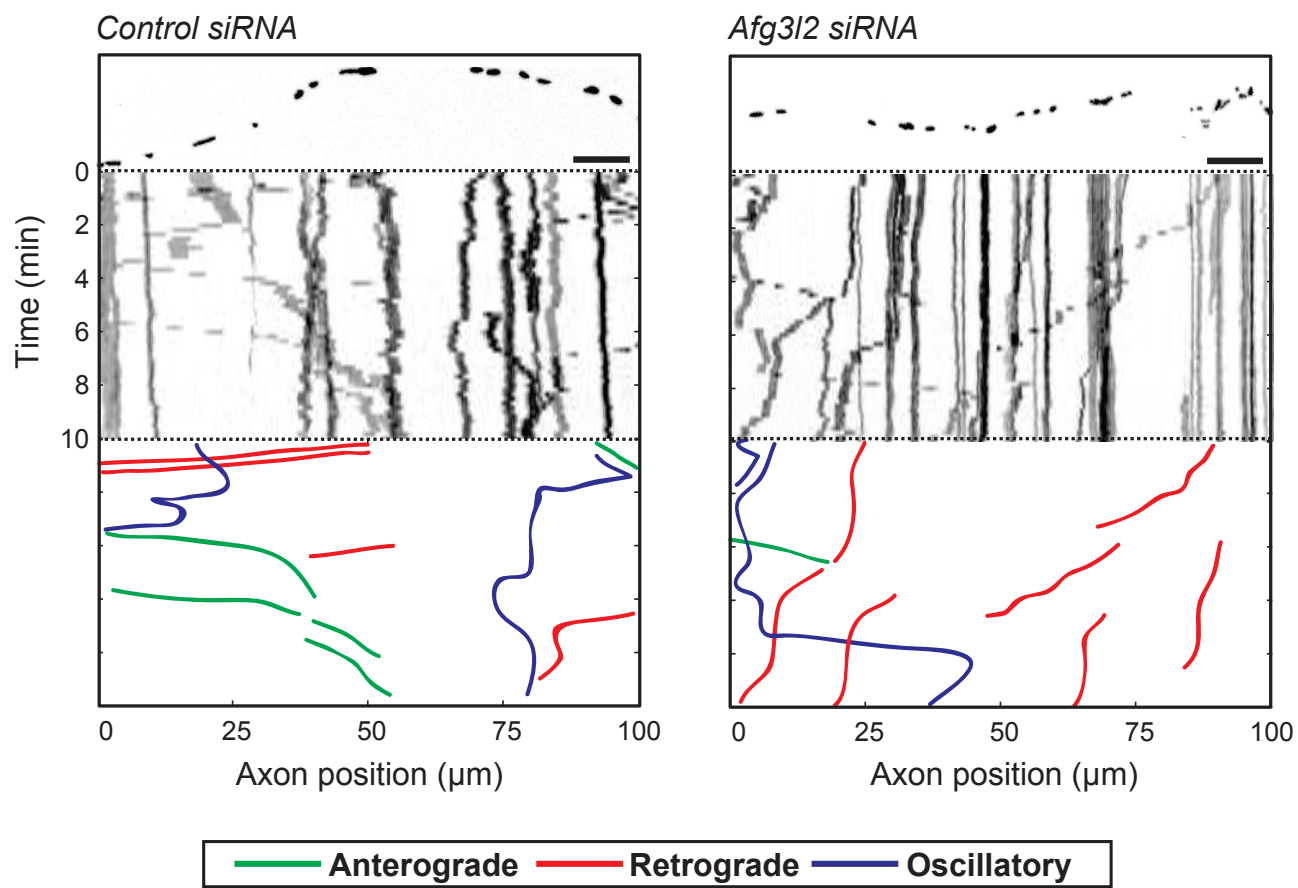
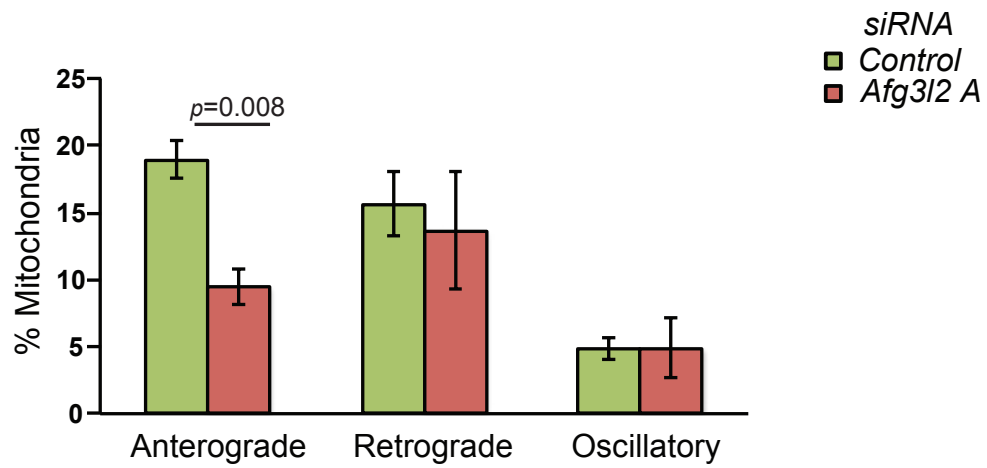
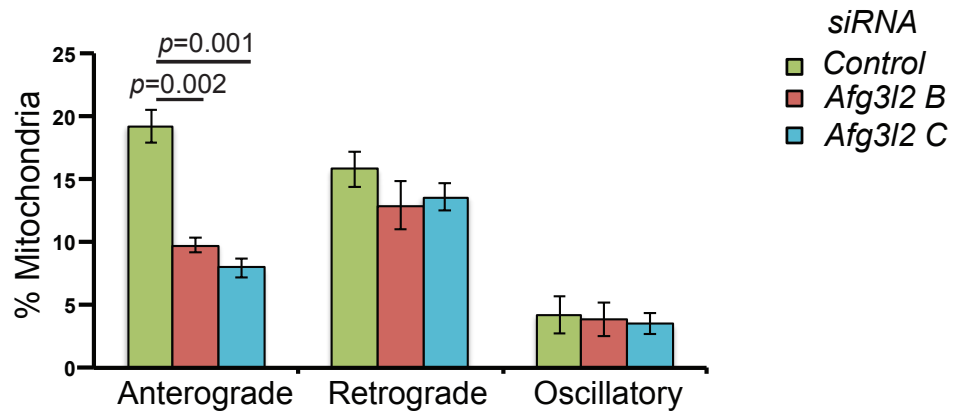
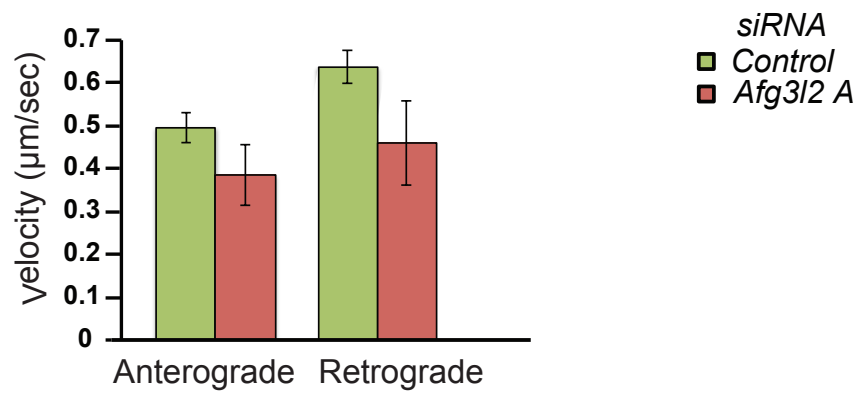


Figure 3.6

A**B****C****Figure 3.7**

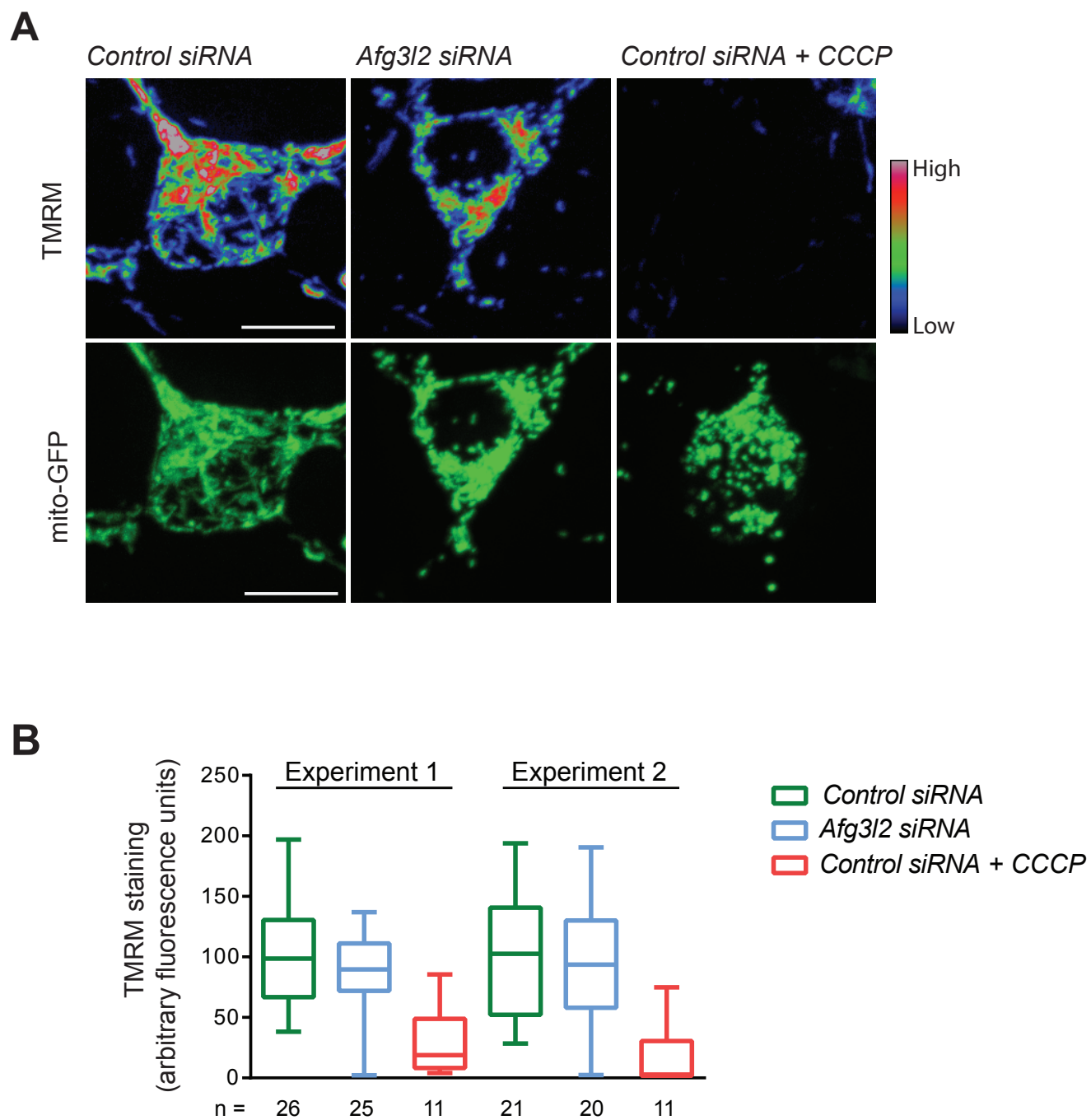


Figure 3.8

3.4) Depletion of OPA1 does not impair mitochondrial transport

It is entirely possible that mere fragmentation of mitochondria can lead to disrupted mitochondrial transport. Therefore, we tested if induction of mitochondrial fragmentation by depleting OPA1, a protein responsible for inner mitochondrial membrane fusion, could lead to disrupted mitochondrial transport in the axons. In our primary murine cortical neurons cultures, we knocked down *Opa1* using two different siRNA oligonucleotides.

3.4.1) Neurons depleted for OPA1 have fragmented mitochondrial morphology and reduced mitochondrial occupancy

We found that mitochondria were fragmented in OPA1 depleted neurons, as expected. The mitochondrial distribution in to different length bins clearly shifted towards the left i.e shorter length bins, by using two siRNA oligonucleotides against *Opa1* when compared to control (Figure 3.9A). Consistently, the frequency distribution of mitochondria belonging to different bins was different by statistical significance as attested by Chi-square test.

We also checked the mitochondrial occupancy in the axons of neurons depleted for OPA1. The mitochondrial occupancies also reduced with two siRNA oligonucleotides with statistical significance attained only with one siRNA oligonucleotide against *Opa1* (Figure 3.9B). This shows that mere mitochondrial fragmentation can also lead to reduced mitochondrial occupancy depending on the extent of knockdown of *Opa1*.

3.4.2) Mitochondrial transport analysis of neurons downregulated for Opa1

Video recordings of control and neurons knocked down for *Opa1* were represented on a kymograph. The axons clearly show mitochondrial fragmentation in neurons depleted for OPA1 when compared to control. Both the control and OPA1 depleted neurons have normal levels of anterograde and retrograde transport (Figure 3.10A).

Quantification of mitochondrial transport further indicated that there is no difference in any kind of mitochondrial transport upon downregulation of *Opa1* (Figure 3.10B). Therefore, mitochondrial fragmentation is not sufficient to cause mitochondrial transport defects as was observed previously (Misko et al., 2010).

FIGURE LEGENDS

Figure 3.9: **Neurons depleted for OPA1 have fragmented mitochondrial morphology and reduced mitochondrial occupancy**

(A) Quantification of mitochondrial length, comparing siRNA oligonucleotides against control and *Opa1* (oligo A & B), shown as the percentage of mitochondria belonging to a given length bin, averaged from 3 independent experiments (131-211 mitochondria were measured in each experiment). Bars represent SEM. *p* values were calculated with the Chi-square test. Control vs. *Opa1* (oligo A): $p = 10^{-4}$; Control vs. *Opa1* (oligo B): $p = 1.4 \times 10^{-6}$.

(B) Histogram showing quantification of mitochondrial occupancy of axons of control neurons and neurons downregulated for *Opa1* (Oligo A & B), ($n = 3$ experiments; at least 8 axons per experiment). *p* value was determined with Student's *t*-test.

Figure 3.10: **Mitochondrial transport analysis of neurons downregulated for *Opa1***

(A) Axons showing representative kymographs from neurons co-transfected with mito-mCherry and control or *Opa1* siRNAs. Schematic of different color-coded transport types is shown below. Scale bars: 10 μm .

(B) Quantification of mitochondrial transport types in the axon (Control Vs siRNA oligonucleotide A & B against *Opa1*). Data represent mean \pm SEM of 3 independent experiments. At least 8 axons from each experiment were analyzed.

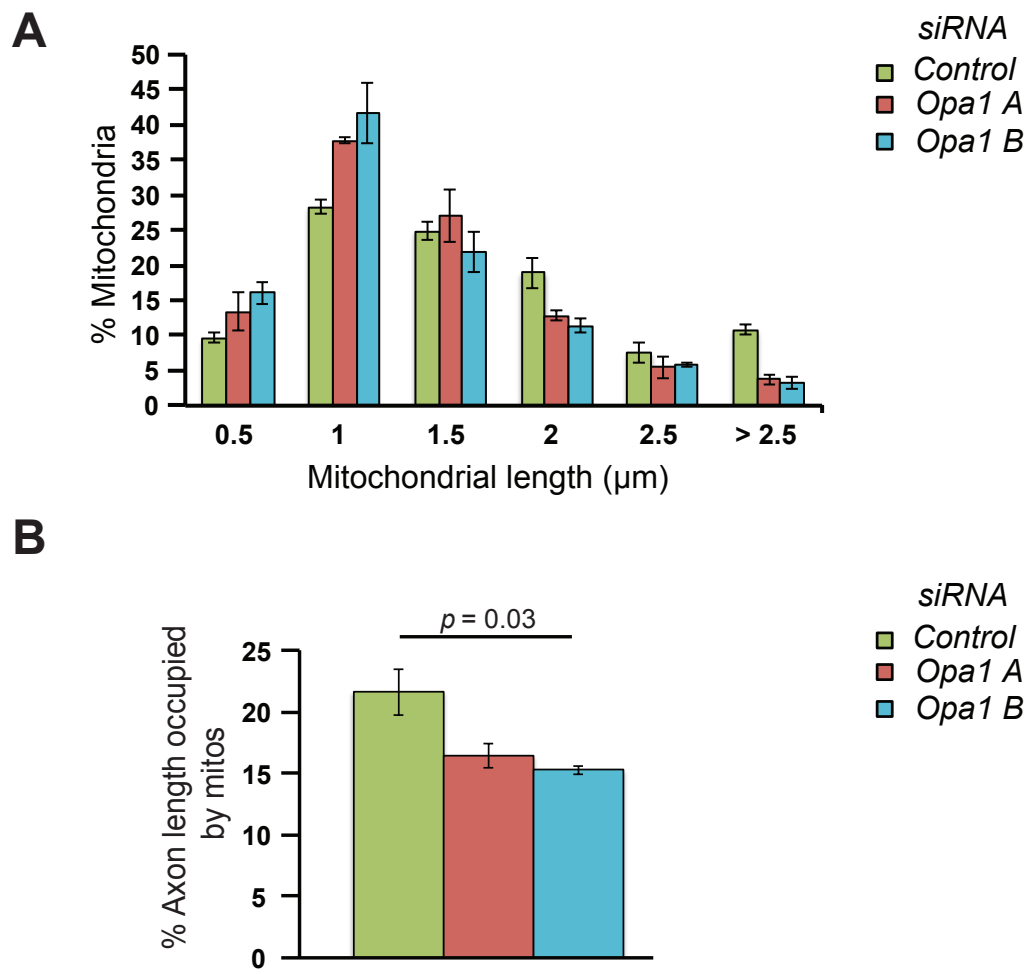


Figure 3.9

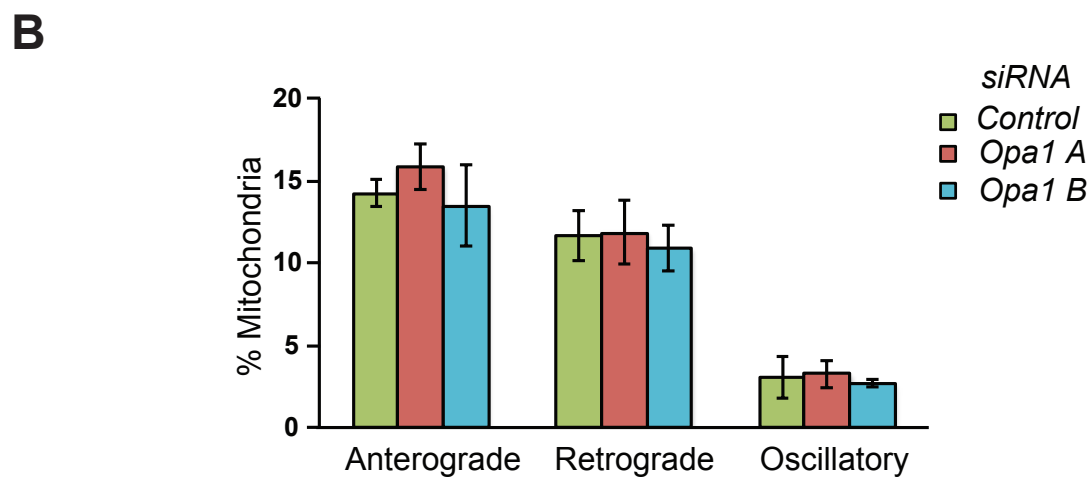
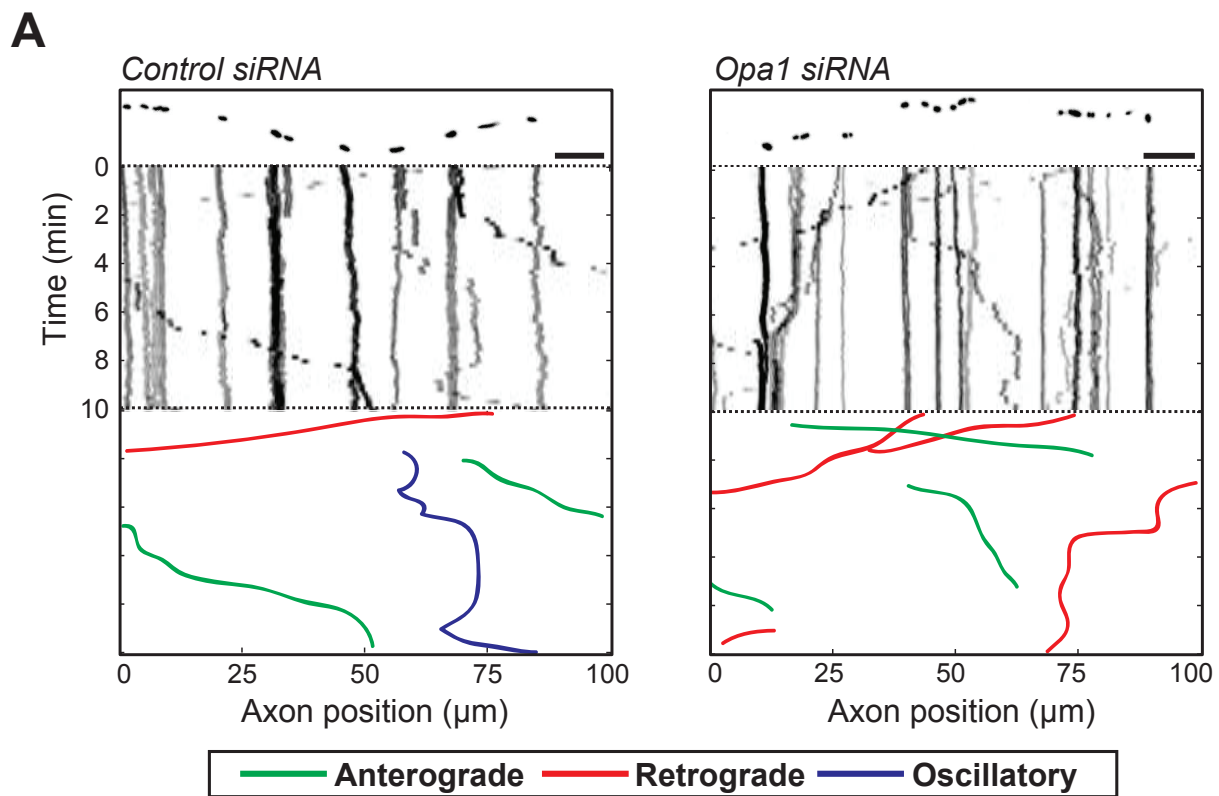


Figure 3.10

3.5) Aberrant mitochondrial transport in neurons depleted for AFG3L2 is independent of OMA1 activation

OPA1, the molecule responsible for inner mitochondrial membrane fusion has 5 forms (a-e) based on proteolytic cleavage of isoforms 'a' and 'b' by proteases OMA1 and YME1L at sites S1 and S2 respectively (Song et al., 2007). Upon depletion of the *m*-AAA protease subunits: AFG3L1 and AFG3L2, OMA1 is activated and long forms of OPA1- 'a' and 'b' are proteolytically cleaved into short forms- 'c' and 'e' (Ehres et al., 2009; Head et al., 2009). Consistently, MEFs concurrently depleted of OMA1 and *m*-AAA protease subunits do not exhibit mitochondrial fragmentation. OMA1 has been proposed to sense mitochondrial abnormalities like reduced ATP levels or mitochondrial membrane potential and process the conversion of long forms into short forms. Therefore, OMA1 could be the sensor for abnormal mitochondrial dynamics in *m*-AAA protease deficient cells and this sensing could further lead to conversion of long forms of OPA1 to short forms. Can it occur that deletion of this possible mitochondrial dysfunction sensor, i.e OMA1, can eventually rescue aberrant mitochondrial dynamics in AFG3L2 depleted neurons?

3.5.1) Mitochondrial morphology and occupancy in Oma1^{-/-} neurons downregulated for Afg3l2

Primary murine cortical neurons from *Oma1^{-/-}* mice were harvested and downregulated for *Afg3l2*. We examined the mitochondrial morphology and found that there is mitochondrial fragmentation in *Oma1^{-/-}* neurons downregulated for *Afg3l2* compared to *Oma1^{-/-}* neurons. However, it is not statistically significant upon comparison of frequency distribution bins by Chi-

square test (Figure 3.11A). There is an increase in percentage of mitochondria only in the 0.5-1 μ M bin with no changes in the remaining bins.

Oma1^{-/-} neurons downregulated for *Afg3l2* also do not indicate any difference in the mitochondrial occupancy when compared to *Oma1*^{-/-} neurons (Figure 3.11B). Therefore, mitochondrial morphology and occupancy remain unaffected upon double depletion of AFG3L2 and OMA1 when compared to depletion of OMA1 alone.

3.5.2) Mitochondrial transport in Oma1^{-/-} neurons downregulated for Afg3l2

Representative kymographs of *Oma1*^{-/-} neurons downregulated with control siRNA oligonucleotides and siRNA oligonucleotides against *Afg3l2* are shown in figure 3.12A. *Oma1*^{-/-} neurons show normal transport of all kinds. However, when there is double depletion of both OMA1 and AFG3L2, we do not observe any rescue of anterograde mitochondrial transport defect indicating that mitochondrial transport defects are independent of OMA1 activation. In fact, a detailed quantification of the same confirmed this observation (Figure 3.12B).

FIGURE LEGENDS

Figure 3.11: ***Oma1*^{-/-} neurons downregulated for *Afg3l2* do not show a significant difference in mitochondrial morphology and occupancy**

(A) Quantification of mitochondrial length in *Oma1*^{-/-} neurons, comparing siRNA oligonucleotides against control and *Afg3l2* (oligo A), shown as the percentage of mitochondria belonging to a given length bin, averaged from 3 independent experiments. (105-200 mitochondria were measured in each experiment). Bars represent SEM.

(B) Histogram showing quantification of mitochondrial occupancy in *Oma1*^{-/-} neurons and *Oma1*^{-/-} neurons downregulated for *Afg3l2* (Oligo A), (n = 3 experiments; at least 8 axons per experiment)

Figure 3.12: ***Oma1*^{-/-} neurons downregulated for *Afg3l2* do not rescue impaired anterograde transport of mitochondria**

(A) Axons showing representative kymographs from *Oma1*^{-/-} neurons co-transfected with mito-mCherry and control or *Afg3l2* siRNAs. Schematic of different color-coded transport types is shown below. Scale bars: 10 μ m

(B) Quantification of mitochondrial transport types in *Oma1*^{-/-} neurons (Control Vs siRNA oligonucleotide A against *Afg3l2*). Data represent mean \pm SEM of 3 independent experiments. At least 8 axons from each experiment were analyzed. *p* value was determined with Student's *t*-test.

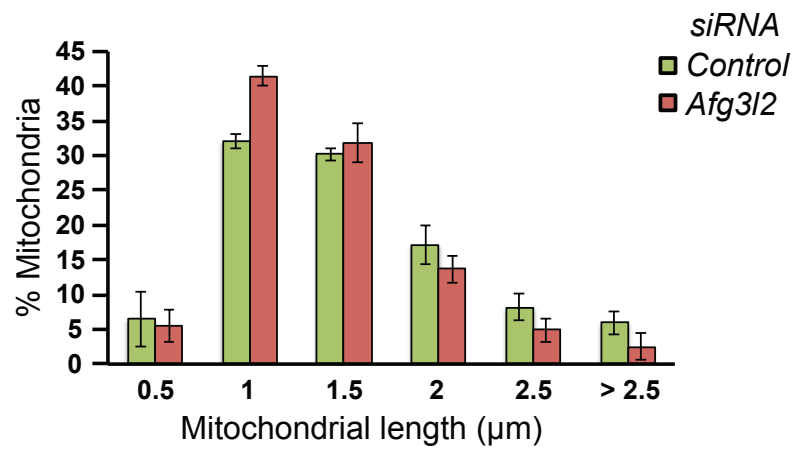
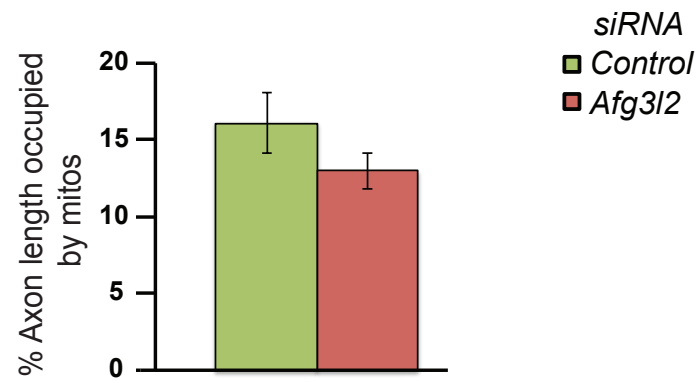
A**B**

Figure 3.11

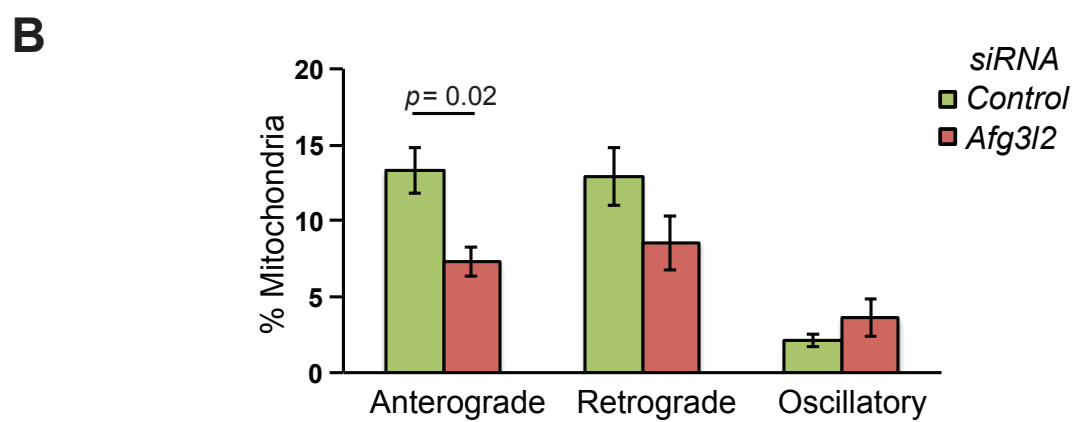
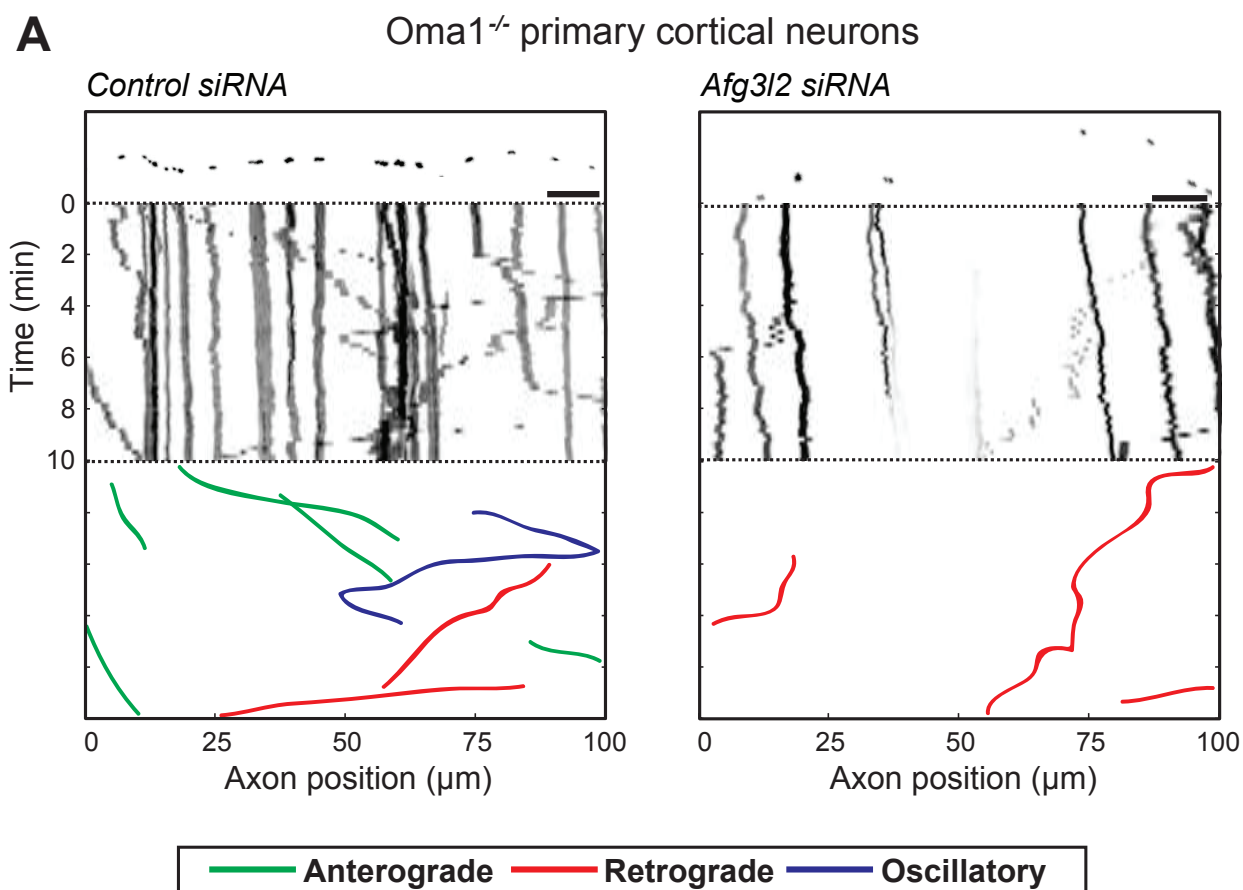


Figure 3.12

3.6) Tau affects mitochondrial dynamics in neurons deficient for AFG3L2

Afg3l2^{Emv66/Emv66} (Constitutive knockout of *Afg3l2*) mice displayed higher levels of tau hyperphosphorylation in their brains (Kondadi et al., 2014). These mice also have smaller cortices with neuronal loss, as shown by Nissl staining, and aberrancies of axonal growth and myelination. *Tau* knockdown rescues milton or miro mediated neurodegeneration in *Drosophila* (Iijima-Ando et al., 2012). On the contrary, overexpression of *tau* causes impaired transport of mitochondria into the axons (Stamer et al., 2002). Therefore, we tested if depletion of tau in AFG3L2 deficient neurons could rescue aberrant mitochondrial dynamics including transport.

3.6.1) Characterization of siRNA oligonucleotides directed against tau

We overexpressed rat *tau* plasmid in MEFs and used siRNA oligonucleotides directed against *tau* to check the efficacy of 3 commercially available siRNA oligonucleotides. All the siRNA oligonucleotides against *tau* were able to deplete the levels of overexpressed *tau*. However, the most efficient siRNA oligonucleotide (*Mapt siRNA 36*) was used for successive experiments (Figure 3.13).

3.6.2) Mitochondrial morphology and occupancy in neurons depleted for AFG3L2 and tau

As observed before, detailed quantification of mitochondrial length revealed that AFG3L2 depletion lead to mitochondrial fragmentation. Interestingly, concurrent depletion of AFG3L2 and tau rescued mitochondrial fragmentation when compared to AFG3L2 depletion alone (Figure 3.14A). This was corroborated by

statistical comparison of frequency distribution differences by a Chi-square test. Neurons downregulated for *Afg3l2* had decreased mitochondrial occupancies as observed previously. However, decreasing the tau levels in AFG3L2 depleted neurons did not rescue the mitochondrial occupancy when compared to AFG3L2 depletion alone (Figure 3.14B). Thus, decreasing tau levels in AFG3L2 depleted neurons rescued mitochondrial fragmentation but not mitochondrial occupancy.

3.6.3) Mitochondrial transport in neurons depleted for AFG3L2 and tau

However, the most tempting assumption to implicate the role of tau in neurodegeneration would be its role in mitochondrial transport. Comprehensive quantification of mitochondrial transport revealed a decrease in anterograde transport of mitochondria in AFG3L2 depleted neurons as observed before. Although partially, it was observed that concurrent depletion of AFG3L2 and tau rescued mitochondrial anterograde transport when compared to AFG3L2 depletion alone (Figure 3.15A). We also checked if the partial rescue in anterograde transport was observed due to an increase in the mitochondrial velocities. However, we do not find any significant change in the velocities of mitochondria moving anterogradely (Figure 3.15B). Similarly, the retrograde mitochondrial velocities did not differ under any condition (Figure 3.15C).

FIGURE LEGENDS

Figure 3.13: **Characterization of siRNA oligonucleotides directed against tau**

Western blot analysis of efficiency of different siRNA oligonucleotides (*Mapt* siRNAs) against overexpressed *tau* in MEFs. *Mapt* siRNA 36 was selected for further studies.

Figure 3.14: **Neurons depleted for AFG3L2 and tau, when compared to AFG3L2 alone, show a rescue in fragmented mitochondrial morphology but not occupancy**

(A) Quantification of mitochondrial length in axons, in respective conditions, shown as the percentage of mitochondria belonging to a given length bin, averaged from 3 independent experiments. (120-210 mitochondria were measured in each experiment). Bars represent SEM. *p* values were calculated with the Chi-square test. Control vs. *Afg3l2*/control: $p = 7 \times 10^{-4}$, control vs. *Afg3l2*/*Mapt*: $p = 9 \times 10^{-3}$, *Afg3l2*/control vs. *Afg3l2*/*Mapt*: $p = 5 \times 10^{-5}$.

(B) Histogram showing quantification of mitochondrial occupancy of respective axons, ($n = 3$ experiments; 7-9 axons per experiment). *p* value was determined with Student's *t*-test.

Figure 3.15: **Neurons depleted for AFG3L2 and tau partially rescue impaired anterograde transport of mitochondria but not mitochondrial velocities when compared to AFG3L2 depletion alone**

(A) Quantification of mitochondrial transport types in the axon. Data represent mean \pm SEM of 3 independent experiments. 7-9 neurons from each experiment

were analyzed. *p* values were determined with Student's *t*-test.

(B & C) Average mitochondrial velocity in the anterograde (B) and retrograde (C) direction. Data represent mean \pm SEM of 3 independent experiments. The velocity of mitochondria was analyzed from 3 axons per experiment.

<i>Mapt</i> OE (Rat)	-	-	-	+	+	+	+	+
Control siRNA	-	+	-	-	+	-	-	-
<i>Mapt</i> siRNA 36	-	-	+	-	-	+	-	-
<i>Mapt</i> siRNA 37	-	-	-	-	-	-	+	-
<i>Mapt</i> siRNA 38	-	-	-	-	-	-	-	+

tau
(55 kDa)

GAPDH
(35 kDa)

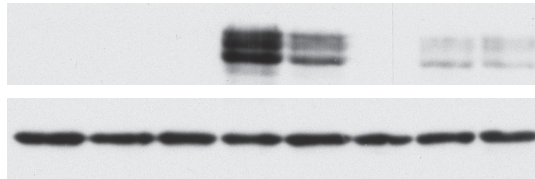


Figure 3.13

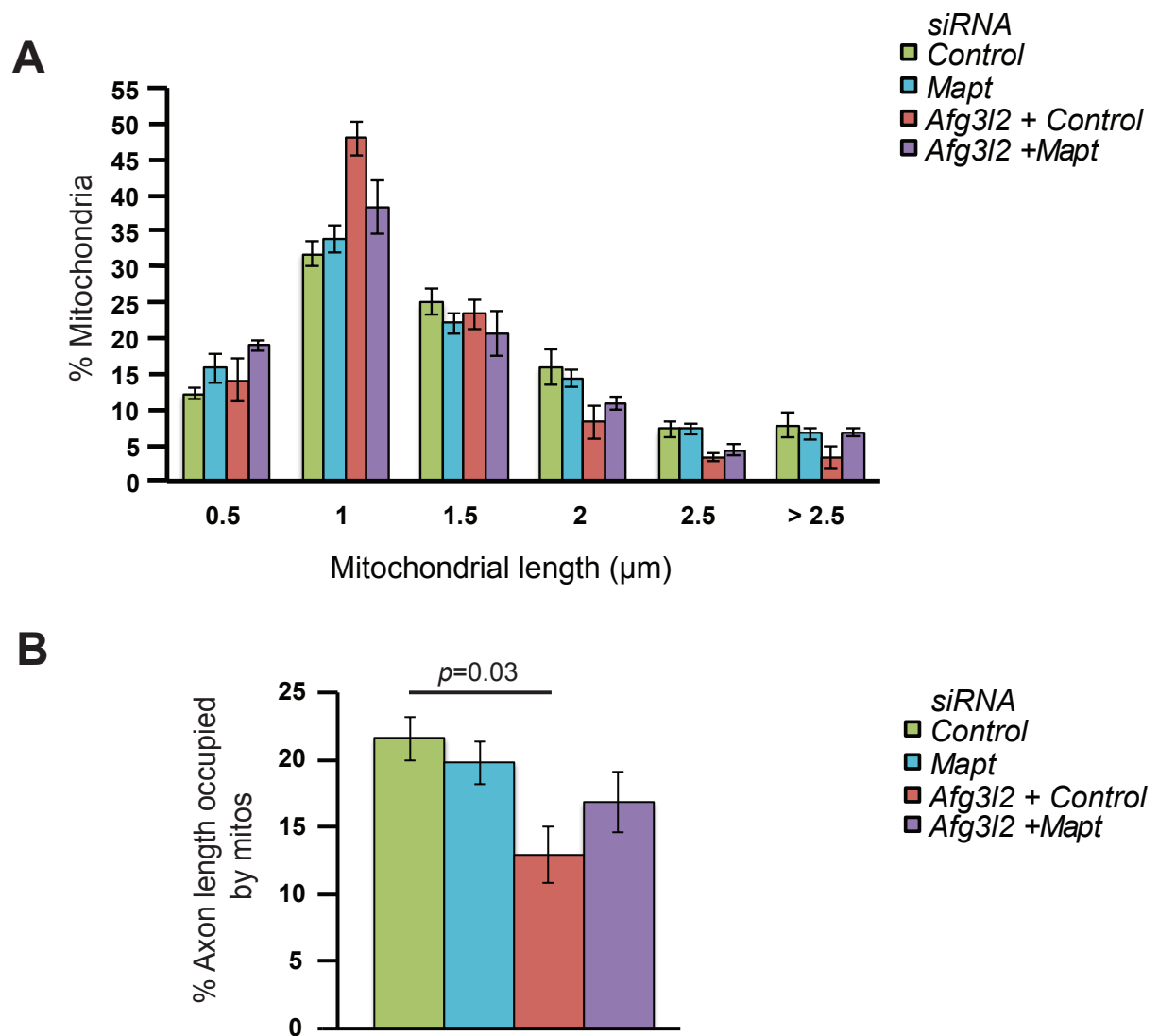


Figure 3.14

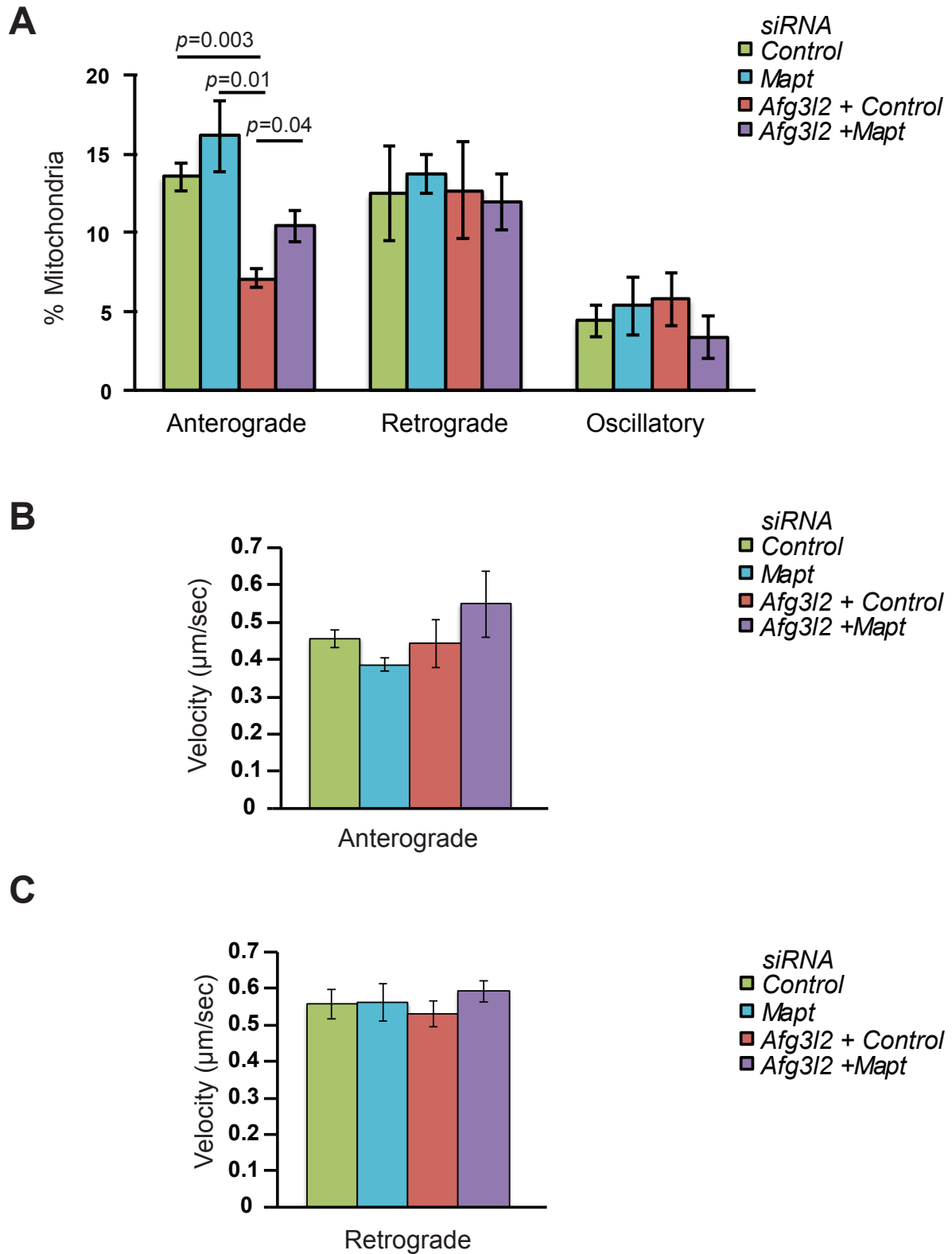


Figure 3.15

3.7) NAC rescues mitochondrial defects observed in neurons depleted for AFG3L2

Genotypic oxidative stress such mutations in superoxide dismutase 2 (SOD2) (Melov et al., 2007) or axonal transport defects caused by deleting kinesin light chain can lead to tau hyperphosphorylation (Falzone et al., 2009). Chemotoxic oxidative stress such as treatment with hydrogen peroxide can also cause mitochondrial transport defects (Fang et al., 2012). Therefore, oxidative stress can be a possible cause of axonal transport defects. We sought to check if interfering with ROS levels in the neurons can have any effect on the mitochondrial transport. N-acetyl cysteine (NAC) is widely used as an antioxidant. In fact, it acts by regulating the amount of glutathione in cells and is efficient as a ROS scavenger (Arakawa and Ito, 2007).

3.7.1) Mitochondrial morphology and occupancy in AFG3L2 depleted neurons grown in the presence of NAC

Analysis of mitochondrial length into different length bins clearly indicated that mitochondrial fragmentation observed upon AFG3L2 depletion was rescued when the neurons were grown in the presence of NAC. This was further confirmed by a Chi-square test that yielded high statistical significance (Figure 3.16A). As observed previously and in this experiment, downregulation of *Afg3l2* lead to a decreased mitochondrial occupancy, which was rescued when the neurons were grown in the presence of NAC (Figure 3.16B). Therefore, AFG3L2 depleted neurons grown in the presence of NAC show a robust rescue in mitochondrial morphology and occupancy.

3.7.2) Kymographic analysis of neurons downregulated for AFG3L2 grown in the presence of NAC

Representative kymographs of AFG3L2 depleted neurons grown in the absence and presence of NAC respectively are shown in figure 3.17. As was observed before, AFG3L2 depleted neurons show reduced anterograde transport as highlighted by the reduced number of green lines. Surprisingly, anterograde transport was restored to normal when the neurons were grown in the presence of NAC.

3.7.3) Mitochondrial transport and velocity in AFG3L2 depleted neurons grown in the presence of NAC

Quantification of mitochondrial transport clearly showed that when AFG3L2 depleted neurons were grown in the presence of NAC, impaired anterograde mitochondrial transport was rescued (Figure 3.18A). In AFG3L2 depleted neurons, approximately 6 % of anterograde transport was observed. When AFG3L2 depleted neurons were grown in the presence of NAC, the impaired anterograde transport increased in the realm of control neurons asserting that a very robust total rescue of anterograde transport was observed. Interestingly, a significant increase in mitochondria possessing oscillatory motion was also observed (Figure 3.18A).

Increased mitochondrial velocities could be a possible explanation by which such a robust increase in the percentage of anterogradely moving mitochondria can be observed. However, we could not find any increase in the average velocity of anterogradely moving mitochondria in AFG3L2 depleted neurons. Interestingly,

the average anterograde velocity of mitochondria increased in control neurons indicating that quenching the basal ROS levels even in control neurons can be beneficial by increasing mitochondrial transport (Figure 3.18B). The retrograde velocities of mitochondria remain unchanged in all the scenarios (Figure 3.18C).

FIGURE LEGENDS

Figure 3.16: **NAC rescues fragmented mitochondrial morphology and occupancy in AFG3L2 depleted neurons**

(A) Quantification of mitochondrial length, comparing siRNA oligonucleotides against control and *Afg3l2* (oligo A), grown in medium with and without NAC, shown as the percentage of mitochondria belonging to a given length bin, averaged from 4 independent experiments. (78-195 mitochondria were measured in each experiment). Bars represent SEM. *p* values were calculated with the Chi-square test. Control vs. *Afg3l2*: $p = 8 \times 10^{-9}$; *Afg3l2* vs. *Afg3l2* with NAC: $p = 1 \times 10^{-12}$.

(B) Histogram showing quantification of mitochondrial occupancy of axons of control neurons and neurons downregulated for *Afg3l2* (Oligo A), grown in medium with and without NAC. ($n = 4$ experiments; 8-10 axons per experiment). *p* values were determined with Student's *t*-test.

Figure 3.17: **Kymographic analysis of neurons downregulated for *Afg3l2* grown in the presence of NAC**

Axons showing representative kymographs from neurons co-transfected with mito-mCherry and control or *Afg3l2* siRNAs, grown in the absence or presence of NAC. Schematic of different color-coded transport types is shown below. Scale bars: 10 μm .

Figure 3.18: NAC rescues impaired anterograde transport in AFG3L2 depleted neurons and increases the velocity of anterogradely moving mitochondria in control neurons

(A) Quantification of mitochondrial transport types in the axon grown in the absence or presence of NAC (Control Vs oligonucleotide A against *Afg3l2*). Data represent mean \pm SEM of 4 independent experiments. 8-10 axons from each experiment were analyzed.

(B) Average mitochondrial velocity (from at least 3 axons per experiment) in the anterograde direction. Data represent mean \pm SEM of 4 independent experiments.

(C) Average mitochondrial velocity (from at least 3 axons per experiment) in the retrograde direction. Data represent mean \pm SEM of 4 independent experiments. *p* values in A and B were determined with Student's *t*-test.

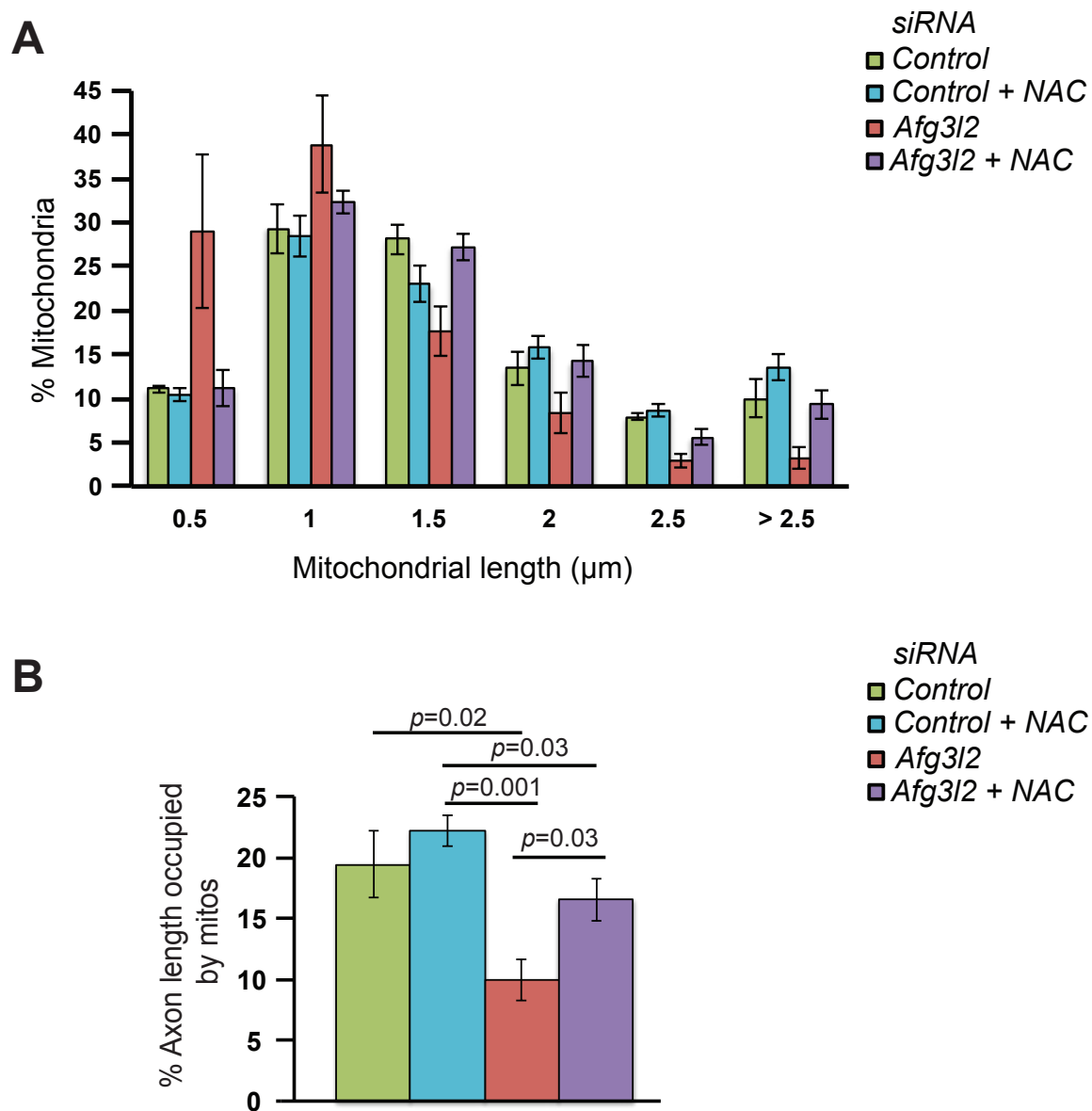


Figure 3.16

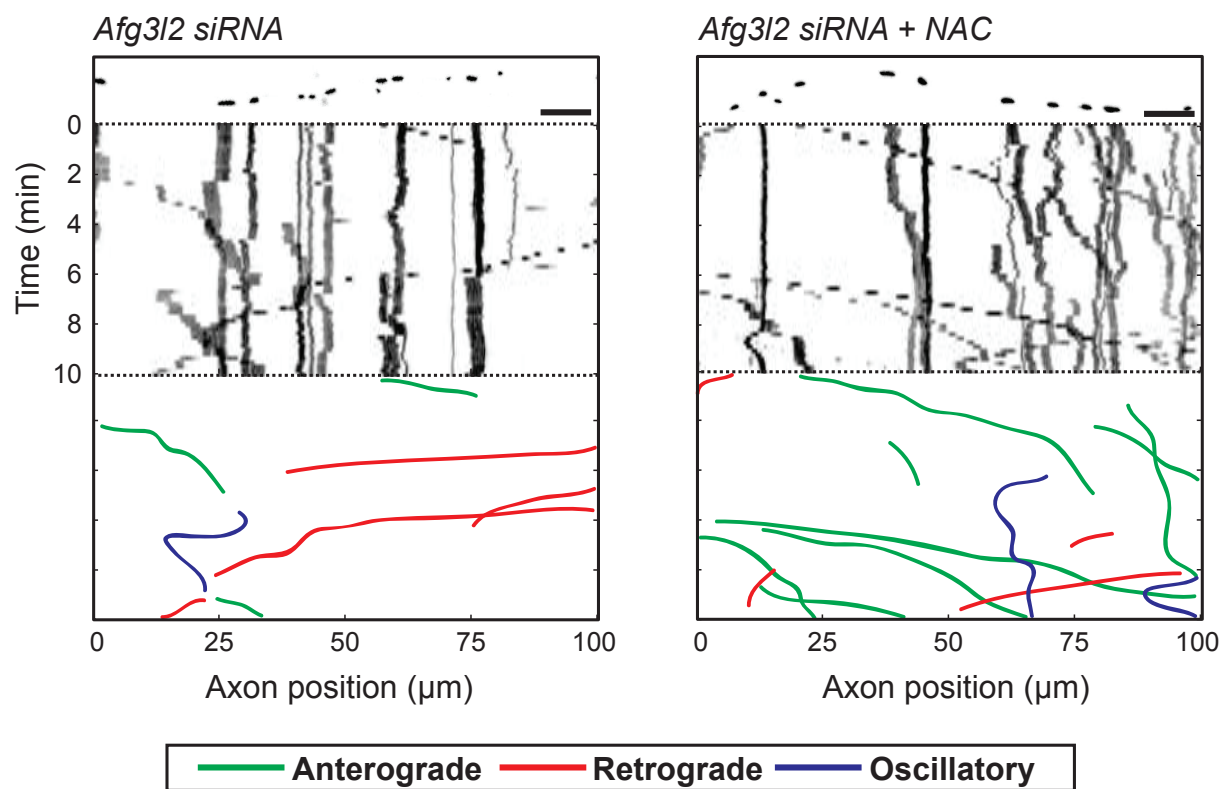
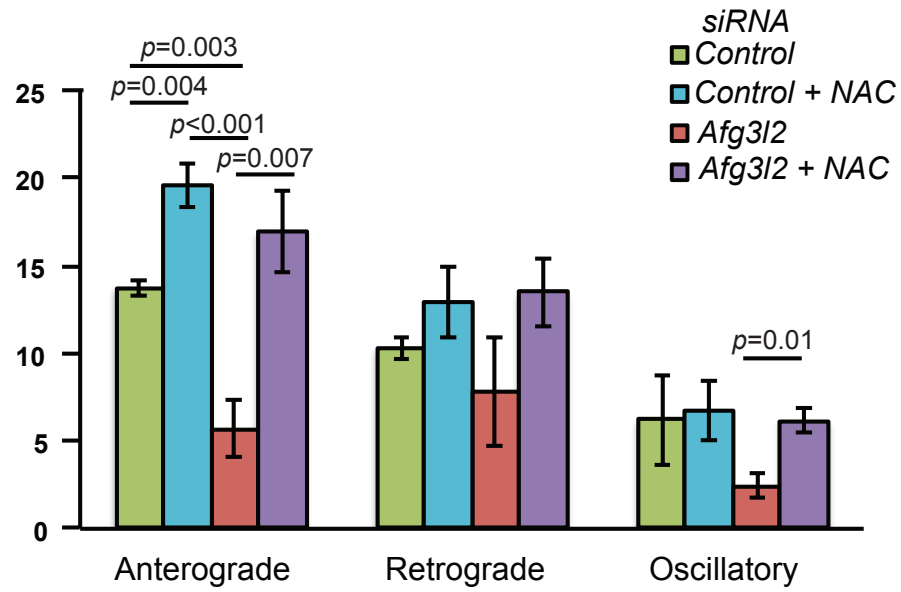
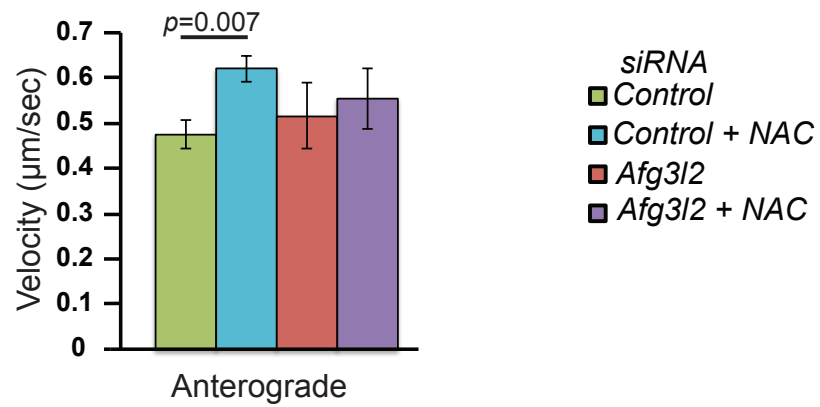
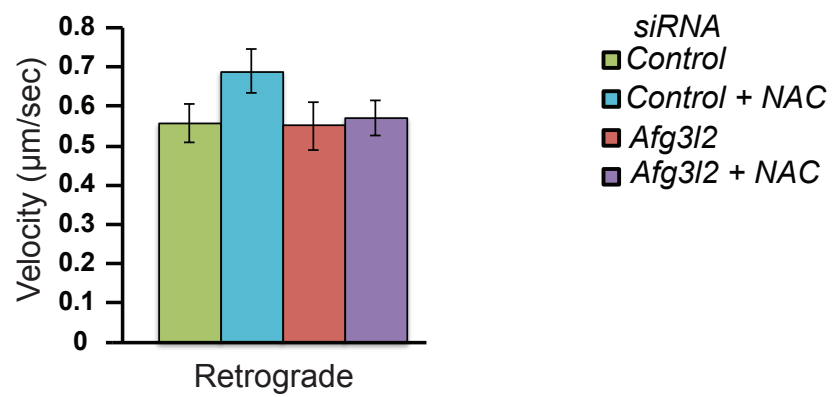


Figure 3.17

A**B****C****Figure 3.18**

3.8) Vitamin E rescues mitochondrial transport defects observed in AFG3L2 deficient neurons

To strengthen the observation that NAC rescues the anterograde mitochondrial transport in AFG3L2 depleted neurons because of its antioxidant activity, we used another antioxidant in vitamin E.

3.8.1) Mitochondrial morphology and occupancy in AFG3L2 depleted neurons grown in the presence of vitamin E

Mitochondrial fragmentation observed in AFG3L2 depleted neurons was not rescued when neurons were grown in the presence of vitamin E (Figure 3.19A). Vitamin E induced fragmentation in control neurons because of some unknown reason as attested by statistical significance by Chi-square test. Nevertheless, we did not observe this fragmentation in AFG3L2 depleted neurons exposed to vitamin E. Consistent with mitochondrial fragmentation, vitamin E also did not rescue the mitochondrial occupancy in neurons downregulated for *Afg3l2* (Figure 3.19B).

3.8.2) Mitochondrial transport in AFG3L2 depleted neurons grown in the presence of vitamin E

When AFG3L2 depleted neurons were grown in the presence of vitamin E, impaired anterograde transport was rescued to the level of control neurons (Figure 3.20A). The retrograde and oscillatory motion of mitochondria did not show any change as before. In summary, we were able to show that both NAC and vitamin E could rescue the decreased anterograde mitochondrial transport

in AFG3L2 deficient neurons. Mitochondrial velocities were unaffected in neurons treated with vitamin E (Figure 3.20B & C)

FIGURE LEGENDS

Figure 3.19: AFG3L2 deficient neurons do not show a significant difference in mitochondrial morphology and occupancy when grown in the presence of vitamin E

(A) Quantification of mitochondrial length, comparing siRNA oligonucleotides against control and *Afg3l2* (oligo A), grown in medium with and without vitamin E, shown as the percentage of mitochondria belonging to a given length bin, averaged from 3 independent experiments. (130-218 mitochondria were measured in each experiment). Bars represent SEM. *p* values were calculated with the Chi-square test. Control vs. control with Vitamin E: $p = 0.01$, control vs. *Afg3l2*: $p = 5 \times 10^{-7}$.

(B) Histogram showing quantification of mitochondrial occupancy of axons of control neurons and neurons downregulated for *Afg3l2* (Oligo A), grown in medium with and without vitamin E. ($n = 3$ experiments; at least 8 axons per experiment). *p* values were determined with Student's *t*-test.

Figure 3.20: Neurons depleted for AFG3L2 rescue impaired anterograde transport of mitochondria when grown in the presence of vitamin E

(A) Quantification of mitochondrial transport types in the axon grown in the absence or presence of vitamin E (Control Vs siRNA oligonucleotide A against *Afg3l2*). Data represent mean \pm SEM of 3 independent experiments. At least 8 axons from each experiment were analyzed. *p* values were determined with Student's *t*-test.

(B) Average mitochondrial velocity (from at least 3 axons per experiment) in the anterograde direction. Data represent mean \pm SEM of 3 independent experiments.

(C) Average mitochondrial velocity (from at least 3 axons per experiment) in the retrograde direction. Data represent mean \pm SEM of 3 independent experiments.

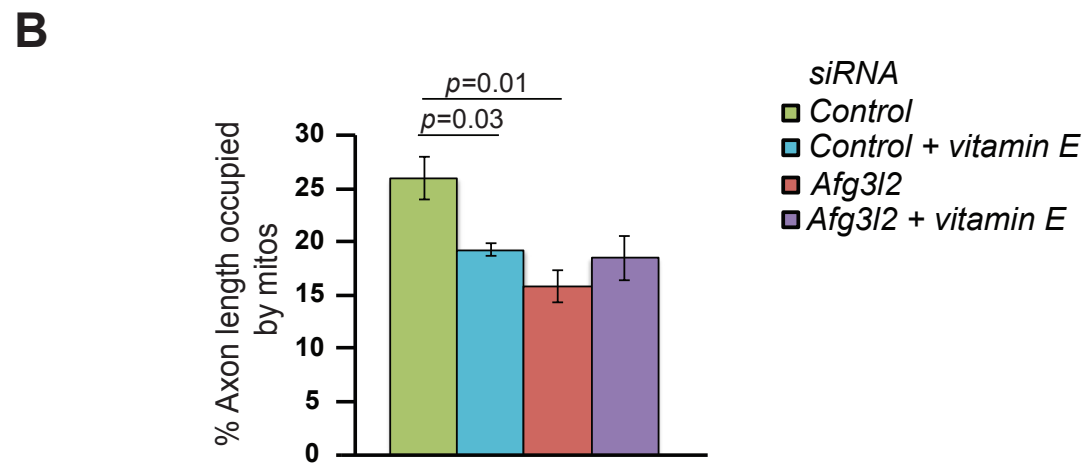
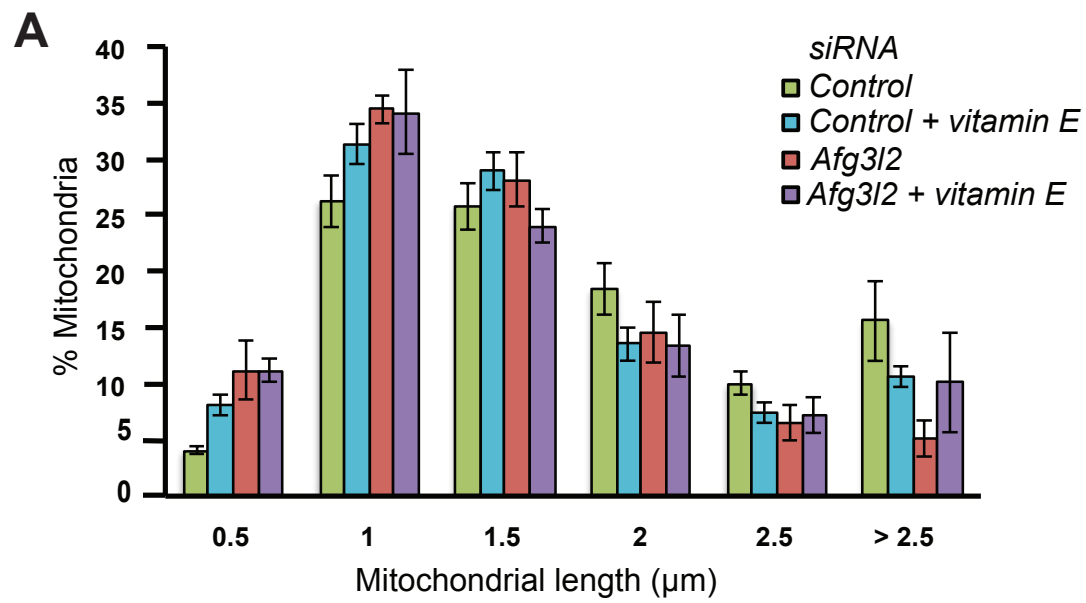


Figure 3.19

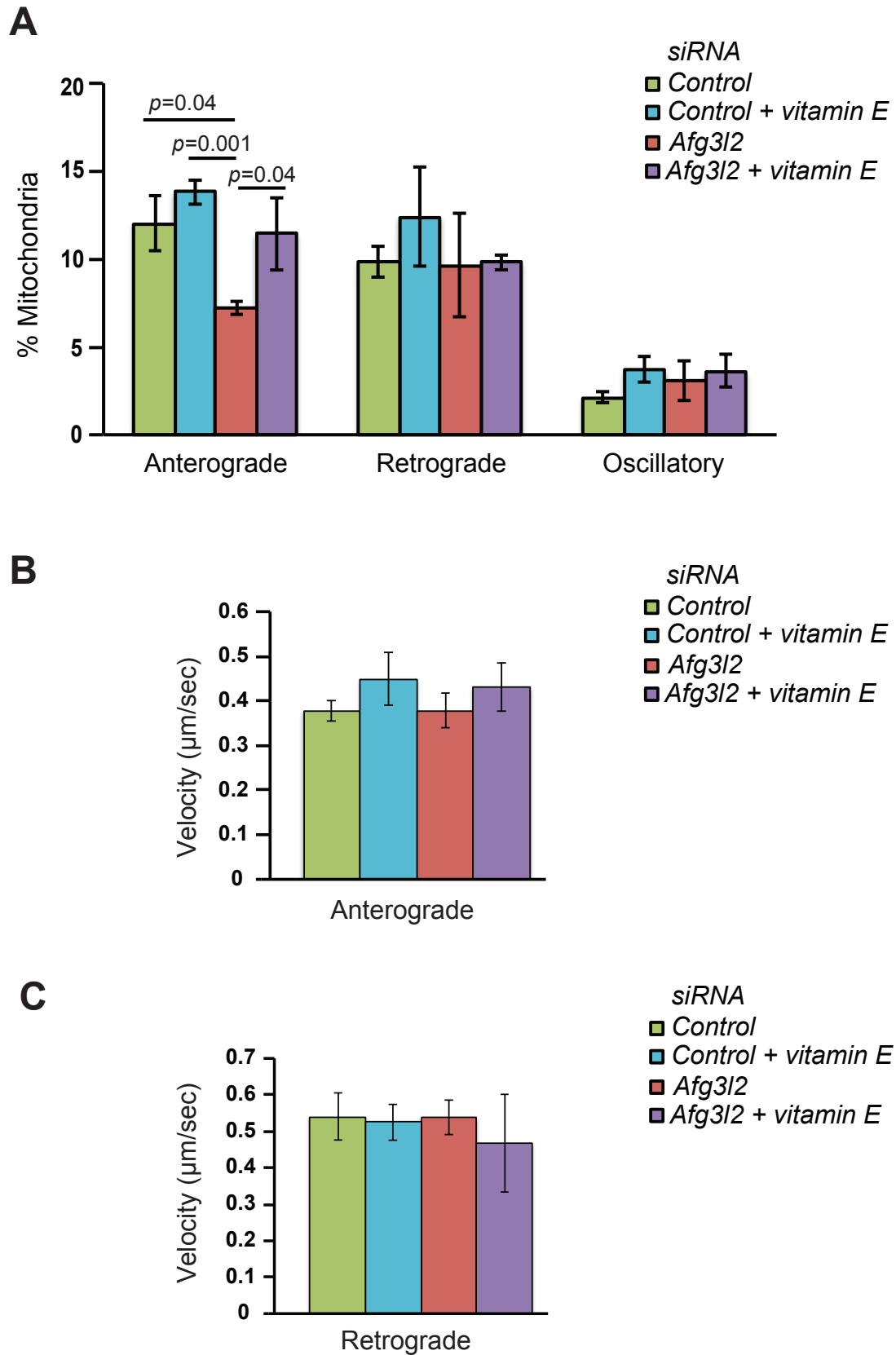


Figure 3.20

3.9) Evaluation of cellular ROS levels in AFG3L2 deficient neurons by CellRox green

The fact that treatment of AFG3L2 depleted neurons with NAC and vitamin E rescues impaired anterograde transport heavily suggests that there could be increased ROS levels in these neurons. CellRox green is a fluorogenic dye that fluoresces brightly upon oxidation and binding to DNA. Results from different experiments do not suggest consistent inferences. We only detected an increase in CellRox green intensity in the soma of neurons in one of the three experiments when *Afg3l2* was downregulated (Figure 3.21A & B). A possible reason could be the level of downregulation achieved in this experiment might be over a critical threshold to cause increased ROS levels. However, since we could not find consistent increase in ROS levels, a representative pseudo-color coded image of intensities showing no difference in the CellRox green intensities is depicted in figure 3.21A.

We then wanted to directly demonstrate that NAC and vitamin E were acting as antioxidants. For this purpose, CellRox green was used. Neurons were exposed to menadione, a chemical which causes oxidative stress by increasing futile redox cycling (Criddle et al., 2006). The pseudo-colour coded intensities of neurons increases strongly when treated with menadione suggesting that CellRox green is able to detect massive changes in the oxidative status of neurons validating it as a reliable dye (Figure 3.22A). Accordingly, the higher intensities of CellRox green in the soma of neurons upon menadione exposure reduced significantly upon addition of NAC and vitamin E suggesting that NAC and vitamin E indeed acted as efficient antioxidants (Figure 3.22A & B).

FIGURE LEGENDS

Figure 3.21: ***Afg3l2* downregulated neurons do not display consistent increase in cellular ROS levels**

(A) Representative images of control and AFG3L2 deficient neurons showing ROS levels by pseudo-colour coded intensities of CellRox green staining in the soma.

(B) Quantification of CellRox green staining in the soma of control and *Afg3l2* downregulated neurons from three different experiments.

Figure 3.22: **NAC and vitamin E display antioxidant activity**

(A) Representative images of neurons treated with different reagents (Menadione, menadione + NAC, menadione + vitamin E) showing ROS levels by pseudo-colour coded intensities of CellRox green staining in the soma.

(B) Quantification of a representative experiment of CellRox green staining of nuclei of neurons treated with different reagents.

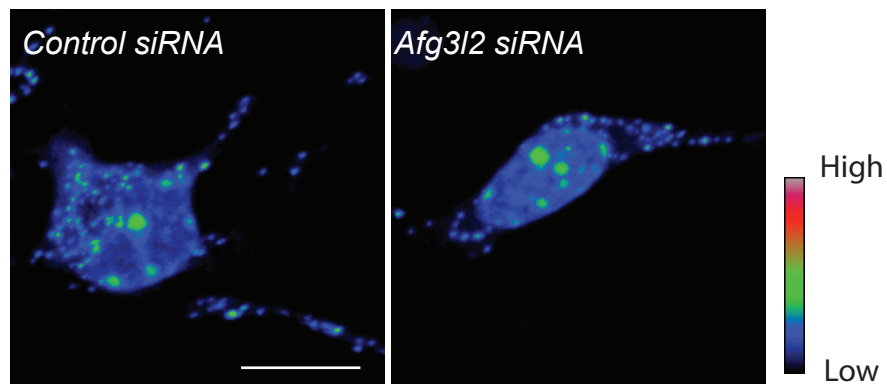
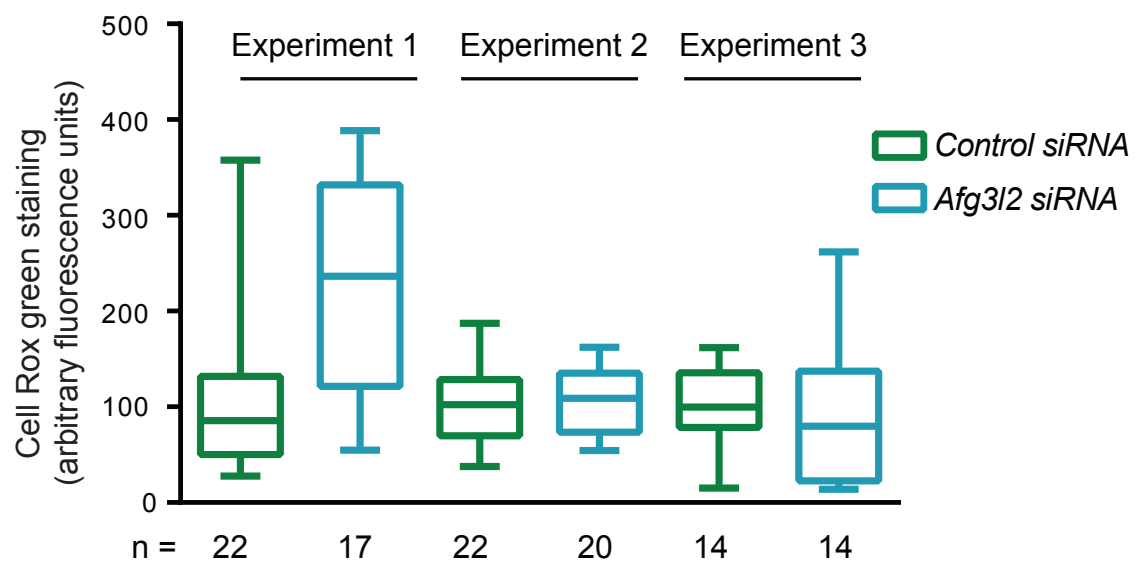
A**B**

Figure 3.21

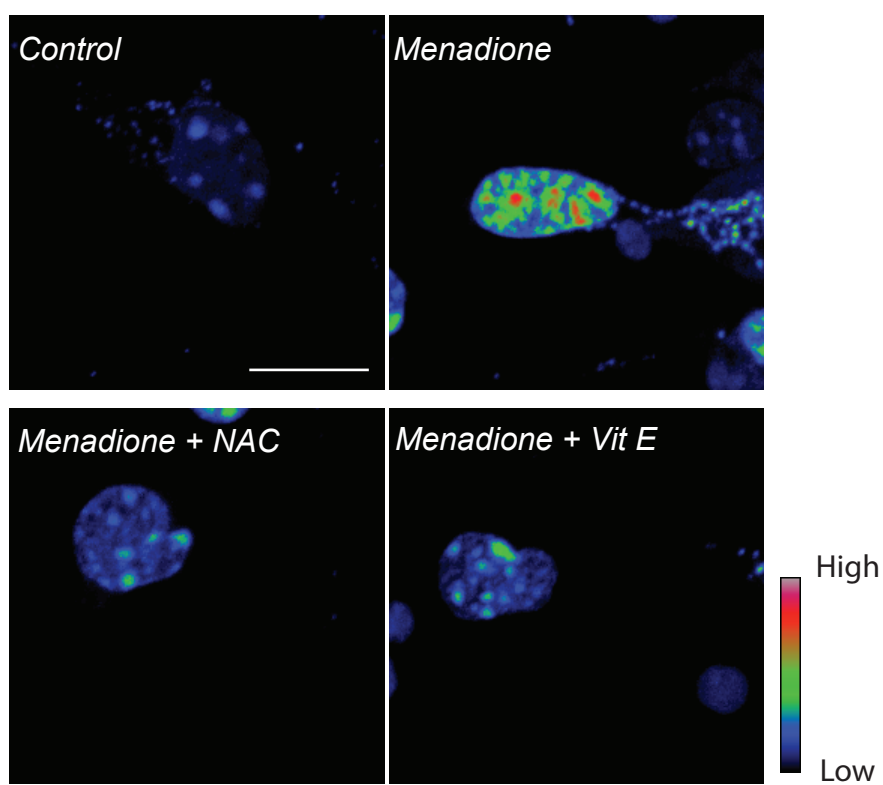
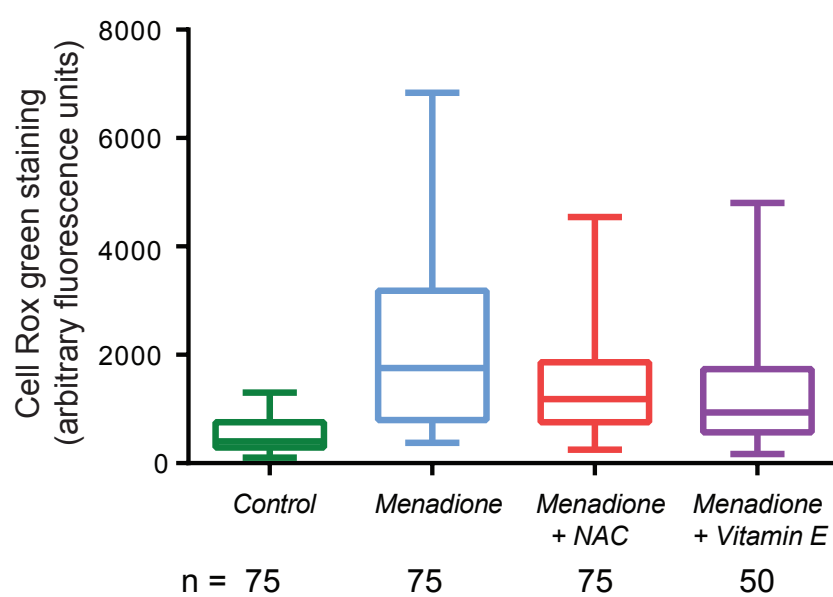
A**B**

Figure 3.22

Table 1: % Stationary Mitochondria

Figure 3.7A	<i>Control siRNA</i>	<i>Afg3l2 siRNA</i>		
	60.5 ± 2.8	71.9 ± 7.8		
Figure 3.7B	<i>Control siRNA</i>	<i>Afg3l2 siRNA (B)</i>	<i>Afg3l2 siRNA (C)</i>	
	60.7 ± 3.4	73.5 ± 2.8*	75.0 ± 1.1*	
Figure 3.10B	<i>Control siRNA</i>	<i>OPA1 siRNA (A)</i>	<i>OPA1 siRNA (B)</i>	
	71.1 ± 3.0	69.0 ± 3.6	72.9 ± 3.2	
Figure 3.12B	<i>Control siRNA in Oma1^{-/-} Neurons</i>	<i>Afg3l2 siRNA in Oma1^{-/-} Neurons</i>		
	70.0 ± 4.4	80.5 ± 2.6		
Figure 3.15A	<i>Control siRNA</i>	<i>Tau siRNA</i>	<i>Afg3l2 + control siRNA</i>	<i>Afg3l2 + tau siRNA</i>
	69.6 ± 2.2	64.8 ± 1.2	74.4 ± 4.0	74.2 ± 1.0
Figure 3.18A	<i>Control siRNA</i>	<i>Control siRNA + NAC</i>	<i>Afg3l2 siRNA</i>	<i>Afg3l2 siRNA + NAC</i>
	69.7 ± 0.4	60.6 ± 1.6	83.9 ± 1.27	63.4 ± 2.3
Figure 3.20A	<i>Control siRNA</i>	<i>Control siRNA + Vit E</i>	<i>Afg3l2 siRNA</i>	<i>Afg3l2 siRNA + Vit E</i>
	76.0 ± 2.6	70.0 ± 2.9	80.1 ± 4.0	75.1 ± 1.72

* Comparison to control shows a significant increase in stationary mitochondria by Student's *t*-test. *p* > 0.05.

Discussion

DISCUSSION:

The *m*-AAA protease present in the inner mitochondrial membrane degrades misfolded polypeptides (Pajic et al., 1994), processes MrpL32 to aid mitochondrial translation (Almajan et al., 2012; Nolden et al., 2005) and has a chaperone-like activity (Arlt et al., 1996). Hence, the basic functions of *m*-AAA protease have been elegantly characterized. Perturbations in the *m*-AAA protease manifest in pathological consequences. Heterozygous missense mutations in AFG3L2 lead to Spinocerebellar ataxia 28 (SCA28) (Di Bella et al., 2010). Mutations in *SPG7* encoding paraplegin cause HSP (Casari et al., 1998). Homozygous mutations in AFG3L2 cause a severe recessive form of spastic-ataxia with early-onset and rapid progression (SPAX5) (Pierson et al., 2011). Mitochondrial fragmentation was previously observed in non-polarised cells (Ehse et al., 2009). However the contribution of mitochondrial dynamics and transport in neurodegeneration has not been studied. The contribution of mitochondrial dynamics to neurodegeneration has been clearly discussed before (Alexander et al., 2000a; Chen et al., 2003; Chen et al., 2007; Delettre et al., 2000; Waterham et al., 2007; Zuchner et al., 2004). To address this question with relation to *m*-AAA protease pathology, we used primary murine cortical neuronal cultures and depleted AFG3L2. Interestingly, AFG3L2 depleted neurons exhibit mitochondrial fragmentation and reduced mitochondrial occupancy (mitochondrial mass present per unit length of axon). Also, we observed a selective defect in anterograde transport of mitochondria with an increase in stationary mitochondria.

Mitochondrial fragmentation observed in AFG3L2 depleted neurons mimicks that in non-polarised cells (Ehses et al., 2009). Is mitochondrial fragmentation sufficient to cause mitochondrial transport defects? We downregulated *Opa1*, a dynamin related GTPase, responsible for inner mitochondrial membrane fusion to cause mitochondrial fragmentation. Fragmentation of mitochondria did not effect any kind of mitochondrial transport in axons indicating that fragmentation is not sufficient to cause mitochondrial transport defect, as was observed previously (Misko et al., 2010).

Axons depleted for AFG3L2 had reduced mitochondrial occupancy meaning less mitochondrial mass was present per unit length of axon. Parkin is known to mediate the turnover of damaged mitochondria (Narendra et al., 2008), but we do not find any parkin recruitment on the mitochondria in AFG3L2 depleted neurons. It is possible that reduced mitochondrial occupancy observed in AFG3L2 deficient neurons is mediated by parkin-independent mechanisms. To this end, it can be comprehended that disposal of damaged mitochondrial portions occur by formation of mitochondrial derived vesicles (MDVs). Such a phenomenon has been proposed to be an early response mechanism much before mitophagy acts as a quality control mechanism (McLelland et al., 2014). In neurons, it has been proposed that autophagosomes are formed at the distal tip and mature as they travel retrogradely by undergoing acidification (Maday et al., 2012). Such a process may involve high-energy expenditure and hence it is advantageous for the neurons to employ MDVs to discard damaged mitochondrial portions. Mitochondrial membrane potential in *Afg3l2* depleted

neuron is largely unchanged disproving the hypothesis that mitochondrial membrane potential and transport are correlated (Miller and Sheetz, 2004).

We observed a selective defect of anterograde transport of mitochondria but not in the velocity of mitochondria. It is also noteworthy that such a defect has been observed in other neurodegenerative conditions. Examples include: 1) aberrations in *SPG4* encoding spastin, a microtubule severing protein, causes HSP. *Spast*^{ΔE7/ΔE7} mice displayed gait defects at 7 months of age. On the cellular level, anterograde transport of mitochondria as well as APP vesicles was impaired in primary cortical neuronal culture. Axonal swellings were observed in spinal cords of *Spast*^{ΔE7/ΔE7} mice and patients, which stained immunopositive for APP, tau, mitochondria and neurofilaments, indicating neurodegeneration (Kasher et al., 2009); 2) Mutations in antioxidant SOD1 result in familial forms of Amyotrophic Lateral Sclerosis (ALS), a motor neuron neurodegenerative disease accompanied by muscle atrophy, spasticity and dysarthria. Motor neurons harvested from SOD1^{G93A} transgenic mice displayed reduced anterograde transport and enhanced retrograde transport of mitochondria (De Vos et al., 2007); 3) Primary striatal neurons expressing mutant Huntington displayed decreased anterograde and retrograde mitochondrial velocities (Trushina et al., 2004). Such a response to decrease the anterograde transport may be solicited as the quality control mechanisms of mitochondria may be compromised (Rugarli and Langer, 2012).

As mentioned before, depletion of *m*-AAA protease activates OMA1, which proteolytic cleaves long isoforms of OPA1 into short forms. OMA1 has been shown to be activated by a variety of stress responses like CCCP (abolishes

mitochondrial membrane potential), Oligomycin (ATP synthase inhibitor), antimycin (complex III inhibitor), rotenone (Complex I inhibitor) and heat shock (Baker et al., 2014). Therefore, OMA1 could be the sensor that senses and transmits the mitochondrial stress to cleave OPA1 into short forms. If this is a possibility then the mitochondrial anterograde transport defect in neurons could be a downstream event. To this end, we used neurons from *Oma1*^{-/-} mice and downregulated *Afg3l2*. We could not observe a rescue of anterograde transport defect of mitochondria upon concomitant depletion of OMA1 and AFG3L2 suggesting that OMA1 mediated mitochondrial fragmentation and mitochondrial transport defects observed in AFG3L2 depleted neurons are independent events.

There is also an increase in the number of stationary mitochondria in axons upon *Afg3l2* downregulation. A possible explanation could be a physical steric hindrance caused by mitochondrial swelling. It was observed that mere mitochondrial swelling, obtained by treatment of neurons with inhibitors of ETC like antimycin and sodium azide, caused mitochondrial transport defects (Kaasik et al., 2007).

Impaired mitochondrial dynamics due to OMA1 activation as a cause of anterograde mitochondrial transport defect was ruled out. However, we observed that concurrent downregulation of *Afg3l2* and *tau* rescued anterograde mitochondrial transport when compared to downregulation of *Afg3l2* alone. Therefore, cytoskeletal modifications can underlie mitochondrial transport defect observed in AFG3L2 deficient neurons. In congruence, constitutive and constitutional mouse models of *Afg3l2* display tau (a microtubule-associated protein (MAP) binding and stabilizing microtubules) hyperphosphorylation in

the cortex and hippocampus (Kondadi et al., 2014) at sites phosphorylated in Alzheimer's disease (Thr181, Ser199, Ser202, Thr205 and Ser396) (Duka et al., 2013). Similarly, tau hyperphosphorylation was observed in fore-brain specific knockout of *Prohibitin 2* succumbing to neurodegeneration (Merkwirth et al., 2012) where Prohibitin 1 and 2 form large scaffold complexes in the inner mitochondrial membrane and stabilize OPA1. Tau overexpression in mature hippocampal neurons led to degeneration of synapses accompanied by missorting of tau into the somatodendritic compartment (Thies and Mandelkow, 2007). MARK2/Par-1 transfected neurons showed a rescue of the aberrations induced by tau via its phosphorylation including mitochondrial transport into the axons. Hence, it was proposed that tau phosphorylation detaches tau from the microtubules laying clear microtubule tracks to efficiently transport mitochondria. However, sustained hyperphosphorylation can lead tau to assemble into paired helical filaments (Alonso et al., 2001; Ballatore et al., 2007) and form insoluble aggregates. Therefore, tau phosphorylation can be beneficial at lower concentrations whereas it can cause pathological consequences at a higher concentration. Overexpression of tau has been shown to impair anterograde transport of organelles including mitochondria (Ebner et al., 1998). Knockdown of *milton*, an adaptor connecting mitochondria and kinesin motor (equivalent to TRAKs in mammals) in *Drosophila* results in neurodegeneration accompanied by tau hyperphosphorylation at Alzheimer's disease related site Ser262 (Iijima-Ando et al., 2012). Depletion of tau rescued the neurodegeneration. Our observation of tau downregulation rescuing the anterograde mitochondrial transport, albeit partially, reinforces the notion that tau reduction is beneficial under pathological conditions.

It is intriguing to observe a selective anterograde transport defect. How can a selective anterograde transport defect occur? Single-molecule studies demonstrated that when single kinesin-GFP motors encountered tau patches, they detached from the MT surface. However, dynein motor was less sensitive having a similar effect only when tau was used at ten times higher concentration (Dixit et al., 2008). Therefore, higher sensitivity of the kinesin motor to tau concentration could be sufficient to induce anterograde transport defect by transporting lesser percentage of mitochondria. Additional mechanisms exist in neurons to hinder transport of unhealthy or inefficient organelles to distal part of the axon. PINK1 (a Ser/Thr kinase) is known to phosphorylate Miro, a protein which anchors motor proteins and mitochondria via Milton (in *Drosophila*) or TRAKs (in mammals). Parkin (a ubiquitin ligase) degrades Miro after its phosphorylation. So, the connection between mitochondria and motors is severed leading to stalling of the mitochondria on the microtubules (Wang et al., 2011). Is it possible that ROS can act as a signal to modify the adaptors or motors?

We observe that antioxidant NAC rescues the mitochondrial transport defects observed in *Afg3l2* downregulated neurons. In this context, it is tempting to speculate that ROS may modify adaptors or motors responsible for organellar transport. Primary neurons treated with hydrogen peroxide also exhibited anterograde transport defect of mitochondria before axonal beading in neurodegeneration (Fang et al., 2012). Hence, anterograde transport defect may be an early event in ROS induced neurodegeneration. *Afg3l2*^{Emv66/+} mice show increased carbonylation of proteins in the mitochondrial fractions of brain

lysates (Maltecca et al., 2009), due to deficiencies in complex I and III (Maltecca et al., 2008). Hence, *m*-AAA deficient mice show enhanced mitochondrial ROS production. Murine neurons treated with Parkinsonian mimetic, MPP⁺ reduces mitochondrial anterograde transport that can be rescued by treatment with NAC. Enhanced autophagy occurs in dopamine axons treated with MPP⁺ (Kim-Han et al., 2011). Consistently, autophagy had been implicated in neurodegeneration. For instance, mice deficient in ATG7 in the central nervous system displayed growth retardation, tremors, abnormal limb-clasping and motor defects (Komatsu et al., 2006). Therefore, it remains to be tested if constitutive and conditional knockout mouse models of *Afg3l2* display aberrant autophagy.

We also observed a rescue of anterograde transport of mitochondria by culturing AFG3L2 depleted neurons in the presence of vitamin E. Vitamin E acts by scavenging peroxy radicals (Yu, 1994). NAC (N-acetyl cysteine) supplies cysteine and helps in the formation of glutathione (which is made of amino acids cysteine, glutamate and glycine). Reduced glutathione gets oxidized to reduce incompletely oxidized ROS and helps to maintain the redox status of the cell (Kerksick and Willoughby, 2005). However, a direct role of NAC in quenching hydrogen peroxide and hydroxyl ions has been proposed. It does not however react with superoxide radicals (Aruoma et al., 1989). NAC has a greater effect while rescuing mitochondrial transport defects compared to vitamin E. It is possible that additional functions of NAC apart from antioxidant activity contribute to this process. In general, NAC decreases the amounts of most of the cytoskeletal components modestly. This can be due to the redox modifications in the protein structure of actin (Dalle-Donne et al., 2001), tubulin (Landino et al.,

2004a) and tau (Landino et al., 2004b). Cell Rox green, a fluorogenic dye showing higher fluorescence upon interacting with ROS, exhibited higher fluorescence in the soma of primary neurons upon treatment with menadione (ROS inducer). This was reduced upon treatment with NAC and vitamin E confirming their antioxidant nature at the concentrations we used. However, consistent pattern of ROS levels could not be obtained in *Afg3l2* downregulated neurons when compared to control neurons. The levels of downregulation obtained in different experiments might not overcome a critical threshold to observe increased ROS levels in all experiments. We observed an interesting connecting between ROS and status of tau hyperphosphorylation (Kondadi et al., 2014). It was shown that antioxidants decrease tau hyperphosphorylation, which correlates to rescue of the mitochondrial transport defects in AFG3L2 depleted neurons. So, the rescue of transport defects might be due to a decreased tau hyperphosphorylation.

Hence, it can be inferred that respiratory deficiencies resulting from loss of AFG3L2 can lead to increased production of ROS (Almajan et al., 2012; Maltecca et al., 2009), which subsequently causes anterograde transport defects. AFG3L2 depletion can cause ROS mediated tau hyperphosphorylation (Kondadi et al., 2014). Antioxidants and tau reduction rescue the mitochondrial transport defects probably by modulating tau hyperphosphorylation. Finally, we propose that ROS can be a central player linking mitochondrial transport and cytoskeletal modifications. Impaired anterograde transport defects characterized by normal retrograde transport could result in depletion of mitochondria in the distal regions of axons causing neurodegeneration. However, the mechanisms by which ROS can manipulate the motors/adaptors to regulate mitochondrial

transport is largely unknown. More experiments need to be done to understand the interplay of ROS, mitochondrial adaptors/motors and transport.

References

REFERENCES:

1. Alavi, M.V., Bette, S., Schimpf, S., Schuettauf, F., Schraermeyer, U., Wehrl, H.F., Ruttiger, L., Beck, S.C., Tonagel, F., Pichler, B.J., *et al.* (2007). A splice site mutation in the murine Opa1 gene features pathology of autosomal dominant optic atrophy. *Brain : a journal of neurology* 130, 1029-1042.
2. Alexander, C., Votruba, M., Pesch, U.A., and Thiselton, D.L. (2000a). OPA1, encoding a dynamin-related GTPase, is mutated in autosomal dominant optic atrophy linked to chromosome 3q28. *Nature*.
3. Alexander, C., Votruba, M., Pesch, U.E., Thiselton, D.L., Mayer, S., Moore, A., Rodriguez, M., Kellner, U., Leo-Kottler, B., Auburger, G., *et al.* (2000b). OPA1, encoding a dynamin-related GTPase, is mutated in autosomal dominant optic atrophy linked to chromosome 3q28. *Nature genetics* 26, 211-215.
4. Almajan, E.R., Richter, R., Paeger, L., Martinelli, P., Barth, E., Decker, T., Larsson, N.G., Kloppenburg, P., Langer, T., and Rugarli, E.I. (2012). AFG3L2 supports mitochondrial protein synthesis and Purkinje cell survival. *J Clin Invest* 122, 4048-4058.
5. Alonso, A., Zaidi, T., Novak, M., Grundke-Iqbal, I., and Iqbal, K. (2001). Hyperphosphorylation induces self-assembly of tau into tangles of paired helical filaments/straight filaments. *Proceedings of the National Academy of Sciences of the United States of America* 98, 6923-6928.
6. Arakawa, M., and Ito, Y. (2007). N-acetylcysteine and neurodegenerative diseases: basic and clinical pharmacology. *Cerebellum* 6, 308-314.
7. Arlt, H., Tauer, R., Feldmann, H., Neupert, W., and Langer, T. (1996). The YTA10-12 complex, an AAA protease with chaperone-like activity in the inner membrane of mitochondria. *Cell* 85, 875-885.
8. Arnold, C.S., Johnson, G.V., Cole, R.N., Dong, D.L., Lee, M., and Hart, G.W. (1996). The microtubule-associated protein tau is extensively modified with O-linked N-acetylglucosamine. *The Journal of biological chemistry* 271, 28741-28744.
9. Arnoldi, A., Tonelli, A., Crippa, F., Villani, G., Pacelli, C., Sironi, M., Pozzoli, U., D'Angelo, M.G., Meola, G., Martinuzzi, A., *et al.* (2008). A clinical, genetic, and biochemical characterization of SPG7 mutations in a large cohort of patients with hereditary spastic paraplegia. *Human mutation* 29, 522-531.
10. Aruoma, O.I., Halliwell, B., Hoey, B.M., and Butler, J. (1989). The antioxidant action of N-acetylcysteine: its reaction with hydrogen peroxide, hydroxyl radical, superoxide, and hypochlorous acid. *Free radical biology & medicine* 6, 593-597.

11. Atorino, L., Silvestri, L., Koppen, M., Cassina, L., Ballabio, A., Marconi, R., Langer, T., and Casari, G. (2003). Loss of m-AAA protease in mitochondria causes complex I deficiency and increased sensitivity to oxidative stress in hereditary spastic paraplegia. *J Cell Biol* 163, 777-787.
12. Augustin, S., Gerdes, F., Lee, S., Tsai, F.T., Langer, T., and Tatsuta, T. (2009). An intersubunit signaling network coordinates ATP hydrolysis by m-AAA proteases. *Molecular cell* 35, 574-585.
13. Baker, M.J., Lampe, P.A., Stojanovski, D., Korwitz, A., Anand, R., Tatsuta, T., and Langer, T. (2014). Stress-induced OMA1 activation and autocatalytic turnover regulate OPA1-dependent mitochondrial dynamics. *The EMBO journal* 33, 578-593.
14. Ballatore, C., Lee, V.M., and Trojanowski, J.Q. (2007). Tau-mediated neurodegeneration in Alzheimer's disease and related disorders. *Nature reviews Neuroscience* 8, 663-672.
15. Beilina, A., Van Der Brug, M., Ahmad, R., Kesavapany, S., Miller, D.W., Petsko, G.A., and Cookson, M.R. (2005). Mutations in PTEN-induced putative kinase 1 associated with recessive parkinsonism have differential effects on protein stability. *Proceedings of the National Academy of Sciences of the United States of America* 102, 5703-5708.
16. Bereiter-Hahn, J., and Voth, M. (1994). Dynamics of mitochondria in living cells: shape changes, dislocations, fusion, and fission of mitochondria. *Microsc Res Tech* 27, 198-219.
17. Bonn, F., Tatsuta, T., Petrunaro, C., Riemer, J., and Langer, T. (2011). Presequence-dependent folding ensures MrpL32 processing by the m-AAA protease in mitochondria. *The EMBO journal* 30, 2545-2556.
18. Bradford, M.M. (1976). A rapid and sensitive method for the quantitation of microgram quantities of protein utilizing the principle of protein-dye binding. *Analytical biochemistry* 72, 248-254.
19. Brickley, K., and Stephenson, F.A. (2011). Trafficking kinesin protein (TRAK)-mediated transport of mitochondria in axons of hippocampal neurons. *The Journal of biological chemistry* 286, 18079-18092.
20. Bullmann, T., Holzer, M., Mori, H., and Arendt, T. (2009). Pattern of tau isoforms expression during development in vivo. *International journal of developmental neuroscience : the official journal of the International Society for Developmental Neuroscience* 27, 591-597.
21. Cagnoli, C., Mariotti, C., Taroni, F., Seri, M., and Brussino, A. (2006). SCA28, a novel form of autosomal dominant cerebellar ataxia on chromosome 18p11.22-q11.2.pdf.
22. Cagnoli, C., Stevanin, G., Brussino, A., Barberis, M., Mancini, C., Margolis, R.L., Holmes, S.E., Nobili, M., Forlani, S., Padovan, S., *et al.* (2010). Missense mutations in the AFG3L2 proteolytic domain account for approximately 1.5% of European autosomal dominant cerebellar ataxias. *Human mutation* 31, 1117-1124.

23. Casari, G., De Fusco, M., Ciarmatori, S., Zeviani, M., Mora, M., Fernandez, P., De Michele, G., Filla, A., Coccozza, S., Marconi, R., *et al.* (1998). Spastic paraplegia and OXPHOS impairment caused by mutations in paraplegin, a nuclear-encoded mitochondrial metalloprotease. *Cell* 93, 973-983.
24. Chan, D.C. (2006). Mitochondrial fusion and fission in mammals. *Annual review of cell and developmental biology* 22, 79-99.
25. Chang, C.R., Manlandro, C.M., Arnoult, D., Stadler, J., Posey, A.E., Hill, R.B., and Blackstone, C. (2010). A lethal de novo mutation in the middle domain of the dynamin-related GTPase Drp1 impairs higher order assembly and mitochondrial division. *The Journal of biological chemistry* 285, 32494-32503.
26. Chen, H., Detmer, S.A., Ewald, A.J., Griffin, E.E., Fraser, S.E., and Chan, D.C. (2003). Mitofusins Mfn1 and Mfn2 coordinately regulate mitochondrial fusion and are essential for embryonic development. *The Journal of cell biology* 160, 189-200.
27. Chen, H., McCaffery, J.M., and Chan, D.C. (2007). Mitochondrial fusion protects against neurodegeneration in the cerebellum. *Cell* 130, 548-562.
28. Chen, H., Vermulst, M., Wang, Y.E., Chomyn, A., Prolla, T.A., McCaffery, J.M., and Chan, D.C. (2010). Mitochondrial fusion is required for mtDNA stability in skeletal muscle and tolerance of mtDNA mutations. *Cell* 141, 280-289.
29. Chen, Y., and Dorn, G.W., 2nd (2013). PINK1-phosphorylated mitofusin 2 is a Parkin receptor for culling damaged mitochondria. *Science* 340, 471-475.
30. Criddle, D.N., Gillies, S., Baumgartner-Wilson, H.K., Jaffar, M., Chinje, E.C., Passmore, S., Chvanov, M., Barrow, S., Gerasimenko, O.V., Tepikin, A.V., *et al.* (2006). Menadione-induced reactive oxygen species generation via redox cycling promotes apoptosis of murine pancreatic acinar cells. *The Journal of biological chemistry* 281, 40485-40492.
31. Dalle-Donne, I., Rossi, R., Milzani, A., Di Simplicio, P., and Colombo, R. (2001). The actin cytoskeleton response to oxidants: from small heat shock protein phosphorylation to changes in the redox state of actin itself. *Free radical biology & medicine* 31, 1624-1632.
32. Davies, V.J., Hollins, A.J., Piechota, M.J., Yip, W., Davies, J.R., White, K.E., Nicols, P.P., Boulton, M.E., and Votruba, M. (2007). Opa1 deficiency in a mouse model of autosomal dominant optic atrophy impairs mitochondrial morphology, optic nerve structure and visual function. *Human molecular genetics* 16, 1307-1318.
33. Dawson, H.N., Ferreira, A., Eyster, V.M., Ghoshal, N., Binder, L.I., and Vitek, M.P. (2001). Inhibition of neuronal maturation in primary hippocampal neurons from tau deficient mice. *Journal of cell science*.
34. De Vos, K.J., Chapman, A.L., Tennant, M.E., Manser, C., Tudor, E.L., Lau, K.F., Brownlees, J., Ackerley, S., Shaw, P.J., McLoughlin, D.M., *et al.* (2007).

- Familial amyotrophic lateral sclerosis-linked SOD1 mutants perturb fast axonal transport to reduce axonal mitochondria content. *Human molecular genetics* 16, 2720-2728.
35. Delettre, C., Griffoin, J.M., Kaplan, J., Dollfus, H., Lorenz, B., Faivre, L., Lenaers, G., Belenguer, P., and Hamel, C.P. (2001). Mutation spectrum and splicing variants in the OPA1 gene. *Human genetics* 109, 584-591.
 36. Delettre, C., Lenaers, G., Griffoin, J.M., Gigarel, N., Lorenzo, C., Belenguer, P., Pelloquin, L., Grosgeorge, J., Turc-Carel, C., Perret, E., *et al.* (2000). Nuclear gene OPA1, encoding a mitochondrial dynamin-related protein, is mutated in dominant optic atrophy. *Nature genetics* 26, 207-210.
 37. Di Bella, D., Lazzaro, F., Brusco, A., Plumari, M., Battaglia, G., Pastore, A., Finardi, A., Cagnoli, C., Tempia, F., Frontali, M., *et al.* (2010). Mutations in the mitochondrial protease gene AFG3L2 cause dominant hereditary ataxia SCA28. *Nature genetics* 42, 313-321.
 38. Dixit, R., Ross, J.L., Goldman, Y.E., and Holzbaur, E.L. (2008). Differential regulation of dynein and kinesin motor proteins by tau. *Science* 319, 1086-1089.
 39. Dubey, M., Chaudhury, P., Kabiru, H., and Shea, T.B. (2008). Tau inhibits anterograde axonal transport and perturbs stability in growing axonal neurites in part by displacing kinesin cargo: neurofilaments attenuate tau-mediated neurite instability. *Cell motility and the cytoskeleton* 65, 89-99.
 40. DuBoff, B., Gotz, J., and Feany, M.B. (2012). Tau promotes neurodegeneration via DRP1 mislocalization in vivo. *Neuron* 75, 618-632.
 41. Duka, V., Lee, J.H., Credle, J., Wills, J., Oaks, A., Smolinsky, C., Shah, K., Mash, D.C., Masliah, E., and Sidhu, A. (2013). Identification of the sites of tau hyperphosphorylation and activation of tau kinases in synucleinopathies and Alzheimer's diseases. *PloS one* 8, e75025.
 42. Duncan, J.E., and Goldstein, L.S. (2006). The genetics of axonal transport and axonal transport disorders. *PLoS genetics* 2, e124.
 43. Ebner, A., Godemann, R., Stamer, K., Illenberger, S., Trinczek, B., and Mandelkow, E. (1998). Overexpression of tau protein inhibits kinesin-dependent trafficking of vesicles, mitochondria, and endoplasmic reticulum: implications for Alzheimer's disease. *The Journal of cell biology* 143, 777-794.
 44. Ehrenberg, B., Montana, V., Wei, M.D., Wuskell, J.P., and Loew, L.M. (1988). Membrane potential can be determined in individual cells from the nernstian distribution of cationic dyes. *Biophysical journal* 53, 785-794.
 45. Ehses, S., Raschke, I., Mancuso, G., Bernacchia, A., Geimer, S., Tondera, D., Martinou, J.C., Westermann, B., Rugarli, E.I., and Langer, T. (2009). Regulation of OPA1 processing and mitochondrial fusion by m-AAA protease isoenzymes and OMA1. *The Journal of cell biology* 187, 1023-1036.

46. Eura, Y., Ishihara, N., Yokota, S., and Mihara, K. (2003). Two mitofusin proteins, mammalian homologues of FZO, with distinct functions are both required for mitochondrial fusion. *Journal of biochemistry* 134, 333-344.
47. Falzone, T.L., Stokin, G.B., Lillo, C., Rodrigues, E.M., Westerman, E.L., Williams, D.S., and Goldstein, L.S. (2009). Axonal stress kinase activation and tau misbehavior induced by kinesin-1 transport defects. *The Journal of neuroscience : the official journal of the Society for Neuroscience* 29, 5758-5767.
48. Fang, C., Bourdette, D., and Banker, G. (2012). Oxidative stress inhibits axonal transport: implications for neurodegenerative diseases. *Molecular neurodegeneration* 7, 29.
49. Ferreira, F., Quattrini, A., Pirozzi, M., Valsecchi, V., Dina, G., Broccoli, V., Auricchio, A., Piemonte, F., Tozzi, G., Gaeta, L., *et al.* (2004). Axonal degeneration in paraplegin-deficient mice is associated with abnormal mitochondria and impairment of axonal transport. *Journal of Clinical Investigation* 113, 231-242.
50. Goldstein, L.S., and Yang, Z. (2000). Microtubule-based transport systems in neurons: the roles of kinesins and dyneins. *Annual review of neuroscience* 23, 39-71.
51. Grundke-Iqbal, I., Iqbal, K., Quinlan, M., Tung, Y.C., Zaidi, M.S., and Wisniewski, H.M. (1986). Microtubule-associated protein tau. A component of Alzheimer paired helical filaments. *The Journal of biological chemistry* 261, 6084-6089.
52. Hanson, P.I., and Whiteheart, S.W. (2005). AAA+ proteins: have engine, will work. *Nature reviews Molecular cell biology* 6, 519-529.
53. Harada, A., Oguchi, K., Okabe, S., Kuno, J., Terada, S., Ohshima, T., Sato-Yoshitake, R., Takei, Y., Noda, T., and Hirokawa, N. (1994). Altered Microtubule organization in small-calibre axons of mice lacking tau protein
54. Harada, A., Takei, Y., Kanai, Y., Tanaka, Y., Nonaka, S., and Hirokawa, N. (1998). Golgi vesiculation and lysosome dispersion in cells lacking cytoplasmic dynein. *The Journal of cell biology* 141, 51-59.
55. Head, B., Griparic, L., Amiri, M., Gandre-Babbe, S., and van der Bliek, A.M. (2009). Inducible proteolytic inactivation of OPA1 mediated by the OMA1 protease in mammalian cells. *The Journal of cell biology* 187, 959-966.
56. Hirokawa, N., Niwa, S., and Tanaka, Y. (2010). Molecular motors in neurons: transport mechanisms and roles in brain function, development, and disease. *Neuron* 68, 610-638.
57. Hirokawa, N., and Noda, Y. (2008). Intracellular transport and kinesin superfamily proteins, KIFs: structure, function, and dynamics. *Physiological reviews* 88, 1089-1118.

58. Iijima-Ando, K., Sekiya, M., Maruko-Otake, A., Ohtake, Y., Suzuki, E., Lu, B., and Iijima, K.M. (2012). Loss of axonal mitochondria promotes tau-mediated neurodegeneration and Alzheimer's disease-related tau phosphorylation via PAR-1. *PLoS genetics* 8, e1002918.
59. Ishihara, N., Nomura, M., Jofuku, A., Kato, H., Suzuki, S.O., Masuda, K., Otera, H., Nakanishi, Y., Nonaka, I., Goto, Y., *et al.* (2009). Mitochondrial fission factor Drp1 is essential for embryonic development and synapse formation in mice. *Nature cell biology* 11, 958-966.
60. Jho, Y.S., Zhulina, E.B., Kim, M.W., and Pincus, P.A. (2010). Monte carlo simulations of tau proteins: effect of phosphorylation. *Biophysical journal* 99, 2387-2397.
61. Jin, S.M., Lazarou, M., Wang, C., Kane, L.A., Narendra, D.P., and Youle, R.J. (2010). Mitochondrial membrane potential regulates PINK1 import and proteolytic destabilization by PARL. *The Journal of cell biology* 191, 933-942.
62. Kaasik, A., Safiulina, D., Choubey, V., Kuim, M., Zharkovsky, A., and Veksler, V. (2007). Mitochondrial swelling impairs the transport of organelles in cerebellar granule neurons. *The Journal of biological chemistry* 282, 32821-32826.
63. Kageyama, Y., Zhang, Z., Roda, R., Fukaya, M., Wakabayashi, J., Wakabayashi, N., Kensler, T.W., Reddy, P.H., Iijima, M., and Sesaki, H. (2012). Mitochondrial division ensures the survival of postmitotic neurons by suppressing oxidative damage. *The Journal of cell biology* 197, 535-551.
64. Karata, K., Inagawa, T., Wilkinson, A.J., Tatsuta, T., and Ogura, T. (1999). Dissecting the role of a conserved motif (the second region of homology) in the AAA family of ATPases. Site-directed mutagenesis of the ATP-dependent protease FtsH. *The Journal of biological chemistry* 274, 26225-26232.
65. Karki, S., and Holzbaur, E.L. (1999). Cytoplasmic dynein and dynactin in cell division and intracellular transport. *Current opinion in cell biology* 11, 45-53.
66. Kaser, M., Kambacheld, M., Kisters-Woike, B., and Langer, T. (2003). Oma1, a novel membrane-bound metallopeptidase in mitochondria with activities overlapping with the m-AAA protease. *The Journal of biological chemistry* 278, 46414-46423.
67. Kashatus, D.F., Lim, K.H., Brady, D.C., Pershing, N.L., Cox, A.D., and Counter, C.M. (2011). RALA and RALBP1 regulate mitochondrial fission at mitosis. *Nature cell biology* 13, 1108-1115.
68. Kasher, P.R., De Vos, K.J., Wharton, S.B., Manser, C., Bennett, E.J., Bingley, M., Wood, J.D., Milner, R., McDermott, C.J., Miller, C.C., *et al.* (2009). Direct evidence for axonal transport defects in a novel mouse model of mutant

- spastin-induced hereditary spastic paraplegia (HSP) and human HSP patients. *Journal of neurochemistry* 110, 34-44.
69. Kerksick, C., and Willoughby, D. (2005). The antioxidant role of glutathione and N-acetyl-cysteine supplements and exercise-induced oxidative stress. *Journal of the International Society of Sports Nutrition* 2, 38-44.
 70. Kim, Y., Park, J., Kim, S., Song, S., Kwon, S.K., Lee, S.H., Kitada, T., Kim, J.M., and Chung, J. (2008). PINK1 controls mitochondrial localization of Parkin through direct phosphorylation. *Biochemical and biophysical research communications* 377, 975-980.
 71. Kim-Han, J.S., Antenor-Dorsey, J.A., and O'Malley, K.L. (2011). The parkinsonian mimetic, MPP+, specifically impairs mitochondrial transport in dopamine axons. *The Journal of neuroscience : the official journal of the Society for Neuroscience* 31, 7212-7221.
 72. Komatsu, M., Waguri, S., Chiba, T., Murata, S., Iwata, J., Tanida, I., Ueno, T., Koike, M., Uchiyama, Y., Kominami, E., *et al.* (2006). Loss of autophagy in the central nervous system causes neurodegeneration in mice. *Nature* 441, 880-884.
 73. Kondadi, A.K., Wang, S., Montagner, S., Kladt, N., Korwitz, A., Martinelli, P., Herholz, D., Baker, M.J., Schauss, A.C., Langer, T., *et al.* (2014). Loss of the m-AAA protease subunit AFG3L2 causes mitochondrial transport defects and tau hyperphosphorylation. *The EMBO journal*.
 74. Koppen, M., Metodiev, M.D., Casari, G., Rugarli, E.I., and Langer, T. (2007). Variable and tissue-specific subunit composition of mitochondrial m-AAA protease complexes linked to hereditary spastic paraplegia. *Molecular and cellular biology* 27, 758-767.
 75. Kosik, K.S., Joachim, C.L., and Selkoe, D.J. (1986). Microtubule-associated protein tau (tau) is a major antigenic component of paired helical filaments in Alzheimer disease. *Proceedings of the National Academy of Sciences of the United States of America* 83, 4044-4048.
 76. Kremmidiotis, G., Gardner, A.E., Settasatian, C., Savoia, A., Sutherland, G.R., and Callen, D.F. (2001). Molecular and functional analyses of the human and mouse genes encoding AFG3L1, a mitochondrial metalloprotease homologous to the human spastic paraplegia protein. *Genomics* 76, 58-65.
 77. LaMonte, B.H., Wallace, K.E., Holloway, B.A., Shelly, S.S., Ascano, J., Tokito, M., Van Winkle, T., Howland, D.S., and Holzbaur, E.L. (2002). Disruption of dynein/dynactin inhibits axonal transport in motor neurons causing late-onset progressive degeneration. *Neuron* 34, 715-727.
 78. Landino, L.M., Moynihan, K.L., Todd, J.V., and Kennett, K.L. (2004a). Modulation of the redox state of tubulin by the glutathione/glutaredoxin reductase system. *Biochemical and biophysical research communications* 314, 555-560.

79. Landino, L.M., Robinson, S.H., Skreslet, T.E., and Cabral, D.M. (2004b). Redox modulation of tau and microtubule-associated protein-2 by the glutathione/glutaredoxin reductase system. *Biochemical and biophysical research communications* 323, 112-117.
80. Lawrence, C.J., Dawe, R.K., Christie, K.R., Cleveland, D.W., Dawson, S.C., Endow, S.A., Goldstein, L.S., Goodson, H.V., Hirokawa, N., Howard, J., *et al.* (2004). A standardized kinesin nomenclature. *The Journal of cell biology* 167, 19-22.
81. Lee, S., Augustin, S., Tatsuta, T., Gerdes, F., Langer, T., and Tsai, F.T. (2011). Electron cryomicroscopy structure of a membrane-anchored mitochondrial AAA protease. *The Journal of biological chemistry* 286, 4404-4411.
82. Lee, V.M., Goedert, M., and Trojanowski, J.Q. (2001). Neurodegenerative tauopathies. *Annual review of neuroscience* 24, 1121-1159.
83. Llorens-Martin, M., Lopez-Domenech, G., Soriano, E., and Avila, J. (2011). GSK3beta is involved in the relief of mitochondria pausing in a Tau-dependent manner. *PloS one* 6, e27686.
84. Lobbe, A.M., Kang, J.S., Hilker, R., Hackstein, H., Muller, U., and Nolte, D. (2014). A Novel Missense Mutation in AFG3L2 Associated with Late Onset and Slow Progression of Spinocerebellar Ataxia Type 28. *Journal of molecular neuroscience : MN* 52, 493-496.
85. Maday, S., Wallace, K.E., and Holzbaur, E.L. (2012). Autophagosomes initiate distally and mature during transport toward the cell soma in primary neurons. *The Journal of cell biology* 196, 407-417.
86. Maltecca, F., Aghaie, A., Schroeder, D.G., Cassina, L., Taylor, B.A., Phillips, S.J., Malaguti, M., Previtali, S., Guenet, J.L., Quattrini, A., *et al.* (2008). The mitochondrial protease AFG3L2 is essential for axonal development. *The Journal of neuroscience : the official journal of the Society for Neuroscience* 28, 2827-2836.
87. Maltecca, F., Magnoni, R., Cerri, F., Cox, G.A., Quattrini, A., and Casari, G. (2009). Haploinsufficiency of AFG3L2, the gene responsible for spinocerebellar ataxia type 28, causes mitochondria-mediated Purkinje cell dark degeneration. *The Journal of neuroscience : the official journal of the Society for Neuroscience* 29, 9244-9254.
88. Mandelkow, E.M., Schweers, O., Drewes, G., Biernat, J., Gustke, N., Trinczek, B., and Mandelkow, E. (1996). Structure, microtubule interactions, and phosphorylation of tau protein. *Annals of the New York Academy of Sciences* 777, 96-106.
89. Mariotti, C., Brusco, A., Di Bella, D., Cagnoli, C., Seri, M., Gellera, C., Di Donato, S., and Taroni, F. (2008). Spinocerebellar ataxia type 28: a novel autosomal dominant cerebellar ataxia characterized by slow progression and ophthalmoparesis. *Cerebellum* 7, 184-188.

90. Martin, L., Latypova, X., Wilson, C.M., Magnaudeix, A., Perrin, M.L., Yardin, C., and Terro, F. (2013). Tau protein kinases: involvement in Alzheimer's disease. *Ageing research reviews* 12, 289-309.
91. Martinelli, P., La Mattina, V., Bernacchia, A., Magnoni, R., Cerri, F., Cox, G., Quattrini, A., Casari, G., and Rugarli, E.I. (2009). Genetic interaction between the m-AAA protease isoenzymes reveals novel roles in cerebellar degeneration. *Human molecular genetics* 18, 2001-2013.
92. McLelland, G.L., Soubannier, V., Chen, C.X., McBride, H.M., and Fon, E.A. (2014). Parkin and PINK1 function in a vesicular trafficking pathway regulating mitochondrial quality control. *The EMBO journal* 33, 282-295.
93. Melov, S., Adlard, P.A., Morten, K., Johnson, F., Golden, T.R., Hinerfeld, D., Schilling, B., Mavros, C., Masters, C.L., Volitakis, I., *et al.* (2007). Mitochondrial oxidative stress causes hyperphosphorylation of tau. *PloS one* 2, e536.
94. Melov, S., Doctrow, S.R., Schneider, J.A., Haberson, J., Patel, M., Coskun, P.E., Huffman, K., Wallace, D.C., and Malfroy, B. (2001). Lifespan extension and rescue of spongiform encephalopathy in superoxide dismutase 2 nullizygous mice treated with superoxide dismutase-catalase mimetics. *The Journal of neuroscience : the official journal of the Society for Neuroscience* 21, 8348-8353.
95. Merkwirth, C., Martinelli, P., Korwitz, A., Morbin, M., Bronneke, H.S., Jordan, S.D., Rugarli, E.I., and Langer, T. (2012). Loss of prohibitin membrane scaffolds impairs mitochondrial architecture and leads to tau hyperphosphorylation and neurodegeneration. *PLoS genetics* 8, e1003021.
96. Miller, K.E., and Sheetz, M.P. (2004). Axonal mitochondrial transport and potential are correlated. *Journal of cell science* 117, 2791-2804.
97. Min, S.W., Cho, S.H., Zhou, Y., Schroeder, S., Haroutunian, V., Seeley, W.W., Huang, E.J., Shen, Y., Masliah, E., Mukherjee, C., *et al.* (2010). Acetylation of tau inhibits its degradation and contributes to tauopathy. *Neuron* 67, 953-966.
98. Misko, A., Jiang, S., Wegorzewska, I., Milbrandt, J., and Baloh, R.H. (2010). Mitofusin 2 is necessary for transport of axonal mitochondria and interacts with the Miro/Milton complex. *The Journal of neuroscience : the official journal of the Society for Neuroscience* 30, 4232-4240.
99. Morris, M., Maeda, S., Vossel, K., and Mucke, L. (2011). The many faces of tau. *Neuron* 70, 410-426.
100. Musova, Z., Kaiserova, M., Kriegova, E., Fillerova, R., Vasovcak, P., Santava, A., Mensikova, K., Zumrova, A., Krepelova, A., Sedlacek, Z., *et al.* (2013). A Novel Frameshift Mutation in the AFG3L2 Gene in a Patient with Spinocerebellar Ataxia. *Cerebellum*.

101. Narendra, D., Tanaka, A., Suen, D.F., and Youle, R.J. (2008). Parkin is recruited selectively to impaired mitochondria and promotes their autophagy. *The Journal of cell biology* 183, 795-803.
102. Narendra, D.P., Jin, S.M., Tanaka, A., Suen, D.F., Gautier, C.A., Shen, J., Cookson, M.R., and Youle, R.J. (2010). PINK1 is selectively stabilized on impaired mitochondria to activate Parkin. *PLoS biology* 8, e1000298.
103. Nolden, M., Ehses, S., Koppen, M., Bernacchia, A., Rugarli, E.I., and Langer, T. (2005). The m-AAA protease defective in hereditary spastic paraplegia controls ribosome assembly in mitochondria. *Cell* 123, 277-289.
104. Ono, T., Isobe, K., Nakada, K., and Hayashi, J.I. (2001). Human cells are protected from mitochondrial dysfunction by complementation of DNA products in fused mitochondria. *Nature genetics* 28, 272-275.
105. Pajic, A., Tauer, R., Feldmann, H., Neupert, W., and Langer, T. (1994). Yta10p is required for the ATP-dependent degradation of polypeptides in the inner membrane of mitochondria. *FEBS letters* 353, 201-206.
106. Pierson, T.M., Adams, D., Bonn, F., Martinelli, P., Cherukuri, P.F., Teer, J.K., Hansen, N.F., Cruz, P., Mullikin For The Nisc Comparative Sequencing Program, J.C., Blakesley, R.W., *et al.* (2011). Whole-exome sequencing identifies homozygous AFG3L2 mutations in a spastic ataxia-neuropathy syndrome linked to mitochondrial m-AAA proteases. *PLoS genetics* 7, e1002325.
107. Pirozzi, M., Quattrini, A., Andolfi, G., Dina, G., Malaguti, M.C., Auricchio, A., and Rugarli, E.I. (2006). Intramuscular viral delivery of paraplegin rescues peripheral axonopathy in a model of hereditary spastic paraplegia. *The Journal of clinical investigation* 116, 202-208.
108. Puls, I., Jonnakuty, C., LaMonte, B.H., Holzbaur, E.L., Tokito, M., Mann, E., Floeter, M.K., Bidus, K., Drayna, D., Oh, S.J., *et al.* (2003). Mutant dynactin in motor neuron disease. *Nature genetics* 33, 455-456.
109. Querfurth, H.W., and LaFerla, F.M. (2010). Alzheimer's disease. *The New England journal of medicine* 362, 329-344.
110. Quiros, P.M., Ramsay, A.J., Sala, D., Fernandez-Vizarra, E., Rodriguez, F., Peinado, J.R., Fernandez-Garcia, M.S., Vega, J.A., Enriquez, J.A., Zorzano, A., *et al.* (2012). Loss of mitochondrial protease OMA1 alters processing of the GTPase OPA1 and causes obesity and defective thermogenesis in mice. *The EMBO journal* 31, 2117-2133.
111. Reid, E., Kloos, M., Ashley-Koch, A., Hughes, L., Bevan, S., Svenson, I.K., Graham, F.L., Gaskell, P.C., Dearlove, A., Pericak-Vance, M.A., *et al.* (2002). A kinesin heavy chain (KIF5A) mutation in hereditary spastic paraplegia (SPG10). *American journal of human genetics* 71, 1189-1194.
112. Rugarli, E.I., and Langer, T. (2012). Mitochondrial quality control: a matter of life and death for neurons. *The EMBO journal* 31, 1336-1349.

113. Sapir, T., Frotscher, M., Levy, T., Mandelkow, E.M., and Reiner, O. (2012). Tau's role in the developing brain: implications for intellectual disability. *Human molecular genetics* 21, 1681-1692.
114. Sheng, Z.H., and Cai, Q. (2012). Mitochondrial transport in neurons: impact on synaptic homeostasis and neurodegeneration. *Nature reviews Neuroscience* 13, 77-93.
115. Shirendeb, U.P., Calkins, M.J., Manczak, M., Anekonda, V., Dufour, B., McBride, J.L., Mao, P., and Reddy, P.H. (2012). Mutant huntingtin's interaction with mitochondrial protein Drp1 impairs mitochondrial biogenesis and causes defective axonal transport and synaptic degeneration in Huntington's disease. *Human molecular genetics* 21, 406-420.
116. Smirnova, E., Griparic, L., Shurland, D.L., and van der Bliek, A.M. (2001). Dynamin-related protein Drp1 is required for mitochondrial division in mammalian cells. *Molecular biology of the cell* 12, 2245-2256.
117. Song, Z., Chen, H., Fiket, M., Alexander, C., and Chan, D.C. (2007). OPA1 processing controls mitochondrial fusion and is regulated by mRNA splicing, membrane potential, and Yme1L. *The Journal of cell biology* 178, 749-755.
118. Stamer, K., Vogel, R., Thies, E., Mandelkow, E., and Mandelkow, E.M. (2002). Tau blocks traffic of organelles, neurofilaments, and APP vesicles in neurons and enhances oxidative stress. *The Journal of cell biology* 156, 1051-1063.
119. Stowers, R.S., Megeath, L.J., Gorska-Andrzejak, J., Meinertzhagen, I.A., and Schwarz, T.L. (2002). Axonal transport of mitochondria to synapses depends on mltin, a novel *Drosophila* protein. *Neuron* 36, 1063-1077.
120. Takei, Y., Teng, J., Harada, A., and Hirokawa, N. (2000). Defects in Axonal Elongation and Neuronal Migration in Mice with Disrupted tau and map1b Genes. *Journal of Cell Biology*.
121. Takuma, H., Arawaka, S., and Mori, H. (2003). Isoforms changes of tau protein during development in various species. *Brain research Developmental brain research* 142, 121-127.
122. Tanaka, Y., Kanai, Y., Okada, Y., Nonaka, S., Takeda, S., Harada, A., and Hirokawa, N. (1998). Targeted disruption of mouse conventional kinesin heavy chain, kif5B, results in abnormal perinuclear clustering of mitochondria. *Cell* 93, 1147-1158.
123. Thies, E., and Mandelkow, E.M. (2007). Missorting of tau in neurons causes degeneration of synapses that can be rescued by the kinase MARK2/Par-1. *The Journal of neuroscience : the official journal of the Society for Neuroscience* 27, 2896-2907.
124. Trushina, E., Dyer, R.B., Badger, J.D., 2nd, Ure, D., Eide, L., Tran, D.D., Vrieze, B.T., Legendre-Guillemain, V., McPherson, P.S., Mandavilli, B.S.,

- et al.* (2004). Mutant huntingtin impairs axonal trafficking in mammalian neurons in vivo and in vitro. *Molecular and cellular biology* 24, 8195-8209.
125. Twig, G., Elorza, A., Molina, A.J., Mohamed, H., Wikstrom, J.D., Walzer, G., Stiles, L., Haigh, S.E., Katz, S., Las, G., *et al.* (2008). Fission and selective fusion govern mitochondrial segregation and elimination by autophagy. *EMBO J* 27, 433-446.
 126. van Spronsen, M., Mikhaylova, M., Lipka, J., Schlager, M.A., van den Heuvel, D.J., Kuijpers, M., Wulf, P.S., Keijzer, N., Demmers, J., Kapitein, L.C., *et al.* (2013). TRAK/Milton motor-adaptor proteins steer mitochondrial trafficking to axons and dendrites. *Neuron* 77, 485-502.
 127. Wagner, U., Utton, M., Gallo, J., and Miller, C.C. (1996). Cellular phosphorylation of tau by GSK-3b influences tau binding to microtubules and microtubule organisation. *Journal of cell science*.
 128. Wakabayashi, J., Zhang, Z., Wakabayashi, N., Tamura, Y., Fukaya, M., Kensler, T.W., Iijima, M., and Sesaki, H. (2009). The dynamin-related GTPase Drp1 is required for embryonic and brain development in mice. *The Journal of cell biology* 186, 805-816.
 129. Wang, X., Su, B., Siedlak, S.L., Moreira, P.I., Fujioka, H., Wang, Y., Casadesus, G., and Zhu, X. (2008). Amyloid-beta overproduction causes abnormal mitochondrial dynamics via differential modulation of mitochondrial fission/fusion proteins. *Proc Natl Acad Sci U S A* 105, 19318-19323.
 130. Wang, X., Winter, D., Ashrafi, G., Schlehe, J., Wong, Y.L., Selkoe, D., Rice, S., Steen, J., LaVoie, M.J., and Schwarz, T.L. (2011). PINK1 and Parkin target Miro for phosphorylation and degradation to arrest mitochondrial motility. *Cell* 147, 893-906.
 131. Waterham, H.R., Koster, J., van Roermund, C.W., Mooyer, P.A., Wanders, R.J., and Leonard, J.V. (2007). A lethal defect of mitochondrial and peroxisomal fission. *The New England journal of medicine* 356, 1736-1741.
 132. Weihofen, A., Thomas, K.J., Ostaszewski, B.L., Cookson, M.R., and Selkoe, D.J. (2009). Pink1 forms a multiprotein complex with Miro and Milton, linking Pink1 function to mitochondrial trafficking. *Biochemistry* 48, 2045-2052.
 133. Weingarten, M.D., Lockwood, A.H., Hwo, S.Y., and Kirschner, M.W. (1975). A protein factor essential for microtubule assembly. *Proceedings of the National Academy of Sciences of the United States of America* 72, 1858-1862.
 134. Witman, G.B., Cleveland, D.W., Weingarten, M.D., and Kirschner, M.W. (1976). Tubulin requires tau for growth onto microtubule initiating sites. *Proceedings of the National Academy of Sciences of the United States of America* 73, 4070-4074.

135. Xia, C.H., Roberts, E.A., Her, L.S., Liu, X., Williams, D.S., Cleveland, D.W., and Goldstein, L.S. (2003). Abnormal neurofilament transport caused by targeted disruption of neuronal kinesin heavy chain KIF5A. *The Journal of cell biology* 161, 55-66.
136. Yu, B.P. (1994). Cellular defenses against damage from reactive oxygen species. *Physiological reviews* 74, 139-162.
137. Zhou, C., Huang, Y., Shao, Y., May, J., Prou, D., Perier, C., Dauer, W., Schon, E.A., and Przedborski, S. (2008). The kinase domain of mitochondrial PINK1 faces the cytoplasm. *Proceedings of the National Academy of Sciences of the United States of America* 105, 12022-12027.
138. Zuchner, S., Mersiyanova, I.V., Muglia, M., Bissar-Tadmouri, N., Rochelle, J., Dadali, E.L., Zappia, M., Nelis, E., Patitucci, A., Senderek, J., *et al.* (2004). Mutations in the mitochondrial GTPase mitofusin 2 cause Charcot-Marie-Tooth neuropathy type 2A. *Nature genetics* 36, 449-451.
139. Zunino, R., Schauss, A., Rippstein, P., Andrade-Navarro, M., and McBride, H.M. (2007). The SUMO protease SENP5 is required to maintain mitochondrial morphology and function. *Journal of cell science* 120, 1178-1188.

ACKNOWLEDGEMENTS

I would like to express my gratitude to my mentor and guide, Elena Rugarli. It has been a pleasant scientific journey with her. She has been encouraging and motivating me to do good science. Passive learning from her can always inculcate patience, meticulous planning and management skills in you. I thank Thomas Langer for being a part of my thesis committee and giving some invaluable suggestions throughout my project.

CECAD imaging facility was the place where I spent a lot of time and learnt many things. I thank Astrid, Christian and Niko for helping with problems through my project.

A good lab coupled with cooperative colleagues is always a stimulating place to do good science. Everyone is always there to appreciate others success and help at the most crucial times. I would take this opportunity to thank my labmates: Esther, Valentin, Desi, Shuaiyu, Henriette, Simon, Jane and Eva. Esther deserves a big thanks from me as she has been kind enough to help in many ways. I enjoyed some nice scientific discussions with Valentin and his sense of humour. The mood in the lab would become lighter because of Desi's presence. I really appreciate Shuaiyu for her cooperation during the collaboration of the project. Henriette has always been a nice person to interact with. Simon was the interpreter for most of the German documents I received. Jane will be remembered for organizing some wonderful outings and packing wonderful birthday gifts. Eva always echoed a positive attitude towards life. I would also like to specially thank my former labmates Paola, Giuse, David and Sabrina.

Playing Cricket on weekends has also been very entertaining for me. I would like to thank all my friends for giving such a nice time on the ground. A bunch of friends have always been there to support me and help me go through some tough times. Thank You Roshini, Vipin and Prachi. Ruchika has been such a wonderful friend and companion through the years that time has really galloped away.

Loss of the m-AAA protease subunit AFG3L2 causes mitochondrial transport defects and tau hyperphosphorylation

Arun Kumar Kondadi¹, Shuaiyu Wang¹, Sara Montagner¹, Nikolay Kladt², Anne Korwitz¹, Paola Martinelli¹, David Herholz¹, Michael J Baker¹, Astrid C Schauss², Thomas Langer^{1,2,3,4}, & Elena I Rugarli^{1,2,4,*}

Abstract

The *m*-AAA protease subunit AFG3L2 is involved in degradation and processing of substrates in the inner mitochondrial membrane. Mutations in *AFG3L2* are associated with spinocerebellar ataxia SCA28 in humans and impair axonal development and neuronal survival in mice. The loss of AFG3L2 causes fragmentation of the mitochondrial network. However, the pathogenic mechanism of neurodegeneration in the absence of AFG3L2 is still unclear. Here, we show that depletion of AFG3L2 leads to a specific defect of anterograde transport of mitochondria in murine cortical neurons. We observe similar transport deficiencies upon loss of AFG3L2 in *OMA1*-deficient neurons, indicating that they are not caused by *OMA1*-mediated degradation of the dynamin-like GTPase OPA1 and inhibition of mitochondrial fusion. Treatment of neurons with antioxidants, such as N-acetylcysteine or vitamin E, or decreasing tau levels in axons restored mitochondrial transport in AFG3L2-depleted neurons. Consistently, tau hyperphosphorylation and activation of ERK kinases are detected in mouse neurons postnatally deleted for *Afg3l2*. We propose that reactive oxygen species signaling leads to cytoskeletal modifications that impair mitochondrial transport in neurons lacking AFG3L2.

Keywords *m*-AAA protease; mitochondrial transport; N-acetylcysteine; Neurodegeneration; tau

Subject Categories Molecular Biology of Disease; Neuroscience

DOI 10.1002/embj.201387009 | Received 26 September 2013 | Revised 23 February 2014 | Accepted 5 March 2014

Introduction

Mitochondria are essential organelles, whose functional integrity is ensured by efficient quality control mechanisms, including maintenance of mitochondrial proteostasis by chaperones and proteases,

ongoing mitochondrial fusion and fission, and removal of dysfunctional mitochondria by mitophagy (Rugarli & Langer, 2012). Neurons are particularly susceptible to defects of any of these systems, which fail in several neurodegenerative conditions (Schon & Przedborski, 2011). Since neurons are highly polarized and need to traffic mitochondria to sites very distant from where mitochondrial biogenesis takes place, mechanisms are likely to exist to couple transport of mitochondria to their functionality. For instance, PINK1 and parkin target the mitochondrial motor adaptor miro for degradation, thus preventing transport of dysfunctional mitochondria (Wang *et al*, 2011).

The mitochondrial protease AFG3L2 is a central component of the intra-mitochondrial quality control system. AFG3L2 forms homooligomeric complexes or hetero-oligomeric hexamers with the homologous subunit paraplegin to constitute the *m*-AAA (matrix-ATPase associated with various cellular activities) protease in the inner mitochondrial membrane (Atorino *et al*, 2003; Koppen *et al*, 2007). This complex exerts ATP-dependent proteolytic activity, leading either to degradation or processing of specific substrates (Gerdes *et al*, 2012). Quality control substrates of the *m*-AAA protease include misfolded polypeptides in the inner membrane, such as subunits of the respiratory chain (Hornig-Do *et al*, 2012), while the best characterized processing substrate is the mitoribosome subunit MRPL32 (Nolden *et al*, 2005; Bonn *et al*, 2011). Mitochondria lacking AFG3L2 show defective assembly of the mitoribosome and reduced levels of mitochondrial protein synthesis (Almajan *et al*, 2012).

Mutations in *AFG3L2* have been linked to two neurodegenerative conditions in humans, a dominant form of spinocerebellar ataxia (SCA28), and a severe recessive form of spastic-ataxia with early-onset, and rapid progression (SPAX5; Di Bella *et al*, 2010; Pierson *et al*, 2011). In contrast, mutations in *SPG7*, encoding paraplegin, are found in patients with a recessive form of hereditary spastic paraplegia (HSP; Casari *et al*, 1998). Given the pleiotropic roles of *m*-AAA proteases in mitochondria, the pathogenic cascade in these diseases is still unclear.

Constitutive *Afg3l2* knockout mice are affected by a severe form of spasticity and muscle weakness, and die before 3 weeks of age

¹ Institute for Genetics, University of Cologne, Cologne, Germany

² Cologne Excellence Cluster on Cellular Stress Responses in Aging-Associated Diseases (CECAD), Cologne, Germany

³ Max Planck Institute for Biology of Ageing, Cologne, Germany

⁴ Center for Molecular Medicine (CMMC), University of Cologne, Cologne, Germany

*Corresponding author. Tel: +49 221 478 84244; Fax: +49 221 478 84261; E-mail: Elena.Rugarli@uni-koeln.de

(Maltecca *et al*, 2008). Strikingly, these mice display a characteristic neurodevelopmental phenotype, characterized by maintenance of neuronal cell number, but failure to develop spinal and peripheral large caliber axons (Maltecca *et al*, 2008). Neurons from *Afg3l2*-deficient mice contain abnormal mitochondria in the cell body and a paucity of neurofilaments in their processes (Maltecca *et al*, 2008). This phenotype led to the proposal that impaired trafficking of mitochondria and other cargos underlies the developmental failure of the axons. AFG3L2 is also required cell-autonomously for survival of adult neurons. Deletion of the gene in Purkinje cells following development provokes dramatic cell loss associated with secondary inflammation (Almajan *et al*, 2012). Notably, the first abnormalities observed in neurons lacking AFG3L2 are mitochondrial fragmentation and clustering, further hinting to impaired mitochondrial dynamics and transport (Almajan *et al*, 2012).

Studies in cell lines have shown that mitochondria lacking AFG3L2 are fragmented and fusion-incompetent owing to activation of OMA1, a mitochondrial protease that cleaves the GTPase fusion molecule OPA1 (Ehses *et al*, 2009; Head *et al*, 2009). OPA1 is essential for inner membrane fusion (Song *et al*, 2007). Various stress conditions activate the peptidase OMA1 in the inner membrane that cleaves OPA1, converting long OPA1 forms into short forms and inhibiting mitochondrial fusion (Duvezin-Caubet *et al*, 2006; Ishihara *et al*, 2006; Griparic *et al*, 2007; Ehses *et al*, 2009; Head *et al*, 2009; Baker *et al*, 2014). It is therefore conceivable that mitochondrial fragmentation impairs the axonal transport of mitochondria in *Afg3l2*-deficient neurons leading to neurodegeneration.

Here, we use primary murine cortical neurons to examine this possibility. We show that depletion of AFG3L2 leads to a specific defect of anterograde transport of mitochondria. Surprisingly, these transport defects are independent of OMA1 activation and mitochondrial fragmentation, but can be rescued by treatment of neurons with antioxidants and by modulation of tau levels. *In vivo*, deletion of *Afg3l2* in cortical and hippocampal neurons leads to tau hyperphosphorylation and activation of ERK kinases. Our data suggest a cross talk between dysfunctional mitochondria and the cytoskeleton, which may have implications for other neurodegenerative conditions characterized by tau aggregations.

Results

Depletion of AFG3L2 in primary neurons leads to fragmentation and defective anterograde transport of mitochondria

To investigate whether mitochondrial transport is affected in neurodegenerative diseases caused by mutations in AFG3L2, we established primary cultures of mouse cortical neurons and downregulated *Afg3l2* using RNA interference while plating the neurons. A construct expressing mCherry targeted to mitochondria (mito-mCherry) was co-transfected together with different *Afg3l2*-specific or control siRNA oligonucleotides (Ehses *et al*, 2009). We imaged morphology and motility of mitochondria in axons with a length of at least 200 μ m. Downregulation of *Afg3l2* resulted in mitochondrial fragmentation in comparison with control neurons (Fig 1A, Supplementary Fig S1A). A significantly different distribution of mitochondrial length was observed in neurons with depleted levels of AFG3L2 (Fig 1B, Supplementary Fig S1B). Furthermore,

the percentage of axonal length occupied by mitochondrial mass, hereafter referred to as mitochondrial occupancy, was reduced upon depletion of AFG3L2 when compared to control (Fig 1C, Supplementary Fig S1C). Mitochondrial fragmentation often precedes mitophagy that in turn could account for the reduced occupancy (Twig *et al*, 2008). The best characterized mitophagic pathway involves recruitment of parkin to depolarized mitochondria (Narendra *et al*, 2008). However, we found no recruitment of parkin to the mitochondrial surface in neurons downregulated for *Afg3l2* (Supplementary Fig S2A). Moreover, mitochondrial membrane potential was not significantly affected in most neurons by AFG3L2 depletion (Supplementary Fig S2B and C).

To analyze mitochondrial transport, we scored the percentage of mitochondria moving in the anterograde direction, in the retrograde direction, changing their directionality (defined as oscillatory), or remaining stationary during the time of recording. Strikingly, depletion of AFG3L2 resulted in a selective defect of anterograde movement of mitochondria into the axons (Fig 1D, Supplementary Fig S1D). The number of stationary mitochondria slightly increased, in some cases to statistically significant values (Supplementary Table S1). Finally, we determined whether downregulation of *Afg3l2* affects the velocity of mitochondrial movement. We found that the average speed of both anterogradely and retrogradely moving mitochondria was not significantly reduced in *Afg3l2*-downregulated neurons (Fig 1E).

Mitochondrial transport defects in *Afg3l2* knockdown axons are independent of OMA1 activation

It is conceivable that mitochondrial fragmentation causes transport defects. To test this possibility, we downregulated *Opa1* in cortical neurons using two different siRNA oligonucleotides and performed live-imaging experiments. As expected, *Opa1* downregulation led to mitochondrial fragmentation (Supplementary Fig S3A and B). It is noteworthy that mitochondrial occupancy was also significantly decreased with siRNA-B (Supplementary Fig S3C). However, mitochondria were normally transported into the axons, as previously observed (Misko *et al*, 2010). This experiment suggests that mitochondrial fragmentation by itself does not impair mitochondrial movement (Supplementary Fig S3D).

To substantiate these findings, we investigated whether *Oma1* deletion could alleviate defects in mitochondrial morphology, occupancy, and transport in primary cortical neurons depleted for AFG3L2. In *Afg3l2*-deficient mouse embryonic fibroblasts (MEFs), long OPA1 forms are processed by the protease OMA1, inhibiting fusion (Ehses *et al*, 2009). In *Oma1* knockout neurons, mitochondrial length was not significantly affected by downregulation of *Afg3l2*, and mitochondrial occupancy was only slightly reduced (Fig 2A-C). Strikingly, anterograde mitochondrial transport was still impaired upon depletion of AFG3L2 (Fig 2D), indicating that the mitochondrial transport defect is independent of OMA1 activation and mitochondrial fragmentation.

Afg3l2 deficiency leads to disruption of the microtubule network and tau hyperphosphorylation *in vivo*

The previous data suggest that dysfunctional mitochondria in *Afg3l2* knockdown neurons might be sensed in the cell body leading to

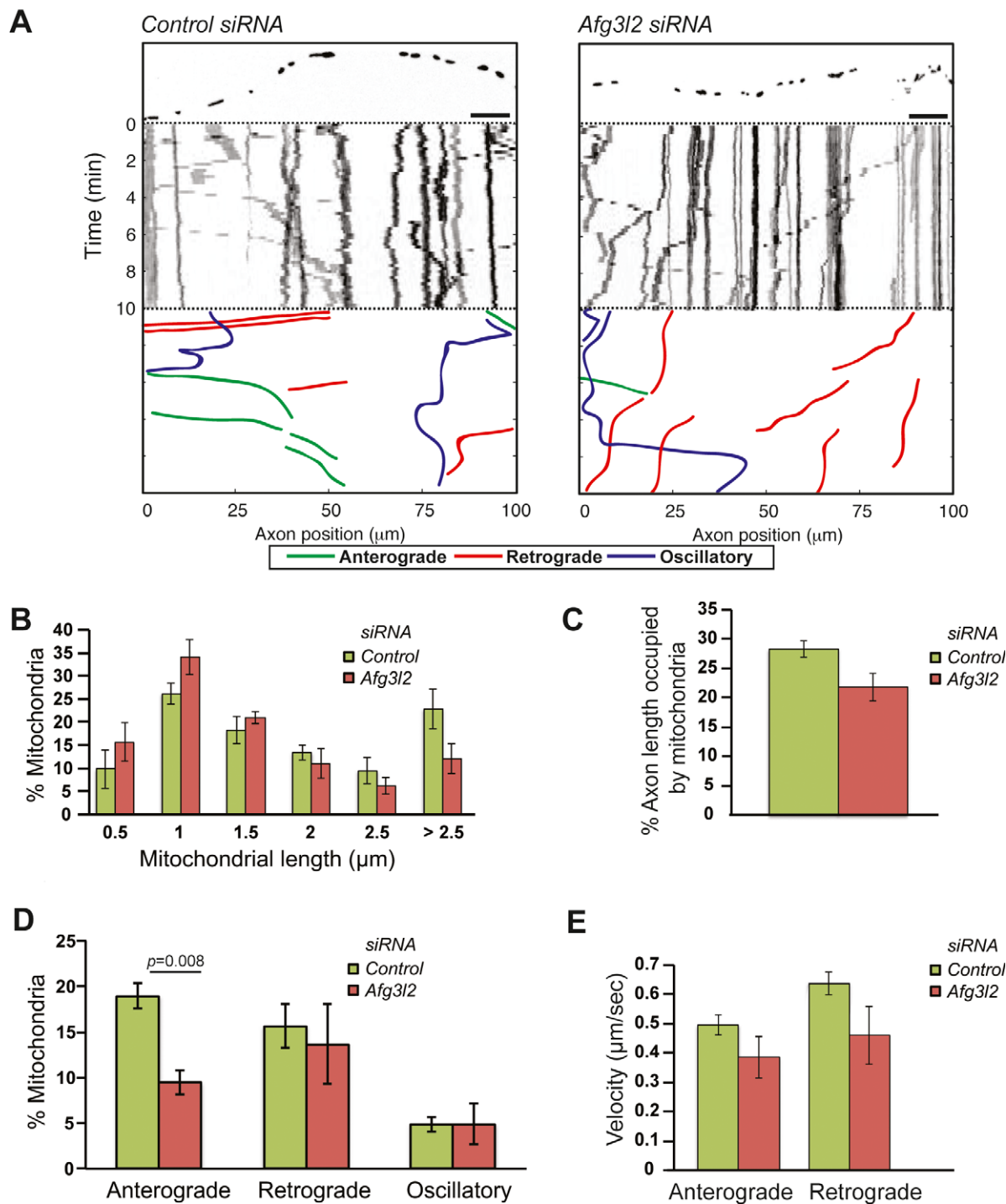


Figure 1. Depletion of AFG3L2 causes mitochondrial defects.

A Representative kymographs of axons (shown above respective kymographs) from neurons co-transfected with mito-mCherry and control or *Afg3l2* siRNAs. Schematic of different color-coded transport types is shown below. Scale bars, 10 μm .

B The percentage of mitochondria belonging to a given length bin was averaged from three independent experiments (120–150 mitochondria were measured in each experiment). Bars represent SEM. Chi-square test: $P = 0.002$.

C Quantification of mitochondrial occupancy per axon ($n = 3$ experiments; 7–8 axons per experiment).

D Quantification of mitochondrial transport types in the axon. Data represent mean \pm SEM of three independent experiments. 7–8 axons from each experiment were analyzed. P -value was determined with Student's t -test.

E Average mitochondrial velocity in the anterograde and retrograde direction. Data represent mean \pm SEM of three independent experiments. The velocity of mitochondria from at least 5 axons per experiment was analyzed.

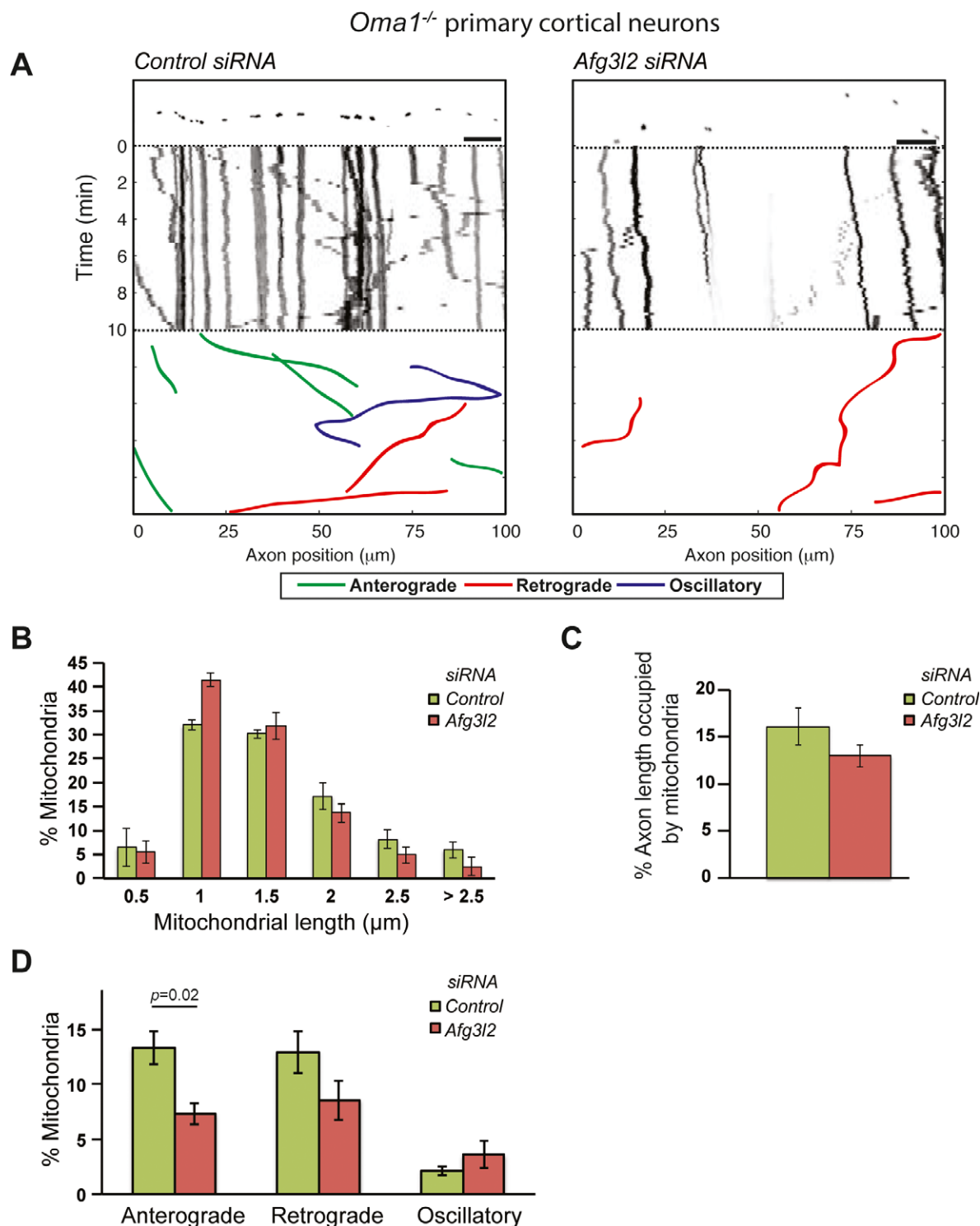


Figure 2. OMA1 ablation does not rescue mitochondrial transport defect of AFG3L2-depleted neurons.

A Representative kymographs of axons (shown above respective kymographs) from neurons isolated from *Oma1* knockout mice co-transfected with mito-mCherry and control or *Afg3l2* siRNAs. Schematic of different color-coded transport types is shown below. Scale bars, 10 μm.

B The percentage of mitochondria belonging to a given length bin was averaged from three independent experiments (105–200 mitochondria were measured in each experiment). Bars represent SEM.

C Quantification of mitochondrial occupancy per axon ($n = 3$ experiments; at least 8 axons per experiment).

D Quantification of mitochondrial transport types in the axon. Data represent mean \pm SEM of three independent experiments. At least 8 axons from each experiment were analyzed. P -value was determined with Student's t -test.

inhibition of the anterograde transport. To elucidate the underlying mechanism, we examined the cerebral cortex of mice constitutively lacking *Afg3l2* (*Afg3l2*^{Emv66/Emv66} mice, from now on referred to as *Afg3l2* KO; Maltecca *et al*, 2008). Nissl staining of serial coronal sections of the brain at postnatal day 14, shortly before *Afg3l2* KO mice die, showed a reduction in the thickness of the cerebral cortex, while the organized six-layered structure was preserved (Fig 3A). Cortical neurons in layer V appeared shrunken and lacked processes, a hallmark of degeneration (Fig 3A).

We performed *in situ* hybridization experiments to evaluate the expression of laminar-specific genes, such as *Cux2* for layers II–IV, *Rorb* for layer IV, and *Er81* for layer V (Molyneaux *et al*, 2007). These genes were expressed in the respective layer, indicating normal migration and specification of cortical neurons during development (Fig 3B). However, *Er81*-positive neurons were decreased, pointing to pronounced secondary degeneration of neurons in layer V.

We then examined neuronal projections by staining brain sections with antibodies against phosphorylated neurofilaments (SMI31) to detect axons, microtubule-associated protein 2 (SMI52) to label dendrites, and myelin basic protein (MBP) to decorate myelin sheaths. A drastic reduction of myelinated axonal projections containing neurofilaments was found in *Afg3l2* KO mice, while dendrites were affected to a lesser degree (Fig 3C). These findings are consistent with previous observations in the spinal cord of these mice (Maltecca *et al*, 2008). To further characterize neuronal alterations in the absence of AFG3L2, we performed ultrastructural studies of the cerebral cortex. Neurons demonstrated pronounced mitochondrial abnormalities. Mitochondria appeared swollen, lost their tubular morphology, and had disrupted cristae pushed to the organelle periphery (Fig 3D). Microtubules in control dendrites and axons were aligned along the major axis, while they were fragmented and disorganized in *Afg3l2*-deficient neuronal processes (Fig 3D).

The microtubule binding protein tau plays an important role in microtubule stabilization (Morris *et al*, 2011). Tau hyperphosphorylation detaches tau from the microtubules, ultimately leading to their instability and fragmentation, similar to our observations in *Afg3l2*-deficient neuronal projections. We therefore assessed the levels of phosphorylated tau species in the brain of *Afg3l2* KO mice. Hyperphosphorylation of tau can be detected with the AT8 antibody, which recognizes epitopes (serine 202 and threonine 205) that are pathologically hyperphosphorylated in Alzheimer's disease and other tauopathies. Immunoreactivity for AT8 antibodies was greatly enhanced in neurons of *Afg3l2* KO mice compared with wild-types (Fig 3E). Western blot analyses confirmed these results and further indicated increased levels of phosphorylation of tau on threonine 181 and serines 199 and 396 (Fig 3F).

In conclusion, constitutive loss of AFG3L2 affects development of long projection axons in the cerebral cortex and is associated with microtubule disorganization and tau hyperphosphorylation.

Deletion of *Afg3l2* in adult cortical neurons causes tau hyperphosphorylation and activation of PKA and ERK1/2 kinases

Tau is highly phosphorylated during embryonic development and in the early postnatal periods at several residues. However, after the majority of axons have reached their target, tau phosphorylation is

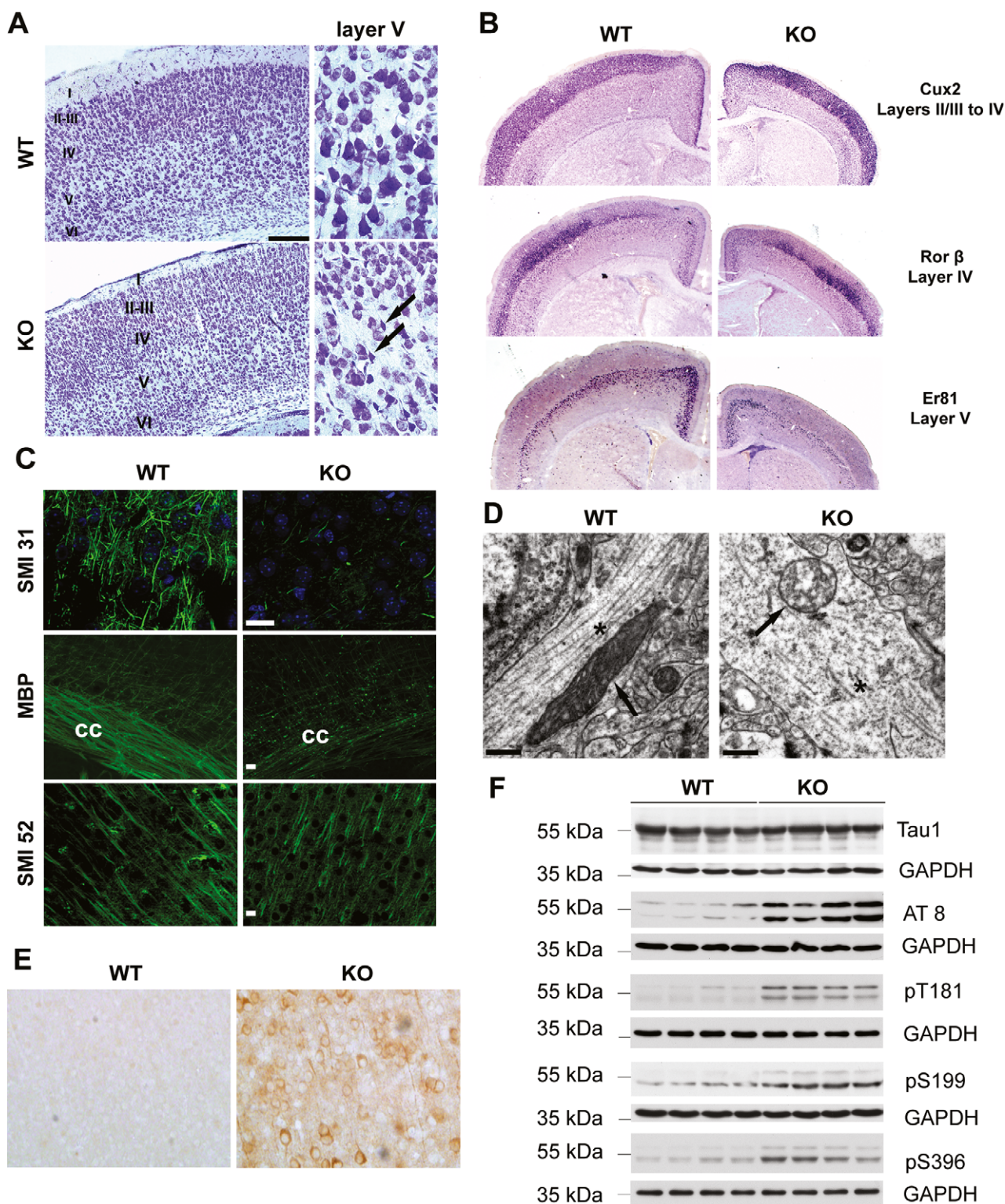
downregulated (Wang & Liu, 2008). Tau hyperphosphorylation in *Afg3l2* null mice may therefore reflect the axonal developmental failure. To test whether lack of AFG3L2 can also lead to tau hyperphosphorylation in adult neurons, we crossed *Afg3l2*^{fl/fl} mice (Almajan *et al*, 2012) with a transgenic line expressing the Cre recombinase under the control of the CamKII α promoter, leading to efficient depletion of AFG3L2 in postnatal neurons of the cortex, and the hippocampus (Minichiello *et al*, 1999; Supplementary Fig S4A). Deletion of *Afg3l2* in neurons (*Afg3l2*^{NKO}) leads to prominent neurodegeneration. At 8 weeks of age, *Afg3l2*^{NKO} mice display evident loss of neurons in both the cortex and the hippocampus, as shown by Nissl staining (Fig 4A). Remarkably, tau hyperphosphorylation was prominent in degenerating neurons and involved similar residues as in the constitutive *Afg3l2* KO mice (Fig 4B and C). Thus, tau phosphorylation is activated during the neurodegenerative process that is triggered by the loss of AFG3L2.

To address the mechanism underlying tau phosphorylation, we examined the activation of potential tau kinases in the *Afg3l2*^{NKO} model. The main tau kinase GSK3 β was found to be inhibited by phosphorylation at serine 9, and activation of MARK, CDK5, or its activator p35 was not observed (Supplementary Fig S4B). In contrast, deletion of *Afg3l2* in adult neurons increased the levels of the phosphorylated active forms of mitogen-activated protein kinase (MAPK) ERK1/2 and of cAMP-dependent protein kinase A (PKA; Fig 4D). Both kinases have been previously implicated in tau phosphorylation in pathological conditions (Martin *et al*, 2013). MAP kinases are activated by oxidative stress, which in turn can lead to tau hyperphosphorylation (Chu *et al*, 2004; Petersen *et al*, 2007). We therefore examined the brains of *Afg3l2* null and NKO mice for signs of oxidative damage, but could not find accumulation of carbonylated proteins or increased levels of the antioxidant SOD2 (Supplementary Fig S5).

We conclude from these experiments that the MAP kinases ERK1/2 and PKA are activated upon loss of AFG3L2 in adult neurons of the cortex and hippocampus leading to tau hyperphosphorylation *in vivo*.

Tau downregulation affects mitochondrial transport in AFG3L2-depleted neurons

Tau binds selectively to anterograde-directed motors and can therefore regulate anterograde transport of mitochondria (Dixit *et al*, 2008). The finding of tau hyperphosphorylation in the absence of AFG3L2 *in vivo* prompted us to examine whether tau levels in primary cortical neurons can affect the mitochondrial transport and morphology defects, associated with acute *Afg3l2* downregulation. *Mapt*-specific siRNA oligonucleotides were tested for their ability to downregulate overexpressed tau in cultured MEFs (Supplementary Fig S6). *Afg3l2* siRNA oligonucleotides were transfected together with a control siRNA or *Mapt* siRNA in cortical neurons, and mitochondrial morphology and transport were evaluated. Notably, tau depletion did not affect mitochondrial length, occupancy, transport, and velocity in wild-type neurons (Fig 5A–E, Table S1). However, mitochondria were less fragmented, and a partial but significant rescue of the anterograde transport defect was detected upon concomitant downregulation of *Afg3l2* and *Mapt* when compared to AFG3L2 depletion alone (Fig 5). Thus, modulation of tau levels affects mitochondrial transport in pathological conditions.



Antioxidants suppress mitochondrial transport defects in AFG3L2-depleted neurons

As oxidative stress triggers tau hyperphosphorylation, we explored the possibility that increased reactive oxygen species

(ROS) production affects mitochondrial motility. Firstly, we tested whether primary neurons downregulated for *Afg3l2* show signs of increased ROS by staining them with CellROX green. This dye becomes highly fluorescent upon oxidation and labels the DNA of both nucleus and mitochondria. However, we did

Figure 3. Constitutive *Afg3l2* deletion leads to microtubule fragmentation and tau hyperphosphorylation.

- A Nissl staining of coronal sections across the cerebral cortex of *Afg3l2* knockout (KO) and wild-type (WT) show normal lamination but degenerating neurons in layer V (arrows).
- B *In situ* hybridization of brain coronal sections of WT and KO using the indicated probes.
- C Immunofluorescence analysis of coronal sections across the cerebral cortex of *Afg3l2* KO and WT mice with the indicated antibodies shows dramatic loss of myelinated axons. cc: corpus callosum.
- D Electron micrographs of cortical neuronal processes show microtubule fragmentation and disorganization, and abnormal mitochondria in KO mice. Arrows: mitochondria; asterisks: microtubules.
- E Cerebral cortex sections were stained with AT8 antibody. Phosphorylated tau accumulates in cell bodies and dendrites of KO mice.
- F Western blot analysis of brain lysates from *Afg3l2* KO and WT littermates using the indicated antibodies. KO brains display increased levels of phosphorylated tau species.

Data information: Scale bar in (A) 200 μ m, in (C) 20 μ m, in (D) 0.5 μ m.

Source data are available online for this figure.

not observe consistent, statistically significant differences in the fluorescence between control and AFG3L2-depleted neurons (Supplementary Fig S7A and B). This result could be due to limited sensitivity of the dye that is suitable to detect massive changes in ROS levels, such as those induced by treating neurons with menadione (Supplementary Fig S7C and D). We therefore asked whether interfering with basal ROS levels by culturing neurons in the presence of antioxidants, such as N-acetylcysteine (NAC) or vitamin E, has an impact on mitochondrial motility. NAC is a drug that affects the redox state of cells and indirectly acts as antioxidant by increasing the pool of reduced glutathione (Kelly, 1998), while vitamin E scavenges the peroxyl radicals and prevents the propagation of free radicals (Niki & Traber, 2012). Both drugs efficiently reduce the levels of ROS induced in primary neurons by menadione (Supplementary Fig S7C and D). Moreover, both NAC and vitamin E reduce the levels of phospho-tau in cultured neurons *in vitro* (Supplementary Fig S7E and F). Strikingly, NAC treatment of primary neurons leads to a global change in cytoskeletal components, by reducing the levels of β -tubulin, tyrosinated and acetylated tubulin, actin, and total tau (Supplementary Fig S7E).

The presence of NAC in the culture medium did not affect the distribution of mitochondrial length or the occupancy of mitochondria in control neurons. Surprisingly, the percentage of mitochondria moving in the anterograde direction and their velocity was significantly increased in control neurons when cultured in medium supplemented with NAC (Fig 6A–F, Supplementary Table S1). Moreover, NAC treatment significantly suppressed the defects observed upon *Afg3l2* downregulation: mitochondrial length, mitochondrial occupancy, and the percentage of mitochondria moving in anterograde direction increased to levels comparable to control (Fig 6A–D).

We then depleted AFG3L2 in cortical neurons grown in medium containing vitamin E. Vitamin E induced slight fragmentation of mitochondria in control neurons, which is reflected in a reduced occupancy (Fig 7A and B). Consistently, vitamin E did not rescue mitochondrial morphology and occupancy of AFG3L2-depleted neurons when compared to controls (Fig 7A and B). However, a significant improvement in the anterograde transport of mitochondria was observed (Fig 7C, Supplementary Table S1). Mitochondrial velocities of anterogradely and retrogradely moving mitochondria were not significantly affected by vitamin E (Fig 7D and E). We conclude that ROS, present at physiological levels, play a pivotal role in coupling quality control of mitochondria to their transport.

Discussion

Neurodegenerative diseases linked to mutations in components of the *m*-AAA protease, paraplegin and AFG3L2, are characterized by late-onset axonal degeneration in cortical motor or cerebellar neurons. Our study shows for the first time that the frequency of anterograde transport of mitochondria, but not the speed of movement, is affected in neurons with reduced levels of AFG3L2, suggesting that defective mitochondrial trafficking contributes to the pathogenic mechanism in the human diseases. Mitochondrial transport defects in *Afg3l2*-deficient neurons are restricted to mitochondria moving from the cell body toward the growth cone. A similar phenotype has been previously described in cortical neurons isolated from mice lacking spastin, a microtubule-severing protein involved in HSP (Kasher *et al*, 2009), in motor neurons derived from SOD^{G93A} transgenic mice, a model of amyotrophic lateral sclerosis (De Vos *et al*, 2007), and in amyloid β -treated neurons (Reddy *et al*, 2012). Even mild impairment of anterograde transport in patients carrying heterozygous mutations in AFG3L2 could lead to progressive depletion of mitochondria from axons causing late-onset neurodegeneration. It is tempting to speculate that impaired anterograde transport of mitochondria underlies the developmental failure of large myelinated axons in absence of AFG3L2 in the mouse.

Surprisingly, our data uncouple mitochondrial trafficking defects from OMA1 activation and mitochondrial fragmentation. Stress-activated OMA1-mediated processing of OPA1 is not required for mitochondrial transport defects in the absence of AFG3L2. Furthermore, reduced OPA1 levels do not affect mitochondrial transport, despite leading to fragmentation, in agreement with previous studies (Misko *et al*, 2010). Our data therefore suggest that alteration of mitochondrial transport and increased processing of OPA1 in absence of AFG3L2 are independent events. Notably, we observed a strict correlation between the degree of mitochondrial fragmentation and the reduction in mitochondrial occupancy, suggesting increased mitochondrial turnover likely by a parkin-independent mechanism.

How are *Afg3l2*-deficient mitochondria hindered from being transported toward the growth cone? We identify tau as a regulator of transport of dysfunctional *Afg3l2*-deficient mitochondria. The primary function of the microtubule-associated protein tau is to bind and stabilize microtubules (Wang & Liu, 2008). Tau was found to largely affect access of the anterograde motor kinesins to microtubules (Dixit *et al*, 2008). Consistently, tau overexpression

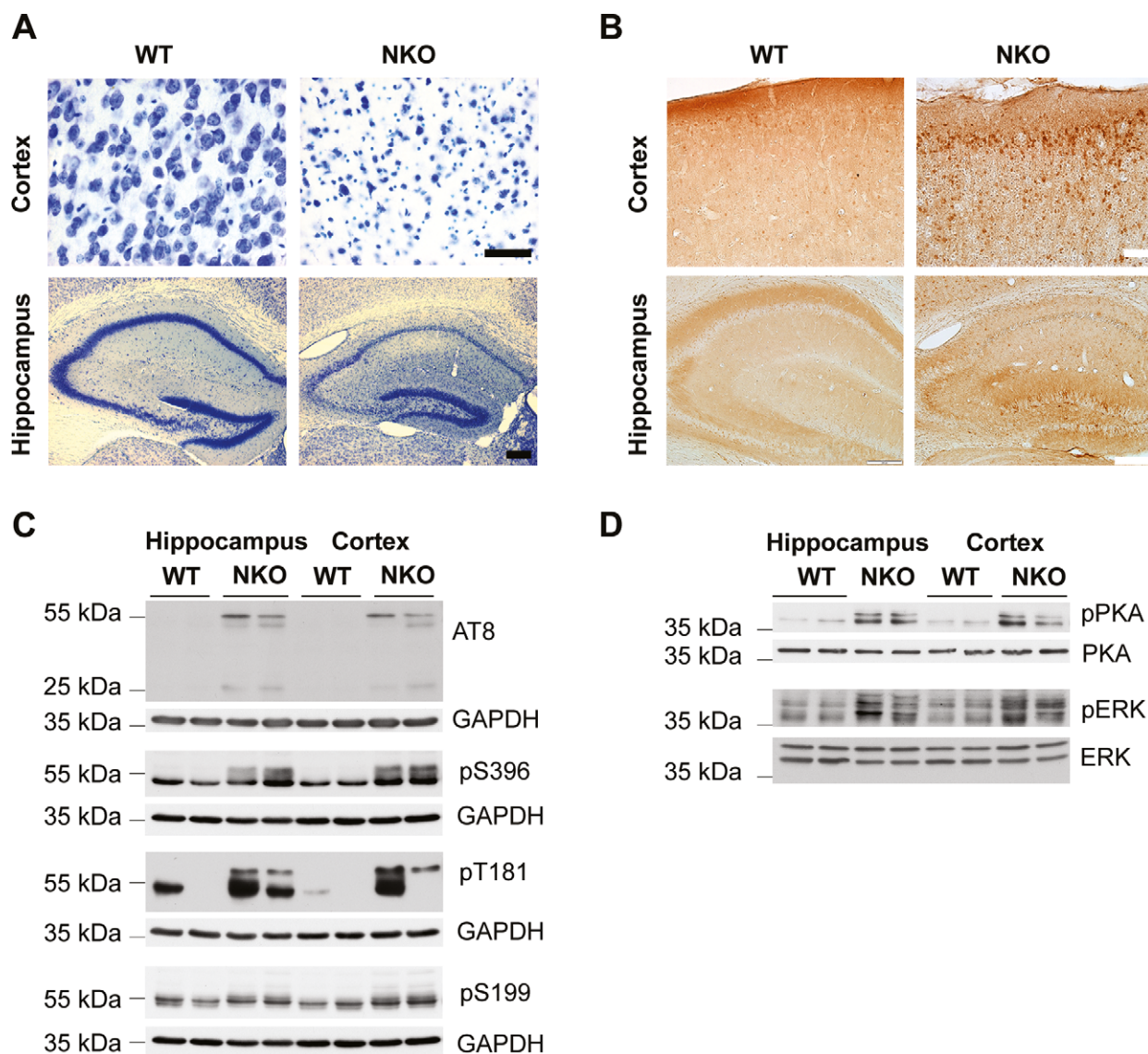


Figure 4. Deletion of *Afg3l2* in adult forebrain neurons causes tau hyperphosphorylation and activation of PKA and ERK1/2 kinases.

A Brain coronal sections of *Afg3l2* forebrain neuronal specific knockout (*Afg3l2*^{NKO}; CamKII α -Cre positive; NKO) and littermate control (*Afg3l2*^{WT}; CamKII α -Cre negative; WT) at 8 weeks of age were stained with Nissl solution. Pronounced neuronal degeneration is observed in the cerebral cortex and hippocampus of *Afg3l2*^{NKO}.
 B AT8 immunohistochemistry staining of adjacent sections from (A) shows accumulation of hyperphosphorylated tau in neuronal cell bodies in both cerebral cortex and hippocampus of *Afg3l2*^{NKO}.
 C Western blot analysis of hippocampus and cerebral cortex lysates from *Afg3l2* NKO and WT littermates using the indicated antibodies detects increased phosphorylation of tau.
 D Western blot analysis of hippocampus and cerebral cortex lysates from *Afg3l2* NKO and WT littermates using the indicated antibodies show activation of PKA and ERK1/2 kinases.

Data information: Scale bar in (A) 50 μ m (cortex) and 200 μ m (hippocampus), in (B) 50 μ m (cortex) and 200 μ m (hippocampus).

Source data are available online for this figure.

inhibits kinesin-dependent transport of cargos, including mitochondria (Ebner *et al*, 1998). Loss of tau function in the mouse still allows normal mitochondrial transport (Yuan *et al*, 2008), whereas tau depletion is beneficial in certain pathological conditions; for example, it improves axonal transport defects of mitochondria in neurons treated with A β peptides (Vossel *et al*, 2010). Similarly, we show that reducing tau levels can partially

rescue the mitochondrial transport defects associated with *Afg3l2* downregulation.

Tau hyperphosphorylation is an important downstream event to the lack of AFG3L2 in cortical neurons *in vivo*. During embryonic and early postnatal periods, tau is hyperphosphorylated at several sites, including Thr181, Ser199, Ser202, and Thr205. Notably, the same residues are also hyperphosphorylated in degenerating

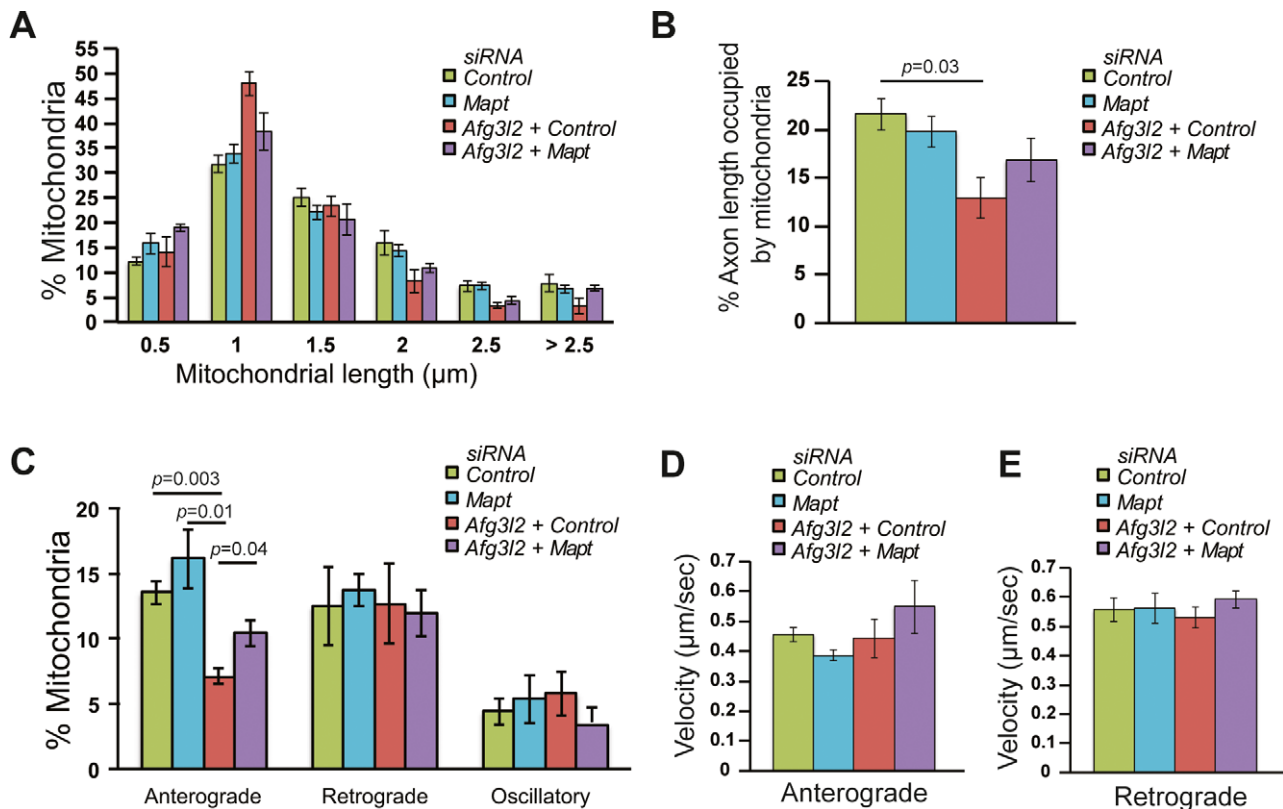


Figure 5. Tau levels affect mitochondrial transport in AFG3L2-depleted neurons.

- A The percentage of mitochondria belonging to a given length bin was averaged from three independent experiments (120–210 mitochondria were measured in each experiment). Bars represent SEM. *P*-values were calculated with the chi-square test. Control vs. *Afg3l2*/control: $P = 7 \times 10^{-4}$, control vs. *Afg3l2*/Mapt: $P = 9 \times 10^{-3}$, *Afg3l2*/control vs. *Afg3l2*/Mapt: $P = 5 \times 10^{-5}$.
- B Quantification of mitochondrial occupancy per axon ($n = 3$ experiments; 7–9 axons per experiment).
- C Quantification of mitochondrial transport types in the axon. Data represent mean \pm SEM of three independent experiments. 7–9 neurons from each experiment were analyzed.
- D, E Average mitochondrial velocity in the anterograde (D) and retrograde (E) direction. Data represent mean \pm SEM of three independent experiments. The velocity of mitochondria from 3 axons per experiment was analyzed.
- Data information: *P*-values in (B) and (C) were determined with Student's *t*-test.

neurons of Alzheimer's disease patients (Wang & Liu, 2008). Upon phosphorylation, tau detaches from microtubules and can potentially improve motility of cargos, such as mitochondria. Consistently, degeneration caused by missorting of tau into neurons can be rescued by increasing its phosphorylation via the tau kinase MARK2 (Thies & Mandelkow, 2007). However, prolonged tau hyperphosphorylation promotes self-aggregation into cytoplasmic inclusions and leads to neurodegeneration (Ballatore et al, 2007). Hyperphosphorylated tau at residues recognized by the AT8 antibody was recently found to inhibit mitochondrial transport in cortical neuronal axons by affecting spacing of microtubules (Shahpasand et al, 2012). In conclusion, tau hyperphosphorylation might be beneficial at early stages in the pathogenic process, but it is conceivable that sustained tau hyperphosphorylation impairs anterograde transport of mitochondria in *Afg3l2*-deficient neurons. In agreement with such a scenario, neuronal microtubules appear severely disrupted in absence of AFG3L2. Notably, interfering with axonal transport by mutating kinesin-1, or by downregulating *miro* or *milton* in *Drosophila*, was sufficient to activate kinase pathways

responsible for tau hyperphosphorylation (Falzone et al, 2009, 2010; Iijima-Ando et al, 2012), suggesting that loss of axonal mitochondria enhances tau pathology.

Accumulation of fibrillary tau inclusions (neurofibrillary tangles) in the central nervous system has been implicated in onset and progression of aging-associated disorders that manifest clinically with progressive cognitive and/or motor impairment (Ballatore et al, 2007). However, the causative link between tau hyperphosphorylation and upstream events in tauopathies is still unclear. Here, we demonstrate that mitochondrial dysfunction can directly trigger tau hyperphosphorylation upon genetic ablation of a mitochondrial protease. Similarly, we found abnormal tau hyperphosphorylation and deposition of tau filaments in *Phb2*-deficient degenerating neurons (Merkwirth et al, 2012). Prohibitins form large protein scaffolds in the inner mitochondrial membrane that interact with the *m*-AAA protease (Merkwirth & Langer, 2009). Together, our data provide genetic evidence for a causal relationship between mitochondrial dysfunction and tau hyperphosphorylation, as suggested by other studies (Hoglinger

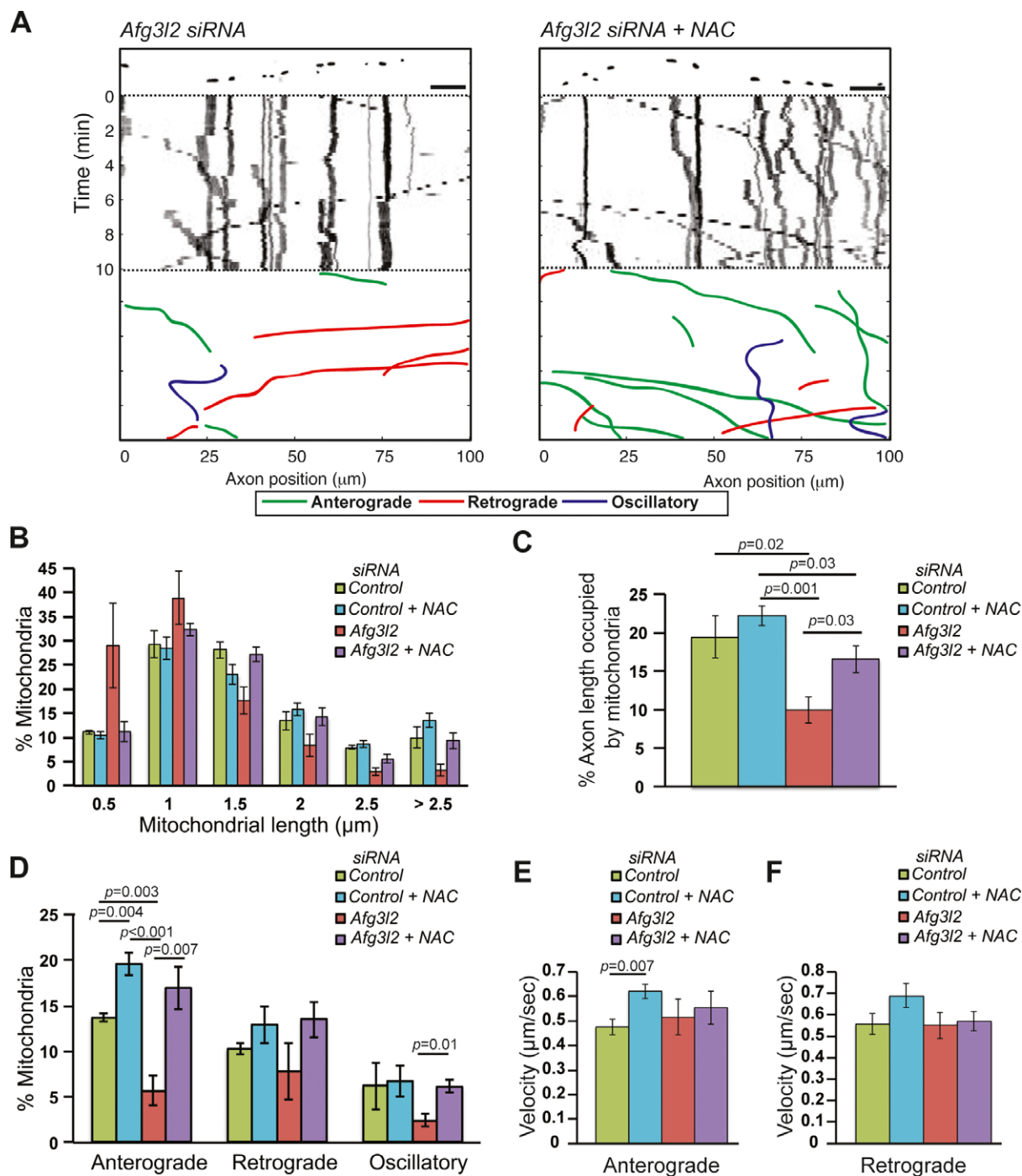


Figure 6. Mitochondrial defects in AFG3L2-depleted neurons are rescued by NAC.

- A** Representative kymographs of axons (shown above respective kymographs) from neurons co-transfected with mito-mCherry and *Afg3l2* siRNAs in the absence or presence of NAC. Schematic of different color-coded transport types is shown below. Scale bars, 10 μm .
- B** The percentage of mitochondria belonging to a given length bin was averaged from four independent experiments (78–195 mitochondria were measured in each experiment). Bars represent SEM. *P*-values were calculated with the chi-square test. Control vs. *Afg3l2*: $P = 8 \times 10^{-3}$; *Afg3l2* vs. *Afg3l2* with NAC: $P = 1 \times 10^{-12}$.
- C** Quantification of mitochondrial occupancy per axon ($n = 4$ experiments; 8–10 axons per experiment).
- D** Quantification of mitochondrial transport types in the axon. Data represent mean \pm SEM of four independent experiments. At least 8 axons from each experiment were analyzed.
- E, F** Average mitochondrial velocity in the anterograde (**E**) and retrograde (**F**) direction. Data represent mean \pm SEM of four independent experiments. The velocity of mitochondria from 3 axons per experiment was analyzed.

Data information: *P*-values in (C–E) were determined with Student's *t*-test.

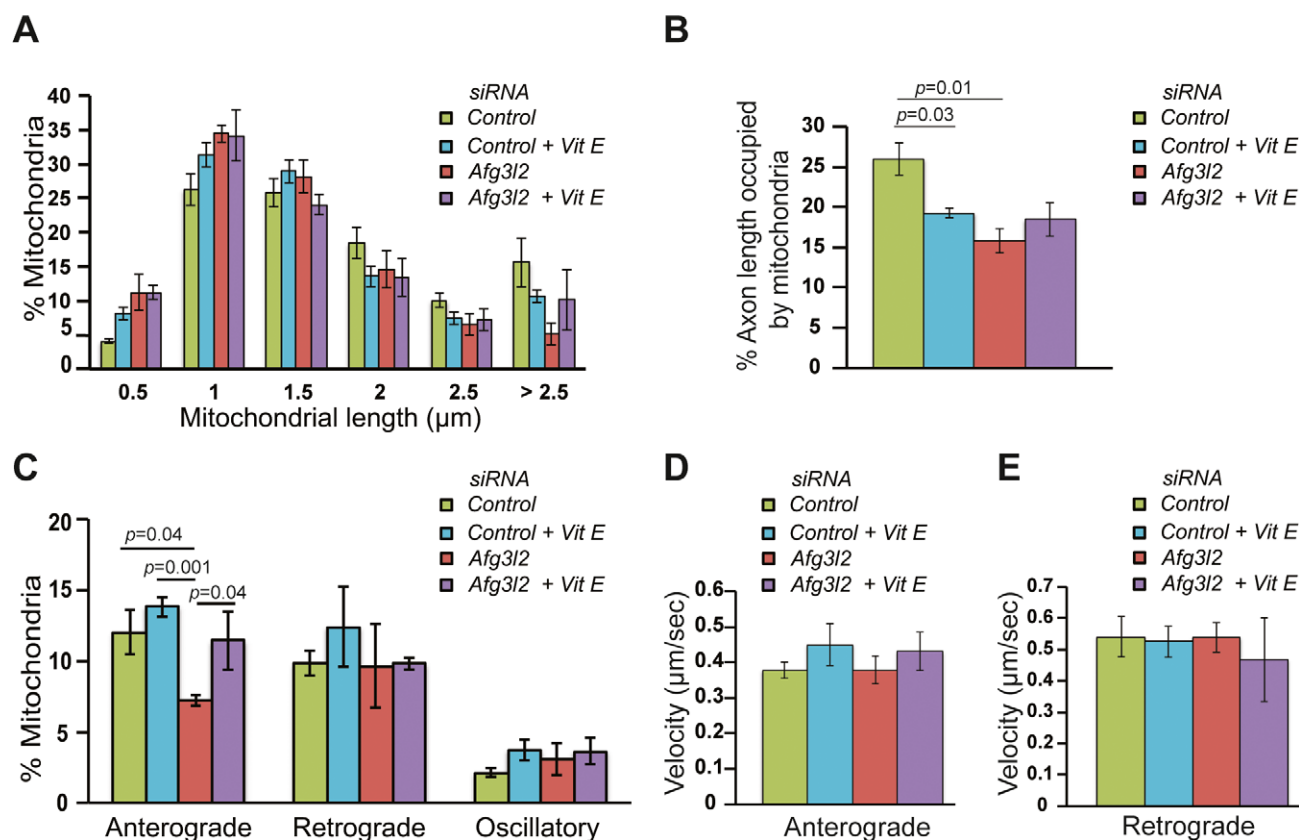


Figure 7. Mitochondrial transport defect in AFG3L2-depleted neurons is rescued by vitamin E.

A The percentage of mitochondria belonging to a given length bin was averaged from three independent experiments (130–218 mitochondria were measured in each experiment). Bars represent SEM. *P*-values were calculated with the chi-square test. Control versus control with vitamin E: $P = 0.01$, control vs. *Afg3l2*: $P = 5 \times 10^{-7}$.

B Quantification of mitochondrial occupancy per axon ($n = 3$ experiments; at least 8 axons per experiment).

C Quantification of mitochondrial transport types in the axon. Data represent mean \pm SEM of three independent experiments. At least 8 axons from each experiment were analyzed.

D, E Average mitochondrial velocity in the anterograde (D) and retrograde (E) direction. Data represent mean \pm SEM of three independent experiments. The velocity of mitochondria from 3 axons per experiment was analyzed.

Data information: *P*-values in (C) and (D) were determined with Student's *t*-test.

et al, 2005; Escobar-Khondiker *et al*, 2007; Melov *et al*, 2007; Ohsawa *et al*, 2008).

In both *Phb2* and *Afg3l2* mouse models, we observed activation of MAPKs (Merkwirth *et al*, 2012). MAPKs have been shown to phosphorylate tau at several residues both *in vitro* and *in vivo* (Zhu *et al*, 2002) and are activated by several cell stresses, including oxidative stress (Son *et al*, 2013). Consistently, we find that antioxidants efficiently reduce levels of phospho-tau in primary neurons. Increased levels of oxidized proteins were detected in the cerebellum of *Afg3l2* heterozygous mice (Maltecca *et al*, 2009), while it is conceivable that neurons die before oxidative damage occurs in the brain of *Afg3l2* knockout mice. Failure to detect a significant increase of ROS levels in *Afg3l2*-deficient neurons may be due to the limited sensitivity of available fluorescent dyes (Murphy *et al*, 2011). However, in support of the hypothesis that ROS play a signaling role in regulating mitochondrial transport, we found that treatment with antioxidants, such as NAC and vitamin E, can rescue the anterograde transport defects of *Afg3l2*-deficient mitochondria. Interestingly, NAC regulates both the frequency of transport and the

velocity of mitochondria in wild-type neurons, stressing the hypothesis that modulating the physiological levels of ROS can affect mitochondrial transport. NAC has a more pronounced effect than vitamin E on mitochondrial transport in *Afg3l2*-deficient neurons. NAC was previously shown to rescue the mitochondrial transport defects observed in dopaminergic neurons treated with MPP⁺, a toxin that inhibits mitochondrial complex I activity (Kim-Han *et al*, 2011). Neurons treated with NAC display a reduction of the levels of actin and β -tubulin. Thus, the beneficial effect of NAC may be also exerted by modulation of redox modifications of cytoskeletal components. In fact, actin has been previously shown to sense oxidative load and to be affected by NAC (Dalle-Donne *et al*, 2001; Farah & Amberg, 2007). An intriguing hypothesis is that ROS-activated signaling cascades can affect mitochondrial transport not only by impinging on tau phosphorylation, but also by targeting motor proteins, or mitochondrial adaptors. Future experiments will be required to investigate this possibility in depth.

In conclusion, we propose a pathogenic model, where deficiency of AFG3L2 leads on one side to mitochondrial fragmentation, via

OMA1-mediated processing of OPA1, and on the other side to increased production of ROS (Fig 8). Increased ROS may result from respiratory incompetence due to defective mitochondrial translation (Almajan *et al*, 2012). ROS may trigger activation of stress-induced kinases, which phosphorylate tau in an attempt to reduce its attachment to the microtubules, thus promoting mitochondrial transport. However, with time, insoluble hyperphosphorylated tau aggregates, disrupts microtubules, and affects mitochondrial anterograde transport. The axonal transport defect may further contribute to sustain pathological tau hyperphosphorylation (Fig 8). Mitochondrial transport defects ultimately lead to late-onset mitochondrial depletion from axons and neurodegeneration. Our data may be of relevance for several neurodegenerative conditions characterized by mitochondrial dysfunction and tau accumulation and open up the possibility that treatment with antioxidants may be beneficial in models of *Afg3l2* deficiency.

Material and Methods

Animal experiments

All animal procedures were conducted in accordance with European (EU directive 86/609/EEC), national (TierSchG), and institutional guidelines and were approved by local authorities (Landesamt für Natur, Umwelt, und Verbraucherschutz Nordrhein-Westfalen) under the license 87–51.04.2010.A219. *Afg3l2*^{Emv66/Emv66} mice were obtained by breeding heterozygous *Afg3l2*^{+/Emv66} (Maltecca *et al*, 2008) in a mixed FVB-C57BL/6 background. Conditional *Afg3l2* floxed mice (Almajan *et al*, 2012) were mated with *CaMKIIa* cre (Minichiello *et al*, 1999) to achieve *Afg3l2* forebrain neuron-specific knockouts. Mice carrying the *Oma1* gene exon 3 flanked by loxP sites were generated by gene targeting in C57BL/6 background.

Oma1 knockout mice were produced by crossing homozygous *Oma1* floxed mice with a transgenic line expressing the Cre recombinase under the β -actin promoter.

Tissue preparation

Mice were deeply anesthetized and perfused transcardially with 4% paraformaldehyde (PFA) in PBS. Tissues were dissected and post-fixed in 4% PFA for immunohistochemistry and in 2% glutaraldehyde in 0.12 M phosphate buffer for electron microscopy. For biochemical analyses, tissues were immediately frozen in dry ice and stored at -80°C until use.

RNA *in situ* hybridization

PCR products obtained by amplification of mouse brain cDNA were used as templates to transcribe either sense or antisense digoxigenin-labeled riboprobes using the DIG RNA labeling kit (Roche). Oligonucleotides used to generate the PCR products contained the SP6 promoter. Sequences are available upon request. RNA *in situ* hybridization was performed on vibratome sections, as previously described (Tiveron *et al*, 1996).

Histology and Immunohistochemistry

Postfixed brains were embedded in 6% agar, and 30- μm sections were cut using a vibratome (Leica). Free-floating sections were stained with 0.25% thionine solution. Immunohistochemistry with AT8 antibody (Thermo Scientific) was performed with M.O.M. Immunodetection kit (Vector Laboratories), according to the manufacturer's protocol. Sections were mounted using Eukitt medium (Fluka). For immunofluorescence, sections were permeabilized and blocked in 0.4% Triton X-100 and 10% goat serum in TBS and

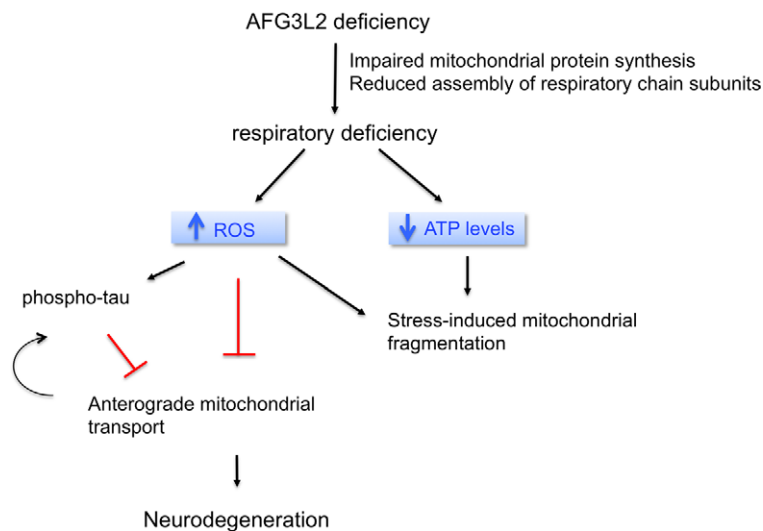


Figure 8. Schematic representation of the pathogenic cascade in neurodegenerative diseases due to AFG3L2 deficiency.

Upon AFG3L2 deficiency, mitochondria become dysfunctional due to impaired mitochondrial protein synthesis and reduced assembly of respiratory chain subunits. The resulting respiratory impairment causes, on one side, stress-induced fragmentation of mitochondria via OMA1 activation and, on the other side, increased ROS production. ROS trigger a pathogenic cascade leading to hyperphosphorylation of tau, which in turn can affect mitochondrial anterograde transport. ROS may also hinder transport via some other yet uncharacterized mechanism. Defects in anterograde transport of mitochondria lead to depletion of mitochondria in axons and neurodegeneration.

incubated with SMI 31, SMI 52, and anti-MBP antibodies (Covance) diluted in 5% goat serum in TBS. Following incubation with anti-mouse Alexa Fluor 488 (Life technologies), sections were mounted using FluorSave Reagent (Calbiochem). Images were acquired using an Axio-Imager M2 microscope equipped with Apotome 2 (Zeiss).

Western blot analysis

Tissues were homogenized in RIPA buffer containing 150 mM NaCl, 50 mM Tris-HCl pH 7.4, 5 mM EDTA, 1% Triton X-100, 1% sodium deoxycholate, 0.1% SDS, and protease inhibitor cocktail (Roche) on ice. After high-speed centrifugation, the supernatant was harvested, and protein concentration was determined using Bradford assay (Bio-Rad). 20–50 µg proteins were separated by 12% SDS-PAGE and blotted onto PVDF membrane (Millipore). The membrane was blocked in 5% milk containing 0.1% Tween-20 in TBS for 1 h at room temperature and probed with primary antibodies overnight at 4°C. We used AT8, AT270 (detecting Tau phosphorylation site Thr181), anti-phospho-Tau-Ser199, anti-phospho-Tau-Ser396 antibodies from Pierce, anti-Tau1, anti-ERK1/2, anti-GAPDH from Millipore, anti-PKA C-α, anti-phospho-PKA C (Thr197), anti-phospho-p44/42MAPK (ERK1/2; Thr202/Tyr204) from Cell Signaling. Following incubation with HRP-conjugated secondary antibodies, signal was detected using ECL (GE Healthcare).

Electron microscopy

After fixation in 2% glutaraldehyde in 0.12 M phosphate buffer, tissues were treated with 1% osmium tetroxide and embedded in Epon (Fluka). About 70-nm ultrathin sections were cut, collected onto 200 mesh copper grids (Electron Microscopy Sciences), and stained with uranyl acetate (Plano GMBH) and lead citrate (Electron Microscopy Sciences). Images were captured by a transmission electron microscope (CM10, Phillips) equipped with Orius SC200W camera.

Primary neuron culture and transfection

Embryos were harvested from wild-type CD1 mice or *Oma1* knock-out mice at E18. Cortices were collected after removing the meninges, cut into small pieces, washed in Earle's balanced salt solution (Gibco), dissociated with glass Pasteur pipette, and centrifuged at 100 g for 5 min in neurobasal medium (Gibco). The supernatant was removed, and fresh medium was added to resuspend the neurons and filtered through a 100-µm filter. 125,000 neurons were transfected using a micro-electroporation system (Microporator MP-100 apparatus, Digital Bio) and then plated on glass-bottom dishes (MatTek corporation) coated with poly-D-lysine hydrobromide (0.1 mg/ml, Sigma-Aldrich). The neurons were grown in neurobasal medium supplemented with B-27 (Gibco) and glutamine at 37°C with 5% CO₂. In each experiment, 0.5 µg of mito-mCherry was co-transfected together with 100 nM of the respective siRNA.

Stealth-small interfering RNAs (siRNAs) were synthesized by Invitrogen with the following sequences:

Afg3l2: 5'-CCUGCCUCCGUACGCUCUAUCAAUA-3'

Mapt: 5'-CAGUCGAAGAUUGGCCUCCUUGGAUA-3'.

The medium GC stealth-negative control (Invitrogen) was used for all experiments.

NAC (Sigma-Aldrich) and vitamin E (Sigma-Aldrich) were supplemented to the complete medium at concentrations of 1 mM and 200 µM, respectively. Vitamin E was replenished every 24 h.

Live-cell imaging

Mitochondria in the axons were imaged using a Perkin-Elmer Ultra View spinning disc confocal microscope, equipped with a CCD camera (Hamamatsu, C9100-50), at 60× magnification (oil-immersion objective, N.A = 1.49, illumination wavelength = 561 nm). Video recordings were acquired at 1000 × 1000 pixel resolution every 10 seconds for a period of 10 min (61 image stacks/movie). The stage enclosing the dishes was set to 37°C and 5% CO₂. Imaging of the axons was performed 72 h after plating the neurons, and they were identified as processes arising from the soma twice or thrice longer than other processes. Axons selected for analyses had a minimum length of 200 µm. Images were acquired at least 50 µm distal to the soma.

Kymograph generation

Mitochondrial movements along an axon were visualized using kymographs, generated with a custom written script (Matlab R2011b incl. image processing toolbox, Mathworks). Initially, an optimal axon centerline between two manually set endpoints was automatically obtained, based on a maximum projection of all image stacks (imaged mitochondria). Then, kymographs were obtained by generating a maximum projection for each image stack (time point) leading to orthogonal projection of maximum intensities in a neighborhood of approximately 1 µm onto the axon centerline.

Assessment of mitochondrial length, occupancy, and axonal transport

Mitochondrial length was quantified from the first image of the video recordings, by drawing a line along the major axis or along the diameter of circular mitochondria. This analysis was performed in Volocity 6.1 (PerkinElmer). Mitochondrial occupancy was calculated as the total length of all mitochondria in an axon divided by axonal length. For quantification of mitochondrial transport, we classified mitochondrial movement over time as anterograde, retrograde, or oscillatory. Mitochondria were defined as oscillatory if they changed direction to move a distance greater than 5 µm, while they were considered stationary if they moved less than 5 µm during the video recordings. In case of a fission event, daughter mitochondria were considered as separate. In case of a fusion event, mitochondrion after fusion was considered as separate from the parent mitochondria. Classification of mitochondrial movements was manually performed from the video recordings obtained in Volocity 6.1 (PerkinElmer) as the position of soma was noted while image acquisition. Mitochondrial velocity was calculated for anterograde and retrograde movements in all the timeframes where a mitochondrion was moving. After establishing a cut-off value of 0.1 µm/s, the average velocity was calculated for each individual mitochondrion.

Statistical analysis

Mitochondrial length was measured from at least three independent experiments. Data were binned, averaged across experiments, and statistical evaluation was performed using the chi-square test. Unpaired two-tailed Student's *t*-test was used for statistical comparison of mitochondrial occupancy, transport, and average velocity. Data are presented as mean \pm standard error (SEM). In all cases, at least three independent experiments were performed, and 8–10 axons analyzed. The *P*-values were calculated using Graphpad Prism software (version 6.02) and are indicated when lower than 0.05.

Supplementary information for this article is available online: <http://emboj.embopress.org>

Acknowledgements

The authors wish to thank Jens Brüning, Thomas Wunderlich, and Markus Schubert for generous sharing of antibodies. We are also grateful to Elisa Motori and Nils-Göran Larsson for sharing reagents and for helpful discussion. We thank Peter Frommolt for discussion on statistical evaluation of data. We thank the CECAD Imaging Facility and Christian Jüngst for their support. This work was supported by grants of the Deutsche Forschungsgemeinschaft to E.I.R. (RU1653/1-1), and T.L. (LA918/8-1), a long-term fellowship of the Alexander-von-Humboldt foundation to M.J.B. and a fellowship of the NRW International Graduate School in Development Health and Disease to A.K.K.

Author contribution

AKK performed imaging experiments, with the help of ACS; NK developed the code required for generating kymographs; SW, SM, AK, PM, and DH performed experiments on the mouse models; MJB produced *Oma1* knockout mice; TL and EIR conceived the study and wrote the manuscript.

Conflict of interest

The authors declare that they have no conflict of interest.

References

- Almajan ER, Richter R, Paeger L, Martinelli P, Barth E, Decker T, Larsson NG, Kloppenburg P, Langer T, Rugarli EI (2012) AFG3L2 supports mitochondrial protein synthesis and Purkinje cell survival. *J Clin Invest* 122: 4048–4058
- Atorino L, Silvestri L, Koppen M, Cassina L, Ballabio A, Marconi R, Langer T, Casari G (2003) Loss of m-AAA protease in mitochondria causes complex I deficiency and increased sensitivity to oxidative stress in hereditary spastic paraplegia. *J Cell Biol* 163: 777–787
- Baker MJ, Lampe PA, Stojanovski D, Korwitz A, Anand R, Tatsuta T, Langer T (2014) Stress-induced OMA1 activation and autocatalytic turnover regulate OPA1-dependent mitochondrial dynamics. *EMBO J* 33: 578–593
- Ballatore C, Lee VM, Trojanowski JQ (2007) Tau-mediated neurodegeneration in Alzheimer's disease and related disorders. *Nat Rev Neurosci* 8: 663–672
- Bonn F, Tatsuta T, Petruccaro C, Riemer J, Langer T (2011) Presequence-dependent folding ensures MrpL32 processing by the m-AAA protease in mitochondria. *EMBO J* 30: 2545–2556
- Casari G, De Fusco M, Ciarmatori S, Zeviani M, Mora M, Fernandez P, De Michele G, Filla A, Coccozza S, Marconi R, Dürr A, Fontaine B, Ballabio A (1998) Spastic paraplegia and OXPHOS impairment caused by mutations in paraplegin, a nuclear-encoded mitochondrial metalloprotease. *Cell* 93: 973–983
- Chu CT, Levinthal DJ, Kulich SM, Chalovich EM, DeFranco DB (2004) Oxidative neuronal injury. The dark side of ERK1/2. *Eur J Biochem* 271: 2060–2066
- Dalle-Donne I, Rossi R, Milzani A, Di Simplicio P, Colombo R (2001) The actin cytoskeleton response to oxidants: from small heat shock protein phosphorylation to changes in the redox state of actin itself. *Free Radical Biol Med* 31: 1624–1632
- De Vos KJ, Chapman AL, Tennant ME, Manser C, Tudor EL, Lau KF, Brownlee J, Ackerley S, Shaw PJ, McLoughlin DM, Shaw CE, Leigh PN, Miller CC, Grierson AJ (2007) Familial amyotrophic lateral sclerosis-linked SOD1 mutants perturb fast axonal transport to reduce axonal mitochondria content. *Hum Mol Genet* 16: 2720–2728
- Di Bella D, Lazzaro F, Brusco A, Plumari M, Battaglia G, Pastore A, Finardi A, Cagnoli C, Tempia F, Frontali M, Veneziano L, Sacco T, Boda E, Brussino A, Bonn F, Castellotti B, Baratta S, Mariotti C, Gellera C, Fracasso V et al (2010) Mutations in the mitochondrial protease gene AFG3L2 cause dominant hereditary ataxia SCA28. *Nat Genet* 42: 313–321
- Dixit R, Ross JL, Goldman YE, Holzbaur EL (2008) Differential regulation of dynein and kinesin motor proteins by tau. *Science* 319: 1086–1089
- Duvezin-Caubet S, Jagasia R, Wagener J, Hofmann S, Trifunovic A, Hansson A, Chomyn A, Bauer MF, Attardi G, Larsson NG, Neupert W, Reichert AS (2006) Proteolytic processing of OPA1 links mitochondrial dysfunction to alterations in mitochondrial morphology. *J Biol Chem* 281: 37972–37979
- Ebneth A, Godemann R, Stamer K, Illenberger S, Trinczek B, Mandelkow E (1998) Overexpression of tau protein inhibits kinesin-dependent trafficking of vesicles, mitochondria, and endoplasmic reticulum: implications for Alzheimer's disease. *J Cell Biol* 143: 777–794
- Ehses S, Raschke I, Mancuso G, Bernacchia A, Geimer S, Tondera D, Martinou JC, Westermann B, Rugarli EI, Langer T (2009) Regulation of OPA1 processing and mitochondrial fusion by m-AAA protease isoenzymes and OMA1. *J Cell Biol* 187: 1023–1036
- Escobar-Khondiker M, Hollerhage M, Muriel MP, Champy P, Bach A, Depienne C, Respondek G, Yamada ES, Lannuzel A, Yagi T, Hirsch EC, Oertel WH, Jacob R, Michel PP, Ruberg M, Höglinger GU (2007) Annonacin, a natural mitochondrial complex I inhibitor, causes tau pathology in cultured neurons. *J Neurosci* 27: 7827–7837
- Falzone TL, Gunawardena S, McCleary D, Reis GF, Goldstein LS (2010) Kinesin-1 transport reductions enhance human tau hyperphosphorylation, aggregation and neurodegeneration in animal models of tauopathies. *Hum Mol Genet* 19: 4399–4408
- Falzone TL, Stokin GB, Lillo C, Rodrigues EM, Westerman EL, Williams DS, Goldstein LS (2009) Axonal stress kinase activation and tau misbehavior induced by kinesin-1 transport defects. *J Neurosci* 29: 5758–5767
- Farah ME, Amberg DC (2007) Conserved actin cysteine residues are oxidative stress sensors that can regulate cell death in yeast. *Mol Biol Cell* 18: 1359–1365
- Gerdes F, Tatsuta T, Langer T (2012) Mitochondrial AAA proteases—towards a molecular understanding of membrane-bound proteolytic machines. *Biochim Biophys Acta* 1823: 49–55
- Griparic L, Kanazawa T, van der Bliek AM (2007) Regulation of the mitochondrial dynamin-like protein Opa1 by proteolytic cleavage. *J Cell Biol* 178: 757–764
- Head B, Griparic L, Amiri M, Gandre-Babbe S, van der Bliek AM (2009) Inducible proteolytic inactivation of OPA1 mediated by the OMA1 protease in mammalian cells. *J Cell Biol* 187: 959–966
- Höglinger GU, Lannuzel A, Khondiker ME, Michel PP, Duyckaerts C, Feger J, Champy P, Prigent A, Medja F, Lombes A, Oertel WH, Ruberg M, Hirsch EC

- (2005) The mitochondrial complex I inhibitor rotenone triggers a cerebral tauopathy. *J Neurochem* 95: 930–939
- Hornig-Do HT, Tatsuta T, Buckermann A, Bust M, Kollberg G, Rotig A, Hellmich M, Nijtmans L, Wiesner RJ (2012) Nonsense mutations in the COX1 subunit impair the stability of respiratory chain complexes rather than their assembly. *EMBO J* 31: 1293–1307
- Iijima-Ando K, Sekiya M, Maruko-Otake A, Ohtake Y, Suzuki E, Lu B, Iijima KM (2012) Loss of axonal mitochondria promotes tau-mediated neurodegeneration and Alzheimer's disease-related tau phosphorylation via PAR-1. *PLoS Genet* 8: e1002918
- Ishihara N, Fujita Y, Oka T, Mihara K (2006) Regulation of mitochondrial morphology through proteolytic cleavage of OPA1. *EMBO J* 25: 2966–2977
- Kasher PR, De Vos KJ, Wharton SB, Manser C, Bennett EJ, Bingley M, Wood JD, Milner R, McDermott CJ, Miller CC, Shaw PJ, Grierson AJ (2009) Direct evidence for axonal transport defects in a novel mouse model of mutant spastin-induced hereditary spastic paraplegia (HSP) and human HSP patients. *J Neurochem* 110: 34–44
- Kelly GS (1998) Clinical applications of N-acetylcysteine. *Altern Med Rev* 3: 114–127
- Kim-Han JS, Antenor-Dorsey JA, O'Malley KL (2011) The parkinsonian mimetic, MPP+, specifically impairs mitochondrial transport in dopamine axons. *J. Neurosci.* 31: 7212–7221
- Koppen M, Metodiev MD, Casari G, Rugarli EI, Langer T (2007) Variable and tissue-specific subunit composition of mitochondrial m-AAA protease complexes linked to hereditary spastic paraplegia. *Mol Cell Biol* 27: 758–767
- Maltecca F, Aghaie A, Schroeder DG, Cassina L, Taylor BA, Phillips SJ, Malaguti M, Previtali S, Guenet JL, Quattrini A, Cox GA, Casari G (2008) The mitochondrial protease AFG3L2 is essential for axonal development. *J Neurosci* 28: 2827–2836
- Maltecca F, Magnoni R, Cerri F, Cox GA, Quattrini A, Casari G (2009) Haploinsufficiency of AFG3L2, the gene responsible for spinocerebellar ataxia type 28, causes mitochondria-mediated Purkinje cell dark degeneration. *J Neurosci* 29: 9244–9254
- Martin L, Latypova X, Wilson CM, Magnaudeix A, Perrin ML, Yardin C, Terro F (2013) Tau protein kinases: involvement in Alzheimer's disease. *Ageing Res Rev* 12: 289–309
- Melov S, Adlard PA, Morten K, Johnson F, Golden TR, Hinerfeld D, Schilling B, Mavros C, Masters CL, Volitakis I, Li QX, Loughton K, Hubbard A, Cherny RA, Gibson B, Bush AI (2007) Mitochondrial oxidative stress causes hyperphosphorylation of tau. *PLoS ONE* 2: e536
- Merkwirth C, Langer T (2009) Prohibitin function within mitochondria: essential roles for cell proliferation and cristae morphogenesis. *Biochim Biophys Acta* 1793: 27–32
- Merkwirth C, Martinelli P, Korwitz A, Morbin M, Bronneke HS, Jordan SD, Rugarli EI, Langer T (2012) Loss of prohibitin membrane scaffolds impairs mitochondrial architecture and leads to tau hyperphosphorylation and neurodegeneration. *PLoS Genet* 8: e1003021
- Minichiello L, Korte M, Wolfer D, Kuhn R, Unsicker K, Cestari V, Rossi-Arnaud C, Lipp HP, Bonhoeffer T, Klein R (1999) Essential role for TrkB receptors in hippocampus-mediated learning. *Neuron* 24: 401–414
- Misko A, Jiang S, Wegorzewska I, Milbrandt J, Baloh RH (2010) Mitofusin 2 is necessary for transport of axonal mitochondria and interacts with the Miro/Milton complex. *J Neurosci* 30: 4232–4240
- Molyneaux BJ, Arlotta P, Menezes JR, Macklis JD (2007) Neuronal subtype specification in the cerebral cortex. *Nat Rev Neurosci* 8: 427–437
- Morris M, Maeda S, Vossel K, Mucke L (2011) The many faces of tau. *Neuron* 70: 410–426
- Murphy MP, Holmgren A, Larsson NG, Halliwell B, Chang CJ, Kalyanaraman B, Rhee SG, Thornalley PJ, Partridge L, Gems D, Nystrom T, Belousov V, Schumacker PT, Winterbourn CC (2011) Unraveling the biological roles of reactive oxygen species. *Cell Metab* 13: 361–366
- Narendra D, Tanaka A, Suen DF, Youle RJ (2008) Parkin is recruited selectively to impaired mitochondria and promotes their autophagy. *J Cell Biol* 183: 795–803
- Niki E, Traber MG (2012) A history of vitamin E. *Ann Nutr Metab* 61: 207–212
- Nolden M, Ehses S, Koppen M, Bernacchia A, Rugarli EI, Langer T (2005) The m-AAA protease defective in hereditary spastic paraplegia controls ribosome assembly in mitochondria. *Cell* 123: 277–289
- Ohsawa I, Nishimaki K, Murakami Y, Suzuki Y, Ishikawa M, Ohta S (2008) Age-dependent neurodegeneration accompanying memory loss in transgenic mice defective in mitochondrial aldehyde dehydrogenase 2 activity. *J Neurosci* 28: 6239–6249
- Petersen RB, Nunomura A, Lee HG, Casadesus G, Perry G, Smith MA, Zhu X (2007) Signal transduction cascades associated with oxidative stress in Alzheimer's disease. *J Alzheimer's Dis* 11: 143–152
- Pierson TM, Adams D, Bonn F, Martinelli P, Cherukuri PF, Teer JK, Hansen NF, Cruz P, Mullikin For The Nisc Comparative Sequencing Program JC, Blakesley RW, Golas G, Kwan J, Sandler A, Fuentes Fajardo K, Markello T, Tift C, Blackstone C, Rugarli EI, Langer T, Gahl WA, Toro C (2011) Whole-exome sequencing identifies homozygous AFG3L2 mutations in a spastic ataxia-neuropathy syndrome linked to mitochondrial m-AAA proteases. *PLoS Genet* 7: e1002325
- Reddy PH, Tripathi R, Troung Q, Tirumala K, Reddy TP, Anekonda V, Shirendeb UP, Calkins MJ, Reddy AP, Mao P, Manczak M (2012) Abnormal mitochondrial dynamics and synaptic degeneration as early events in Alzheimer's disease: implications to mitochondria-targeted antioxidant therapeutics. *Biochim Biophys Acta* 1822: 639–649
- Rugarli EI, Langer T (2012) Mitochondrial quality control: a matter of life and death for neurons. *EMBO J* 31: 1336–1349
- Schon EA, Przedborski S (2011) Mitochondria: the next (neurode) generation. *Neuron* 70: 1033–1053
- Shahpasand K, Uemura I, Saito T, Asano T, Hata K, Shibata K, Toyoshima Y, Hasegawa M, Hisanaga S (2012) Regulation of mitochondrial transport and inter-microtubule spacing by tau phosphorylation at the sites hyperphosphorylated in Alzheimer's disease. *J Neurosci* 32: 2430–2441
- Son Y, Kim S, Chung HT, Pae HO (2013) Reactive oxygen species in the activation of MAP kinases. *Methods Enzymol* 528: 27–48
- Song Z, Chen H, Fiket M, Alexander C, Chan DC (2007) OPA1 processing controls mitochondrial fusion and is regulated by mRNA splicing, membrane potential, and Yme1L. *J Cell Biol* 178: 749–755
- Thies E, Mandelkow EM (2007) Misrouting of tau in neurons causes degeneration of synapses that can be rescued by the kinase MARK2/Par-1. *J Neurosci* 27: 2896–2907
- Tiveron MC, Hirsch MR, Brunet JF (1996) The expression pattern of the transcription factor Phox2 delineates synaptic pathways of the autonomic nervous system. *J Neurosci* 16: 7649–7660
- Twig G, Elorza A, Molina AJ, Mohamed H, Wikstrom JD, Walzer G, Stiles L, Haigh SE, Katz S, Las G, Alroy J, Wu M, Py BF, Yuan J, Deeney JT, Corkey BE, Shirihai OS (2008) Fission and selective fusion govern mitochondrial segregation and elimination by autophagy. *EMBO J* 27: 433–446
- Vossel KA, Zhang K, Brodbeck J, Daub AC, Sharma P, Finkbeiner S, Cui B, Mucke L (2010) Tau reduction prevents Abeta-induced defects in axonal transport. *Science* 330: 198

- Wang JZ, Liu F (2008) Microtubule-associated protein tau in development, degeneration and protection of neurons. *Prog Neurobiol* 85: 148–175
- Wang X, Winter D, Ashrafi G, Schlehe J, Wong YL, Selkoe D, Rice S, Steen J, LaVoie MJ, Schwarz TL (2011) PINK1 and Parkin target Miro for phosphorylation and degradation to arrest mitochondrial motility. *Cell* 147: 893–906
- Yuan A, Kumar A, Peterhoff C, Duff K, Nixon RA (2008) Axonal transport rates in vivo are unaffected by tau deletion or overexpression in mice. *J Neurosci* 28: 1682–1687
- Zhu X, Lee HG, Raina AK, Perry G, Smith MA (2002) The role of mitogen-activated protein kinase pathways in Alzheimer's disease. *Neurosignals* 11: 270–281

ERKLÄRUNG

Ich versichere, dass ich die von mir vorgelegte Dissertation selbständig angefertigt, die benutzten Quellen und Hilfsmittel vollständig angegeben und die Stellen der Arbeit - einschließlich Tabellen, Karten und Abbildungen -, die anderen Werken im Wortlaut oder dem Sinn nach entnommen sind, in jedem Einzelfall als Entlehnung kenntlich gemacht habe; dass diese Dissertation noch keiner anderen Fakultät oder Universität zur Prüfung vorgelegen hat; abgesehen von der unten angegebenen Publikationen - noch nicht veröffentlicht worden ist sowie, daß ich eine solche Veröffentlichung vor Abschluß des Promotionsverfahrens nicht vor nehmen werde.

Die Bestimmungen der Promotionsordnung sind mir bekannt. Die von mir vorgelegte Dissertation ist von Frau Prof. Dr. Elena Rugarli betreut worden.

Köln,

Mai 2014

Arun Kumar Kondadi

Publikation im Rahmen dieser Arbeit:

Kondadi, A.K., Wang, S., Montagner, S., Kladt, N., Korwitz, A., Martinelli, P., Herholz, D., Baker, M.J., Schauss, A.C., Langer, T., *et al.* (2014). Loss of the m-AAA protease subunit AFG3L2 causes mitochondrial transport defects and tau hyperphosphorylation. The EMBO journal.

CURRICULUM VITAE

Arun Kumar Kondadi

Laboratory of Prof. Elena Rugarli
CECAD Research Center
University of Cologne, Germany
akondadi@smail.uni-koeln.de

AUSBILDUNG

October 2010 – Present	Ph.D University of Cologne, Cologne, Germany
2004 – 2006	M.Sc. Biosciences (Biotechnology), Sri Sathya Sai Institute of Higher Learning, (SSSIHL) Puttaparthi, India
2001 – 2004	B.Sc. Biosciences (Hons) (SSSIHL) Bangalore, India

BERUFSERFAHRUNG

October 2010 – Present	Research Assistant University of Cologne, Cologne, Germany
2009 – 2010	Project Assistant Indian Institute of Science (IISc), Bangalore, India
2007 – 2009	Junior Research Fellow National Centre for Biological Sciences, Bangalore, India

AUSZEICHNUNGEN

- Secured a **fellowship** from the North Rhine Westphalia International Graduate School in Development, Health and Disease (IGSDHD) for doctoral studies
- Awarded **first prize** for a **poster** presentation during Alumni day of the GSfBS, Cologne in 2012
- Secured an all India rank of 75 with **99.24 percentile** in **GATE** 2006
- Received **Gold medal for academic excellence** in B.Sc. (Hons), (Biosciences) (2004)
- Qualified for the Council of Scientific and Industrial Research (CSIR)-Lectureship NET (National Entrance Test), June 2008

PUBLIKATION

- **Arun Kumar Kondadi**, Shuaiyu Wang, Sara Montagner, Nikolay Kladt, Anne Korwitz, Paola Martinelli, David Herholz, Michael J Baker, Astrid C Schauss, Thomas Langer & Elena I Rugarli - 'Loss of the *m*-AAA protease subunit AFG3L2 causes mitochondrial transport defects and tau hyperphosphorylation' in The EMBO Journal (published online 28.03.14)

KONFERENZEN

- Mitochondria: from signaling to disease (Cell symposia) – 5-7 May, 2013, Lisbon including **a poster presentation**
- Mitochondria in life, death and disease (FEBS/EMBO course) – 9-13 May, 2012, Crete including **a poster presentation**
- Seeing is believing: Imaging the processes of life (EMBO/EMBL symposia) – 3-6 October, 2013, Heidelberg
- Neural Circuits: Development, function and degeneration (Cologne Spring meeting) – Feb 27-March 1, 2013, Cologne

PERSÖNLICHE DATEN

Date of Birth: August 29, 1983

Nationality: Indian

Marital Status: Married

Language: Fluent in spoken and written English